Modeling the Effect of Cross Flow Roughness on Solid Oxide Fuel Cells

by

Kimberly Lynne Christman

A Thesis Submitted to the Graduate

Faculty of Rensselaer Polytechnic Institute

in Partial Fulfillment of the

Requirements for the degree of

MASTER OF SCIENCE

Major Subject: Mechanical Engineering

Approved:

____

Michael K. Jensen, Thesis Adviser

Rensselaer Polytechnic Institute
Troy, New York

May, 2009

CONTENTS

LIST OF TABLES

LIST OF FIGURES

ACKNOWLEDGMENT

This work has been possible due to contributions from a number of people. I would like to thank the Claire Boothe Luce Program for providing the financial support for my education. I would also like to express my gratitude to my advisor Professor Jensen for providing encouragement and guidance throughout this research and to Professor Lewis for his help and support. Above all, I would like to thank my family and friends for their love, affection, and everlasting support through my entire education; providing encouragement whenever needed.

ABSTRACT

A three-dimensional SOFC model was used to study the use of enhanced heat transfer and mixing techniques to possibly increase the performance and available power density in a planar solid oxide fuel cell (SOFC). Fluid transport within the channel dictates the ability of the reactants to reach the reacting surface. Transport also is essential to prevent damaging temperature gradients from developing across the fuel cells. The objective of this study was to determine if applying mixing techniques to fuel cells had the potential to improve the heat/mass transport properties of the cell and to subsequently increase the performance of the cells.

FLUENT computational fluid dynamics software was used for modeling the SOFC fuel cells. Complementary numerical results showed that the introduction of various shaped fins and ribs into duct flow at very low Reynolds numbers can achieve modest enhanced mixing. These hydrodynamic results indicated that the ideal rib shape and pitch spacing were rectangular ribs spaced 3.5 mm apart.

A three-dimensional model of a single SOFC unit cell was modeled using several rib geometries developed in the preliminary hydrodynamic study and the results of the fuel cell model were analyzed. From the sharp edged sawtooth design in which the area of the electrolyte increased 16% over the plane channel design, the power density increased 13.3% if the power density is calculated from the plan area of the cells. However, if the power density is calculated from the actual area of the electrolyte, the power density of the sharp edged sawtooth design decreases 2.3% with respect to the power density produced in the plane channel fuel cell design. Similar results were obtained with the other fuel cell designs in this study. These results indicated that the enhanced mixing and heat transfer techniques had a modest effect on improving the heat and mass transport in the cell. The techniques predominantly increased the surface area of the fuel cell which led to increased volumetric power density.

1. Introduction

1.1 Significance of the Problem

There is a current movement towards environmentally friendlier and more efficient power production based on environmental concerns including global warming and the depletion of fossil fuels. Conventional power generation relies on fossil fuels, which produce a significant amount of pollutants and are of limited supply. In 2003, transportation in the US resulted in the emission of 1,866.7 Tg CO_2 [1]. This equates to approximately 5 metric tons of CO_2 per person in the US. According to the U.S. Department of Energy (DOE), transportation energy use is expected to increase 48 percent between 2003 and 2025, despite modest improvements in the efficiency of vehicle engines [2]. Another 2,328.2 Tg CO_2 was produced during electricity generation [3]. To decrease US impact on the greenhouse effect, new technological solutions must be introduced which fit within the present cultural requirements.

One possible solution is the fuel cell, which provides high energy conversion efficiency particularly at higher operating temperatures. Because of the mechanism of operation of fuel cells, they produce little or no pollutants depending on the type. The DOE is projecting that if 10% of automobiles used in the US were powered by fuel cells, 60 Tg CO_2 would be eliminated from the yearly greenhouse gas production [4]. The DOE has also stated that fuel cells using natural gas could potentially reduce carbon dioxide emissions from the electricity sector by 60% compared to a conventional coal plant and by 25% compared to today's natural gas plants.

For this to happen, fuel cells must meet the US government's cost and lifetime durability guidelines. The DOE specified these targets in the Hydrogen Fuel Cell Program [5]. For the transportation sector, the fuel cell should perform and cost the same as today's internal combustion engine vehicles. Thus, the guidelines state that a fuel cell should operate at \$30 per kW over 5,000 hours of durability. In 2004, fuel cells cost \$120 per kW and had ~1000 hours of durability [6]. More advancements need to be made to meet these production guidelines.

While there are many types of fuel cells, solid oxide fuel cells (SOFCs) show great promise for high efficiency and performance in the field of fuel cells. The high temperatures of SOFC technology allows for operating temperatures ranging from 600-1000^{o}C and efficiencies up to 70% [7]. Of the fuel cell technologies currently under development, only SOFC technology offers the advantage of solid-state construction, multi-fuel operational capability, high electrical conversion efficiency, and a simpler balance of plant compared to other fuel cell types. However, the high temperatures create some material issues within the fuel cells. Mismatch of thermal expansion between components and large temperature gradients across the cell can lead to the failure of the materials and the cells. As with all types of fuel cells, development is still needed to meet the government automotive and distributed energy goals.

Presently, SOFC designs follow two main forms: tubular and planar. Each design addresses a specific challenge that faces the technology. However, other design efforts exist. The tubular fuel cell design addresses the critical materials issues caused by thermal expansion and large temperature gradients. In the tubular fuel cell (Figure 1.1) the oxidant side of the fuel cell is shielded from the fuel side by a bayonet tube. Oxygen is fed into the end of the bayonet tube so that counter-flow is developed across the electrode assembly. The bayonet tube shape increases the strength properties of the fuel cell and eliminates the need for fragile seals. The counter-flow design helps to decrease the temperature gradient across the electrolyte. However, the geometry tubular SOFCs limits the volumetric power density of a stack.

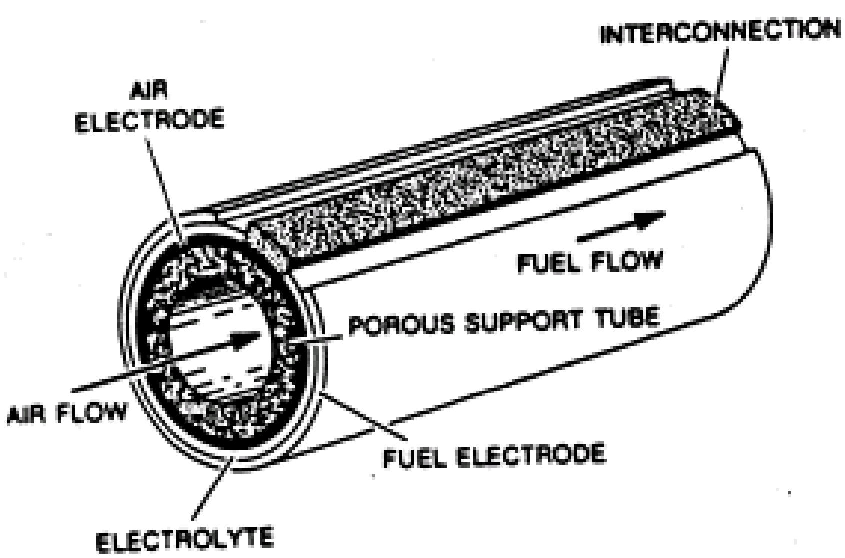

Figure 1.1 Tubular SOFC schematic [8]

The planar geometry is the most common SOFC design due to its simple construction and potential for large current densities. The construction of a planar fuel cell is similar to a sandwich (Figure 1.2). The oxidant and fuel are separated by the electrode assembly and sealant at the inlets and outlets. The flows can be arranged as co-flow, counter-flow or cross flow. The flat components and seals in the planar SOFC are more susceptible to thermal and mechanical stresses than the tubular geometry. However, the flat design of the planar fuel cell allows for efficient stacking of individual cells in a stack. This results in a larger volumetric power density than the tubular fuel cells. While these cells can achieve large power densities, improvements must are still needed before commercial goals are met.

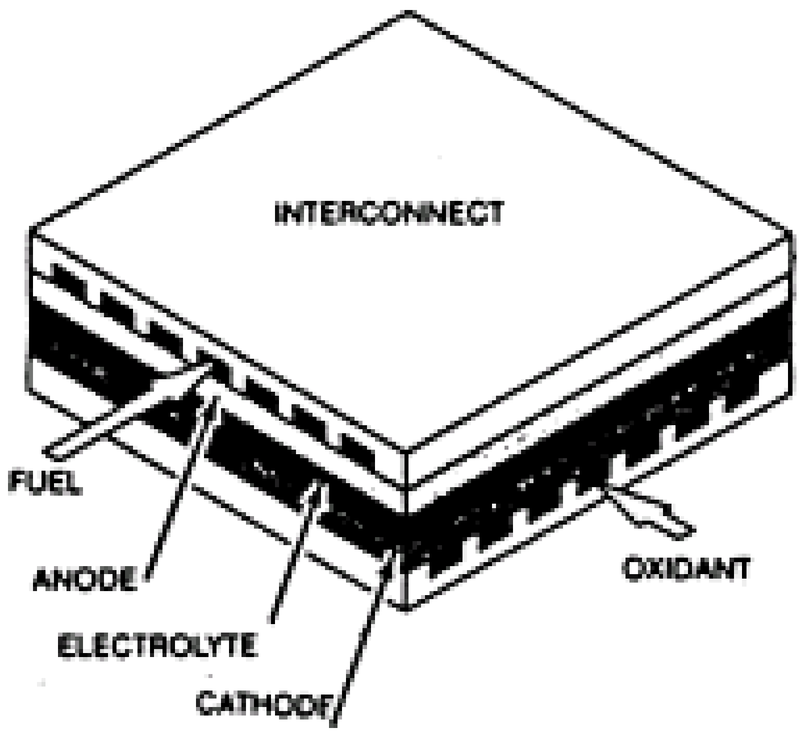

Figure 1.2 Planar SOFC schematic [8]

The majority of research on SOFCs has focused on discovering and incorporating new materials into the cells to improve performance characteristics, such as power density and mechanical stability. To address the issues of the mechanical stability of the fuel cells, research has focused on engineering materials with compatible thermal expansion coefficients. To decrease activation losses and increase the power density of the fuel cells, additional emphasis has been placed on increasing the activation properties of materials. Finally, to decrease cell ohmic and concentration losses, much effort has been made to engineer materials to increase the transport rate of ions and reactants near the electrolyte. Each of these research areas center on the fuel cell's microstructure. Thus, numerical results have often focused on the progression of reactions within specific material or on a black-box, system-wide basis highlighting specific material choices.

Activation and ohmic losses are most aptly addressed with vast material science knowledge and by designing new materials. Concentration polarization can be addressed in a wider variety of ways. One such method is to approach the problem from a hydrodynamic perspective. Fluid transport within the channel dictates the ability of the reactants to reach the reacting surface. This transport also is essential to prevent damaging temperature gradients from developing across the fuel cells. These are just a few ways that enhancing heat and mass transport within a fuel cell would be beneficial. Heat/mass transfer enhancements are widely used in industry to decrease the size or increase the performance of a system. Applying mixing mechanisms to fuel cells has the potential to improve the heat/mass transport properties of the cell and to subsequently increase the performance of the cells.

1.2 Literature Review

A review of the available literature on the enhancement of fluid flow and heat transfer in SOFCs and closely related topics has been performed. The survey has been divided into the following sections:

SOFC development and Implementation

Efforts to Increase Performance of Planar SOFC

Mixing and Enhanced Heat Transfer

Note that an additional literature survey on the physics of fuel cell operation, electrochemistry, and fluid flow is separately discussed in Chapter 2.

1.2.1 SOFC Development and Implementation

Even though fuel cells are one of the oldest energy conversion technologies, the development of the technology has been slow. Commercial fuel cells do not presently meet government cost and performance goals for automotive and distributive energy applications. The DOE predicts that, for a fuel cell to be successful, it must cost the same per kW and be as durable in an application as the carbon-burning counterparts in the same application. Despite this, there are many companies and labs pursuing SOFC development and manufacturing. Many strides have been made to create innovative designs and develop niche markets to guide SOFC technology towards commercialization.

Tubular SOFC

At the beginning of SOFC development tubular cells were the focus. Ceramic manufacturing technology and material quality were poor. The tubular fuel cell offered a stronger mechanical design while flat discs resulted in bulky stacks that had difficulties with fuel crossover. The technology leader, at the time, was Westinghouse Electric Corporation. The first tubular fuel cells were constructed using bell-and-spigot joints (Figure 1.3). These cells were cylindrical in shape with the fuel flowing by the anode in the center of the tube and the cathode on the outer surface of the tube.

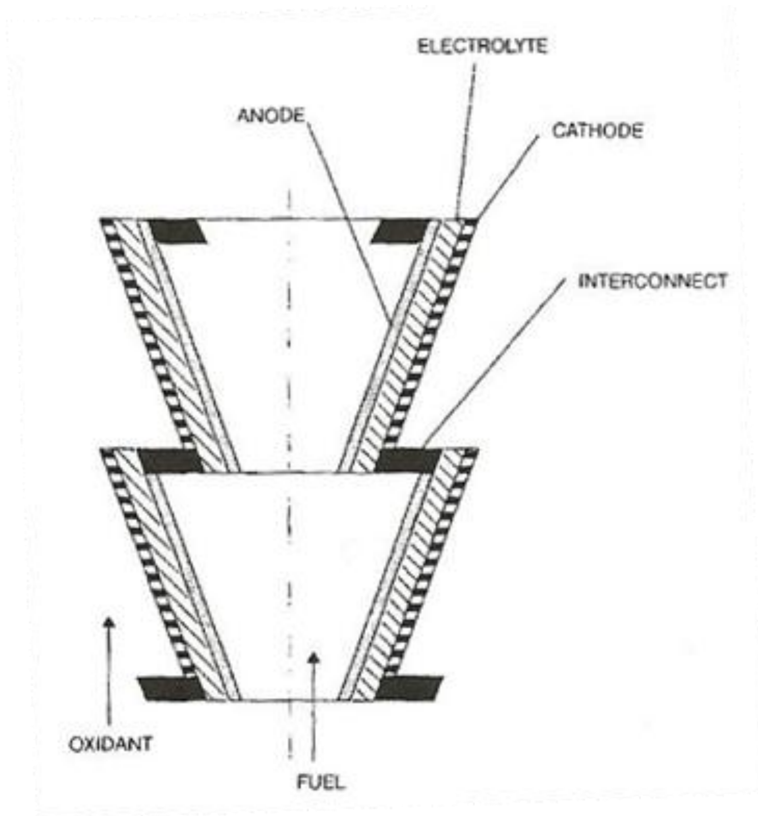

Figure 1.3 Segmented-cell-in-series solid-oxide fuel cell (bell-and-spigot design) [9]

This design was further developed by Brown Boveri in 1975 [10]. The company's segmented-in-series-bell-and-spigot design consisted of conical tubular cells fitted one into the next. The interconnect served both to seal the channels and electrically connect the cells in series. A stack with 120 cells achieved a total voltage of 110-120 V and a maximum power output of 0.115 kW. This corresponded to a 0.22 W/cm^2 power density at 1000^{o}C with H_2 and air as the reactants. However, this design was not appropriate for large scale use due to the relatively expensive manufacturing processes required to construct and assemble the many cells.

The banded segmented-cell-in-series tubular design (Figure 1.4) was a simplification of the bell-and-spigot design, and was developed by Rolls Royce and Mitsubishi Heavy Industries [11]. This design took advantage of thin-film processing techniques to apply banded layers of electrodes, electrolyte, and interconnect material on a porous ceramic support. These assemblies were stacked as rings with fuel flowing inside the porous support layer and oxidant flowing outside of the ring. This design suffers from the expense of vapor deposition techniques needed to apply to the components, as well as greater electrical losses than other cells due to a long current path [12].

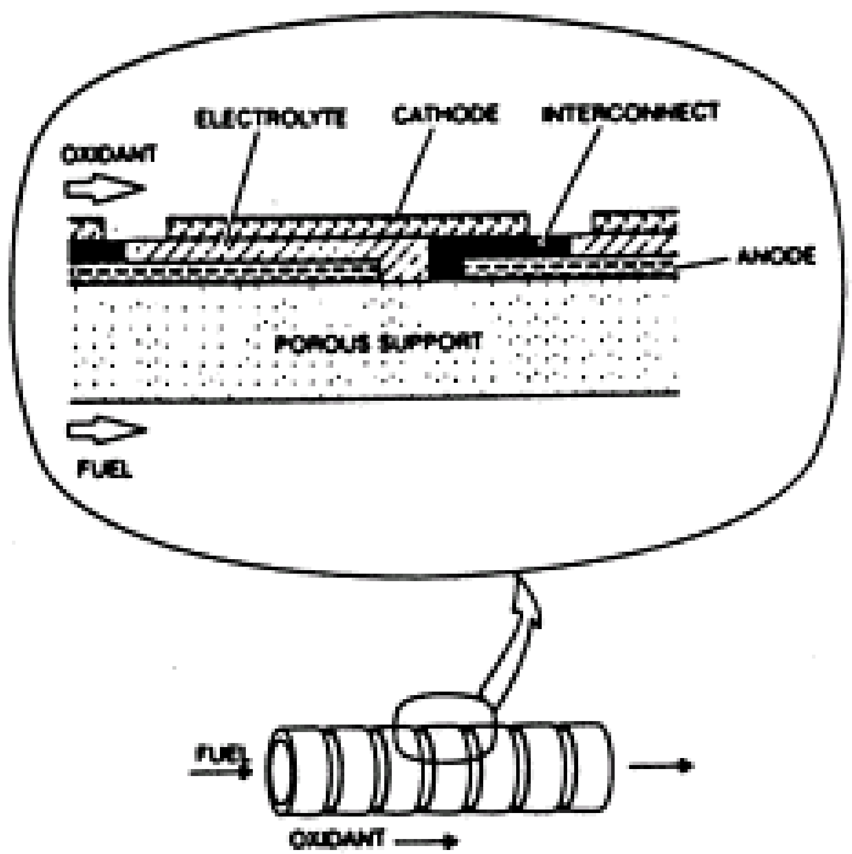

Figure 1.4 Segmented-cell-in-series SOFC design [8]

The non-segmented tubular design was first proposed in 1980 and is the most widespread of the tubular designs. From here on, this geometry will simply be referred to as tubular. The single biggest advantage of the tubular design is that it is sealless. With no seals, the electrical connections and current collection can be made in the anode chamber rather than the cathode chamber. Removing the connections from the oxygen rich environment eases the material requirements of the interconnects. The cells are bundled in pairs by nickel felts. The parallel bundles are connected in series.

Fabrication of these cells is comparatively inexpensive with the use of extrusion and spray techniques to manufacture most of the components. However, due to the stacking scheme and the high ohmic resistance of this concept, operating temperatures between 900^{o}C and 1000^{o}C are required to reach power densities of 0.2 W/cm^2 [10]. Other disadvantages include the long current path and mass transport limitations of gas diffusion through the length of the tubes.

The most advanced tubular SOFC development has occurred at Siemens Westinghouse Power Corporation (SWPC). The SWPC tubular cells for mass power generation are 1.8 m in length with an outer diameter of 22 mm. These cells are placed in 6 × 3 arrays to form stacks. In an effort to overcome the power density limitations of the tubular design, SWPC has modified the traditional tubular design by creating flattened tubes with internal ribs to shorten the current path within the cell. Both of these cell designs and a stack are shown in Figure 1.5. A similar design is under development at Kyocera [10, 12].

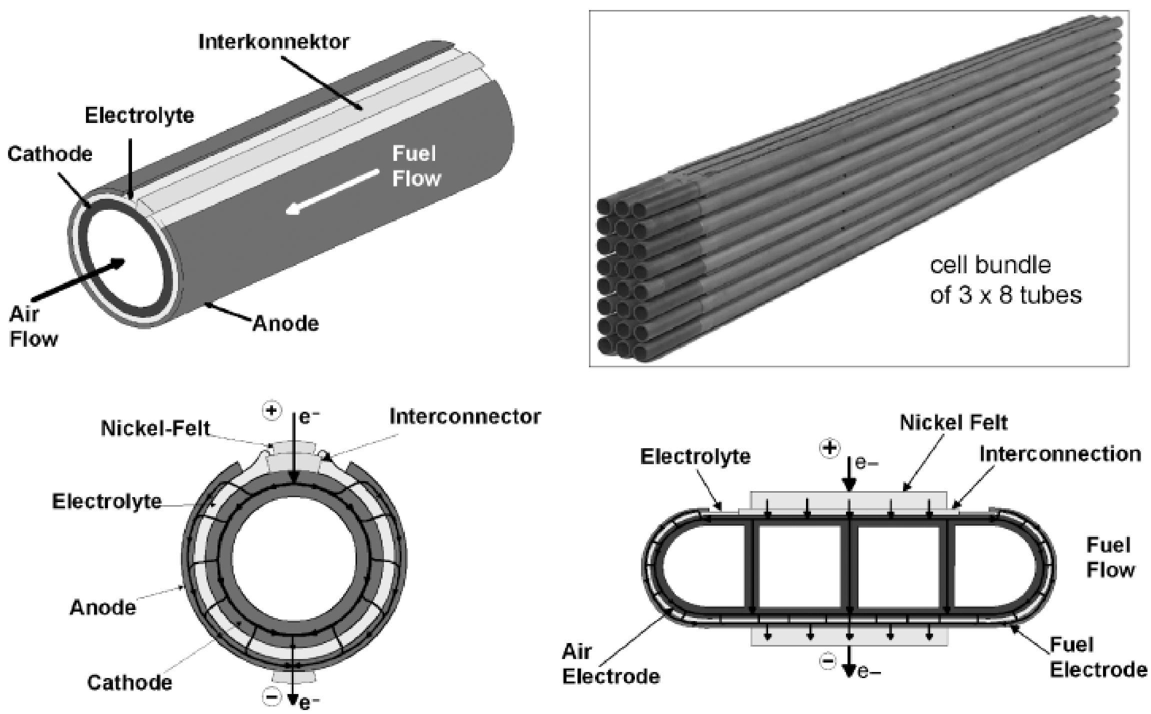

Figure 1.5 SWPC tube design, cell bundle and flattened tube [12]

The tubular design developed at Mitsubishi Heavy Industries (MHI) differs from the SWPC design in that it combines modern tubular cells with segmented technologies mentioned above. The MHI cell was shown schematically in Figure 1.4 above. It consists of 15 small cell segments deposed over a 41cm length of tube. Fuel is injected in the center of the tube rather than the air in SWPC cells. MHI has constructed a 1 kW module of 48 tubes [12].

The Japanese company TOTO is developing a tubular SOFC with less expensive manufacturing technologies. The TOTO tubes are shorter, at 0.5 m in length, and have an outer diameter of 16 mm. The company Acumentrics also has developed a relatively short tubular SOFC, with 45-cm length and an outer diameter of 15 mm [11, 12]. Recently, Acumentrics has formed a consortium to test and demonstrate its 1 kW tubular SOFC micro combined heat and power (mCHP) system [13]. The prototype of this technology indicates it will produce at 1 kW electric energy and 25 kW thermal energy [14]. The company has also recently performed an operational test of a 5 kW system in excess of 10,000 hours. This system is designed to provide stationary, auxiliary, and backup power for commercial, industrial, and military applications [15].

Planar SOFC

Presently, the planar or flat plate SOFC design has become the most widely investigated of the two SOFC classifications. Planar SOFC are viewed to have the most potential at delivering the least expensive SOFC unit. The development of planar SOFCs has increased with advancements of manufacturing technologies. With fewer defects in the ceramic electrolyte, the materials have become more resistive to mechanical and thermal stresses. Planar fuel cells are now a feasible technology. The SOFC industry is beginning to focus more on the flat geometries because of the ease of manufacture and the potential for greater power density.

SWPC in Germany developed and tested a 10 kW planar SOFC. A stack of 80 cell layers were mounted between bipolar plates where each layer contained 16 parallel cells. The stack would produce 5.4 kW at 950^{o}C and 4.1 kW at 850^{o}C. SWPC has discontinued research on planar fuel cells to focus on the tubular SOFC [8]. The Fraunhofer Gesellshaft department IKTS in Dresden has continued to develop this technology. The company's new 1 kW stack is predicted to have a lifetime of 40,000 hours and a system efficiency of over 80% [16].

Ceramic Fuel Cell Ltd. (CFCL) in Australia has developed a 5 kW planar SOFC stack containing 400 cells. Each cell contains a 10 cm × 10 cm × 100 μm YSZ electrolyte sheet connected with stainless steel interconnects. CFCL has tested single cells up to 2500 hours with good performance. Small stacks with power densities above 0.3 W/cm^2 have been operated. The company is presently completing its fifth generation pre-commercial unit for CHP applications [17].

Sulzer Hexis in Switzerland has developed a radial flow planar SOFC with a hybrid ceramic/metal stack and metallic interconnects. As seen in Figure 1.6, fuel is supplied to the center and air to the outer rim of circular cell plates where excess fuel is burned. A stack of up to 70 cells each 120 mm in diameter has delivered 1.1 kW at 950^{o}C [12]. Recently, Sulzer altered the design to a single-plate concept to reduce manufacturing costs. The company's Galileo 1000N SOFC heating units have been in field test in Europe since early 2007 [18].

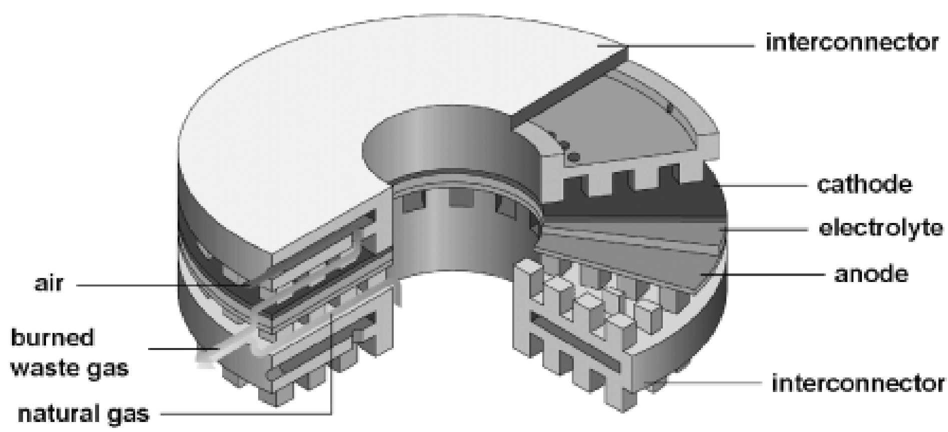

Figure 1.6 Sulzer Hexis cell and stack [12]

Forschungszen Jurlich was one of the first companies to develop an anode-supported planar fuel cell. Changing the support to the anode allowed the electrolyte thickness to be reduced to 5 to 10 μm. This stack has operated in co-flow and cross-flow arrangements. The cross-flow fuel cell has shown the most promise. A 40-layer stack has delivered 5.4 kW at 800°C using methane fuel that is internally reformed. A more recent 60-layer stack can deliver 11.9 kW at 800°C using internally reformed methane as fuel [12].

1.2.2 Efforts to Increase Performance of Planar SOFC

Since SOFC must see improved performance before DOE cost of power guidelines are met, much research has been undertaken to study the elements that affect power density in SOFCs. Improvements could result in lower material cost. Power density, $P = \frac{VI}{A}$ is a function of the potential of the cell, V, the current in the cell, I, and the area over which reactions can take place in the cell, A. The majority of research focuses on the three types of polarization that affect the potential of the cell. Activation polarization is the extra potential necessary to overcome the energy barrier of the rate-determining step of the reaction so that the electrode reaction occurs at the desired rate. Ohmic polarization is the loss that occurs due to resistance to flow of ions in the electrolyte and electrons through the electrode materials. Concentration polarization is the gas transport loss within the cell. Recently, there have been a few efforts to increase the active area of the fuel cell while not adversely affecting the total size of the fuel cell.

Chan *et al.* [19] completed a numerical model for solid oxide fuel cells that accounts for diffusion in low pore diameter materials. This report does not take into account concentration polarization on the macro scale. The model shows the cathode having a lower concentration polarization in both anode and electrolyte supported SOFCs. Chan, *et al.* concluded that the sensitivity of cell voltage due to change in element thickness was greatest for changes in the electrolyte and weakest for changes in the anode. Anode-supported fuel cells preformed better than cathode-supported cells, even under pressurized conditions at the cathode to compensate for cathode's greater concentration overpotential. This study did not attempt to optimize the reactant flows at the macro scale level.

Chan and Xia [20] completed a numerical study of the effects of activation, ohmic, and concentrations polarization on the overall polarization in solid oxide fuel cells based on the thermodynamic principles for the calculation of cell voltage. Their model shows the cathode has a lower activation polarization than the anode. They attribute this to the lower exchange current density of the cathode material. They further show that concentration polarization has a strong dependence on electrode thickness. In their work, Chan and Xia determined that electrode material-related factors (e.g. catalytic activity, reactions sites, etc.), which determine the magnitude of the exchange current density, are targets for improvement. Based on the Chan model, humidification plays an important role in minimizing anode concentration polarizations. They did not explain why this might be.

Bessler and Gewies [21] completed a series of studies on gas concentration impedance of solid oxide fuel cell anodes. The first part of the study showed that gas transportation has a strong influence on cell impedance in button cells. The second part of the study was a 1-dimensional numerical study of gas transport in a reactive anode without thickness to negate porous gas transport processes. This study concluded that gas concentration resistance significantly contributes to a cell's overall polarization resistance and that the concentration resistance depends on operational parameters such as gas concentration, temperature, and polarization.

Lin *et al*. [22] completed a numerical study of the effect that interconnect rib width has on concentration polarization. This study is based on the understanding that, while wide ribs may reduce the electrical resistance in the interface of the cell and reduce the current path in the electrode material, they also cover a large fraction of fuel cell area, and the chemical species do not diffuse easily underneath wide ribs. The study showed that when the rib width is small compared with the characteristic penetration distance of the reactants, the gas concentration is uniform. The study also showed that the optimal rib design characterized by the ratio of rib width to channel width is strongly affected by electrical resistance. If the rib has high electrical resistance, the larger the rib width fraction should be. In reasonable fuel cell applications this fraction should be between 1/3 and 2/3 of the channel width.

Li *et al*. [23] conducted work analyzing the current collection process in solid oxide fuel cells and worked to optimize gas delivery and current collection to obtain higher power densities for solid oxide fuel cells. This optimization is a matter of maximizing the area over which the electrochemical reaction can occur while minimizing the distance the current from the reaction has to travel through thin electrode layers before it can be collected. In Li's design, wide flow channels with distributed cylindrical current collectors replace the traditional series of narrow rectangular channels and collectors. This design has the potential to increase mixing within the gas delivery field and can decrease the amount of fuel cell area covered by current collectors, while limiting the current path to a collector site. The power density of their system underwent nearly a 100% increase between the lowest and highest reported values in their optimization. Li noted the sensitivity of the ideal geometric ratio of current collectors to concentration polarization but did not look at the sensitivity the concentration polarization to current collector array design.

Inspired by the work of Li *et al*., Ji *et al.* [24] created a model to investigate scaling effects, particularly miniaturization, on the performance of SOFC. The work consisted of a parametric study evaluating channel scale effects on temperature, species concentration, local current density, and power density of a thin film SOFC cell. The work showed that lowering the height of the flow channels in narrow channels can lower the average solid temperature and improve cell efficiency. This is due to a higher heat/mass transfer coefficient between the channel wall and the flow stream and a shortened current path. SOFCs with thin-film electrolytes can operate at lower temperatures with high performance; however, the miniaturized technology is more susceptible to thermal stresses.

Hasan *et al*. [25] completed a 2-dimensional computational study of the effects of fuel cell size scale on electric potential and convective flux within solid oxide fuel cells. This work also included a study of the effect of placing rectangular protrusions to increase the surface area of electrodes in the fuel cell. The research indicated that higher concentrations of oxygen and fuel in the cell results in higher performance. Overall, the larger dimensional fuel cell performed the best in terms of convective flux, diffusive flux, and power output. The case with the rectangular protrusions in the electrodes showed improvement over the plane channel case. This result seems to counter the previous research on the effect of electrode thickness on fuel cell potential and is likely due to the model allowing electrochemical reactions in the entire electrode volume rather than only at the triple phase boundary between the electrolyte and electrodes. Even so, these results suggest that increasing the reaction area and the convective flux can greatly increase the performance of a fuel cell.

Mono-block-layer SOFC

The monolithic, or mono-block-layer (MOLB), SOFC is an innovative adaptation of the traditional SOFC designs in an attempt to improve fuel cell performance. This design takes advantage of increasing reactive area while maintaining the volume of a traditional planar cell. The MOLB design was first proposed by Argonne National Laboratory in 1984. The goal of this design was high power density though increasing the size of the active area. Taking advantage of the moldable ceramic structure, the active electrode-electrolyte assembly was formed in a corrugated shape (Figure 1.7). The anode and cathode created the flow channels for the fuel and air. This simplifies the design of the interconnects, and plane ceramic plates can be used. The power density of the monolithic was calculated to be 4 kW/l [26].

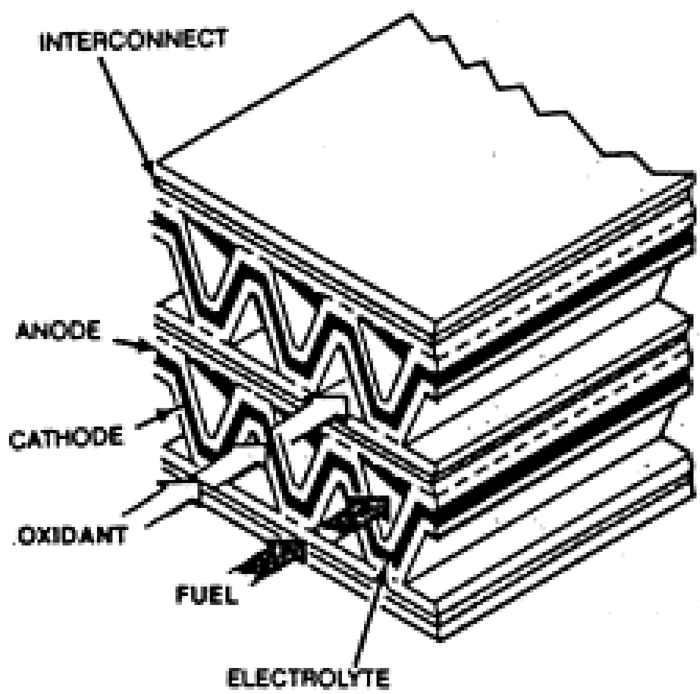

Figure 1.7 Monolithic SOFC schematic [8]

Further development of this design was completed by Chubu Electric Power Company (CEPCO) and Mitsubushi Heavy Industry (MHI) where a 5 kW SOFC was successfully tested. CEPCO and MHI have developed a 5 kW planar SOFC. The cells are supported by the electrode/electrolyte assembly which is corrugated to create gas flow channels. In tests, the stacks have achieved a power density of 0.22 W/cm^2 with a 38% fuel utilization [8]. The largest stack of this type contained 40 cells. This stack generated 2.5 kW at 1000^{o}C [12]. Development of this design has been slow since the intricacies of the electrode assembly compounds, the fabrication issues, and material issues inherent in SOFCs [11, 12].

Siemens Westinghouse has recently developed Delta8, an alternate version of their tubular SOFC, creating a monolithic geometry tube fuel cell. Figure 1.8 depicts the triangular tube geometry. The fuel cell assembly includes a centered air delivery tube. The tubes are stacked like planar cells. Fuel flows in the spaces between the electrode assembly tubes and the bottom of the tube stacked above it [27]. Siemens has operated a stack of 24 Delta8 cells, in four bundles of six cells each achieving a 14 kW rating at maximum power [28].

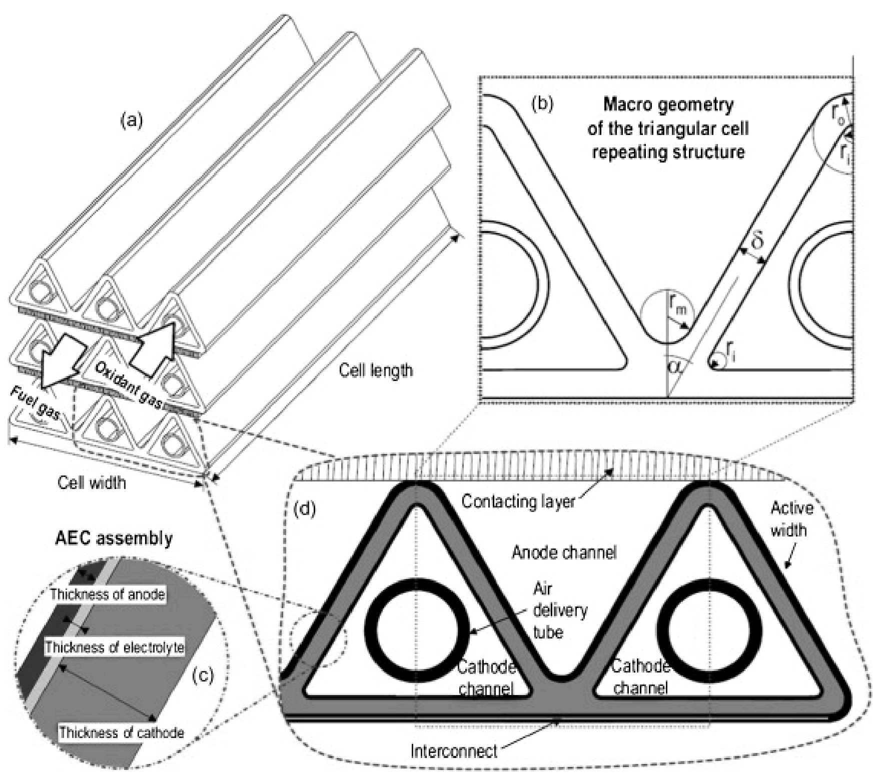

Figure 1.8 Siemens Westinghouse Delta8 triangular tube cell geometry [27]

Hwang *et al.* [29] created a numerical model to simulate transport phenomena in MOLB-type SOFCs. The MOLB fuel cell studied was anode-supported and had a 0.2 mm thick electrolyte and processed hydrocarbon fuel. In their model, the oxygen mass fraction had a local minimum in the channel corner due to low convection. The mass fraction was also minimized where the cathode met the current collection plate where the oxygen is transported by diffusion. Parallel phenomenon occurred with the fuel side of the cell. The current density in MOLB fuel cells is interesting. Each incline plane of the electrode assembly shows increasing current density towards the cathode side current collector. This is due to the direction of current flow. The long current paths within the cell, however, could create a greater ohmic polarization within the cell.

Hwang *et al.* [30] used the model in a separate work make comparisons of fluid flow, concentration, and electric fields in a planar SOFC and a MOLB-type SOFC. Comparing the species concentration between the two systems, the planar system shows an oxygen concentration gradient across the channel with a minimum concentration under the interconnectors where fresh air cannot access easily. Hydrogen concentration is uniform across the flow channel but decreases along the length of the channel. In the MOLB cell, oxygen concentration is lowest along the plateau where the cathode contacts the interconnect. Hydrogen has a noticeable concentration gradient across the flow channel. The flow has concentration minimums in areas with increased diffusion: where the anode meets the interconnect and in the corners of the electrode where it approaches the cathode-side interconnect. The MOLB cell has a lower mean concentration of H_2/O_2 indicating a higher level of fuel/oxidant utilization in the cell. This higher utilization is reflected in the increased current density of the cell over the planar SOFC. However, the paths that the current must travel are shown to be longer in the MOLB-type fuel cell.

Hwang [31] made further use of the model to compare anode- and cathode-supported MOLB-type SOFC. This comparison showed similar concentration gradient results as were previously discussed. However, the anode-supported SOFC showed higher current density, by about 5%, when compared to the cathode-supported SOFC.

Yang *et al*. [32] created a simulation of MOLB-type SOFCs to compare the temperature distributions, species concentrations, and current densities in co-flow and counter-flow cell designs. The study indicated that a co-flow case has a more uniform temperature distribution and a smaller temperature difference from inlet to outlet. Current density distributions are also more uniform in a co-flow case. In qualitative comparisons to planar SOFC designs, the average temperatures in MOLB-type SOFC are higher than planar but the temperature difference is lower. This is attributed to the increase in hydrogen consumed in the larger active areas resulting in a greater amount of accumulated reaction heat. Current densities in the MOLB-type SOFC are also higher than planar but the distributions are less uniform which is a disadvantage to MOLB systems.

Yang *et al*. [33] quantified the MOLB-type SOFC comparison with planar SOFC in a further computational study. This study looked at the effects of operating conditions on the temperature and species distribution in the fuel cell designs. In the co-flow test case, the planar SOFC had an average temperature of 979^{o}C and a 137^{o}C drop along the cell while the MOLB-type SOFC had an average temperature of 1014^{o}C and a 76^{o}C drop along the cell. In the counter-flow test case, the planar SOFC had an average temperature of 996^{o}C and a 165^{o}C drop along the cell while the MOLB-type SOFC had an average temperature of 1014^{o}C and a 76^{o}C drop along the cell. The MOLB temperature is suspect in the counter-flow cases based on the previous study and is likely a typographical error in the journal paper. The study also concluded that the increase of fuel concentration in the cell increases the temperature of the cell due to the increased reactions at the electrolyte. However, the temperature of the planar SOFC was more sensitive to changes in fuel concentration. This indicates that MOLB-type fuel cells are more appropriate for used in stack designs that call for elevated fuel flow rates in conjunction with exhaust afterburners.

Non-Industry Designs

Other SOFC designs have been proposed outside of industry. These designs have largely been created on a small scale and are inhibited by complex manufacturing processes.

Ramakrishna *et al.* [34] have proposed an alternate method to enhance power density within a SOFC. In the design shown in Figure 1.9, a thin wall splits the inlet section of the cell and allows fresh reactants to enter the flow channel halfway along its length. This design increases the performance of the cell. The maximum power density in the cell with the thin wall was 1.18 W/cm^2 at an efficiency of 60% compared to a 0.88 W/cm^2 and an efficiency of 50% in the plane geometry. However, the local current density of the adjusted cell has a local minimum just before the addition of the fresh fluid. The higher current density is attributed to elevated pressure in the adjusted fuel cell. The local minimum of the current density is attributed to the decrease in species concentration before the addition of the fresh fluid. The increase in pressure and the large current density gradients will be obstacles for this technology.

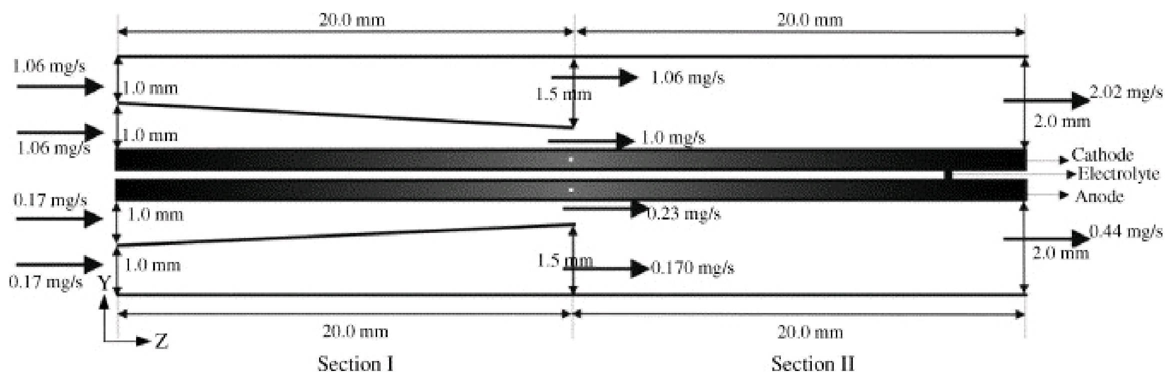

Figure 1.9 Split flow channel design to increase SOFC performance [34]

Another SOFC design that has recently been developed is based on a honeycomb geometry. The honeycomb fuel cell geometry adapts well to miniaturization which is the leading approach to reduce operating temperatures, size, and hasten start-up and shut-down operations. The miniaturization is possible due to the honeycomb's structural advantages, such as the ability to have large electrode area per unit volume and design freedom. In the cathode supported honeycomb shown in Figure 1.10, the electrolyte and anode layers can be prepared as thin films on the channel surface. All of the channels are the fuel channels and the body is used to supply the oxidant. Under humidified hydrogen flow, volumetric power density above 2 and 3 W/cm^3 at 0.7 V were exhibited at 700 and 750^{o}C, respectively [35].

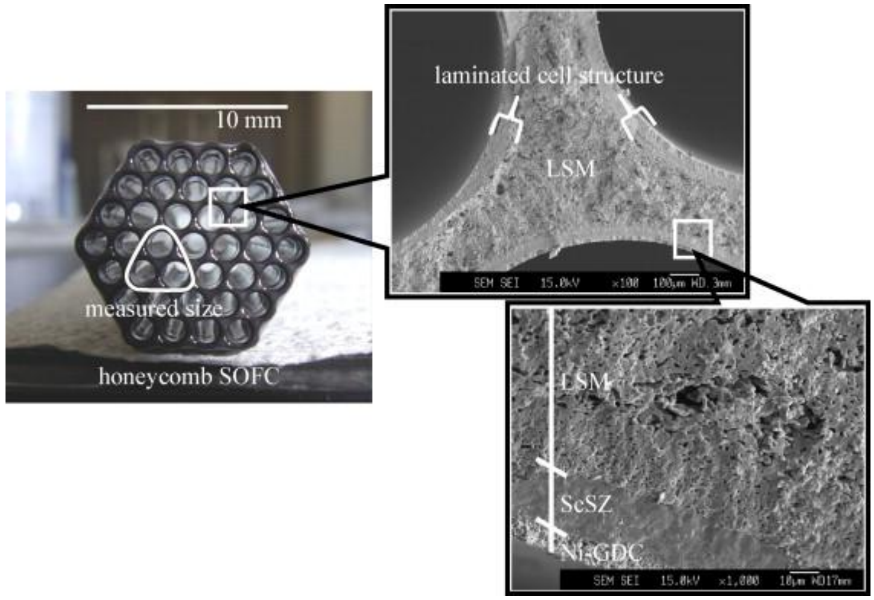

Figure 1.10 Micro-structure of the honeycomb SOFC [35]

1.2.3 Mixing and Enhanced Heat Transfer

Few studies have investigated improving SOFCs based on hydrodynamic performance of reactant flows; that is, by enhancing mixing of a flow near the surfact, reaction rates should be increased. In heat transfer applications, the use of enhanced heat transfer techniques is to optimize fluid/surface interfaces for increased transport of heat and mass. Generally, the objectives of the use of enhanced heat transfer are: to reduce the size of a heat/mass transfer system, to increase heat/mass exchange within a system, or to reduce the pumping power of a system with a fixed heat duty. As mentioned above, SOFCs need cost and reliability improvements, so application of the first two enhanced heat transfer objectives might also be appropriate to SOFCs.. In passive enhancement devices, three basic methods are employed to increase heat transfer: increasing the heat transfer coefficient, *h*, without appreciable transfer area increase, increase transfer area without appreciably increasing *h*, or increase both *h* and transfer area [36].

These types of enhancements can be applied fuel cells to try to counteract the concentration polarization loss, which is one of the major losses within a SOFC. Concentration related losses in the cell can be thought of in two ways: the direct losses at the electrolyte interface due to the speed at which species are consumed and supplied to the reaction, and the dilution of the species concentration in the flow near the reaction wall due to consumption or addition of product species. Macro-scale concentration loss was partially addressed by Ramakrishna *et al.* [34] in the split channel design. The design made use of the first type of passive enhancement device listed above, where the heat transfer coefficient was altered but the transfer surface area remained constant. The design proposed a method in supplying fresh reactant flows to the center of the fuel cell, but it did not address the issue of concentration gradient boundary layer that develops across the electrolyte/electrode surface along the length of the cell. The concentration boundary layer is similar to fluid and thermal boundary layers in that it is the area of flow near the surface that does not have the same properties as the bulk flow. In heat transfer and fluid flow, mixing mechanisms are often used to minimize the effects of boundary layers. Studying mixing efforts in heat transfer and fluid flows gives insight to methods to address concentration boundary layers as well.

High Reynolds Number Flows

The majority of research on mixing mechanisms has been done in the turbulent flow regime. In internal flows, like those in fuel cells, the transition to turbulent flow occurs at Reynolds numbers between 2000 and 4000. Flows at these rates are not applicable to fuel cells, but the research gives insights to the available technology in the field.

Han *et al.* [37] investigated the effects of small ribs placed on a wall surface perpendicular to flow direction with varied rib shape, angle of attack, and pitch-to-height ratio on friction factors and heat transfer in parallel plate experiments for Reynolds numbers from 3000 to 30,000. The study showed that rib symmetry had no effect on heat transfer. The shape of the ribs, however, affected the friction factor and only mildly affected the heat transfer. The study concluded that the most efficient rib arrangement with respect to heat transfer verses friction power were ribs with a 45^{o} angle of attack.

Murata and Mochizuki [38] numerically simulated heat transfer in rib-roughened ducts at Reynolds numbers of 50 (laminar flow) and 350 (turbulent flow). The rib angles in the study were 60^{o} and 90^{o}. In the laminar 90^{o} case, there did not appear to be any reattachment of the flow after the ribs. The absent reattachment resulted in no ideal heat transfer enhancement. The laminar 60^o case induced secondary flow. The turbulent 90^o case produced high heat transfer around the ribs. The turbulent 60^o case also observes elevated heat transfer around the rib, but the highest heat transfer area shifted towards the wall because of the more intense reattachment at that point.

Tatsumi *et al.* [39] numerically simulated heat transfer and fluid characteristics in a duct with rib turbulators. They studied perpendicular ribs that extended across the channel, as well as discrete ribs that did not. The Reynolds number of the flow was chosen to be 30,000. At this high of Reynolds number, the flow in the duct was highly three-dimensional for both ribbed cases. For the discrete rib case, the flows created counter-rotating large-scale vortices which enhanced flow mixing above that of the full ribbed channel.

Gao and Sundén [40] completed a study of thermal and hydraulic performance of rib-roughened rectangular ducts for Reynolds numbers from 1000 to 6000. The rib geometries included: parallel ribs and V-shaped ribs pointing upstream and downstream of the flow direction. For each case the hydraulic diameter ratio was 0.06, the attack angle was 60^o, and the relative roughness ratio was 10. The temperature distribution in the length of the flow showed a sawtooth trend attributed to flow reattachment. The Nusselt number was greatest for the downstream V-shaped ribs followed by the upstream V-shape and the parallel ribs. The friction factor was the greatest for the V-shaped ribs and marginally lower for the parallel ribs.

Gao and Sundén [41] followed their study with a optical visualization study of flow characteristics in ducts with 60^o angled, crossed, and V-shaped ribs. These tests were carried out at a Reynolds number of 5800. The few tests operated at a Reynolds number of 1000 showed no obvious local maximum to indicate flow reattachment. The flow adjacent to the ribs was observed to flow from the upstream end of the ribs to the downstream end supporting the enhanced flow mixing at the wall seen in Tatsumi *et al*. above. In the V-shaped ribbed cases, the V-shapes pointing downstream lead to a higher heat transfer enhancement than the upstream-pointing ribs.

Tanda [42] also performed a study of transverse and V-shaped broken ribs in rectangular channels. The ribs in this study had rectangular cross-sections in transverse arrays or in V-shapes with an angle of 45^o or 60^o relative to the flow direction. The

Reynolds number in these experiments ranged from 5000 to 50,000. The study found that broken ribs resulted in high heat transfer coefficients due to the high turbulence levels cause by tip-endwall interactions. The transverse ribs with relative roughness pitch of 4 and 8 resulted in the higher heat transfer enhancement. However, these rib designs also resulted in the highest friction factors. When pressure drop was considered, the transverse broken ribs at relative roughness pitch of 4 and 13.3 resulted in the best thermal performance.

Nagano *et al.* [43] numerically simulated heat transfer in turbulent channel flows with transverse-rib roughness. The study found that in turbulent flows with angled ribs the velocity and temperature are asymmetric. The study also found that the flow behind tall ribs can be stagnant; however, low ribs are likely to produce vortices. Rib height directly influenced turbulent mixing enhancement; however, rib height can also adversely influence laminar flows where laminar shear layers and flow stagnation are an issue. The study also determined that keeping the ribs short can keep the mixing near the wall, decreasing the amount of drag in the channel and increasing heat transfer performance.

Layek *et al.* [44] conducted an experimental investigation on heat transfer and turbulent fluid flow in a duct with transverse chamfered rib-groove roughness. The relative roughness pitchs in these experiments were in the range 4.5 to 10. The maximum heat transfer enhancement in these tests occurred at a relative roughness pitch of 6 and a relative groove position of 0.4. The highest Nusselt number occurred for the case with the rib angled 18^{o} to the channel axis. This was attributed to the balance of deflecting streamlines of flow towards the heat transfer surface to create early reattachment and keeping the flow attached to the top surface of the ribs. The friction factor increased with chamfer angle in this roughness design. As the chamfer angle increases, the deflection of the streamlines increased creating more friction.

Mixing in Low Reynolds Number Flows

The flows in SOFC are well within the laminar region, so it is important to look at ways roughness induced mixing is applied in fields where there is laminar flow. In the solar air heaters industry, heat transfer is important, and the fluid flow rates are low. To attain higher heat transfer coefficients in solar heaters, it is desirable for there to be turbulence at the heating surface, but the fan or blower required may require an excessive amount of energy. For this reason, the solar heater industry has focused on creating turbulence only in the region very close to the heating surface. The goal for roughness elements in solar heaters is to keep the height of the element small in comparison with the duct dimension. The key parameters that characterize the roughness in heaters are roughness element height and pitch.

Focke [45] studied the mechanism of transfer enhancement by eddy promoters. He determined that the diffusion in laminar flows depended on promoter spacing. He reports that when turbulence promoters cause gradual constriction and expansion of the flow channel, no separation occurred at low flow rates. However, separation did occur at higher flow rates, even in the laminar regime. A free shear layer developed and separated the bulk flow from a recirculating region. The heat transfer at the wall across the laminar shear layer was greater than if there were no rib; however, there was a substantial increase in the local transfer in the reattachment region.

Olsson and Sundén [46] investigated flow and heat transfer in rib-roughened rectangular channels. The rib geometries studied included: cross ribs, parallel ribs, cross V-ribs, parallel V-ribs, and multiple V-ribs (swirl flow). Heat transfer and pressure drop data were analyzed over a range of Reynolds number from 500 to 15000. The study showed that at low Reynolds numbers, the friction factor in rib-roughened ducts was only slightly greater than a smooth channel. The heat transfer coefficient was the greatest for the parallel, upstream-facing V-shaped ribs, with the other designs closely grouped. The swirl flow tube showed the most promising heat transfer ability over the entire range of Reynolds numbers. The other geometries presented marginal improvement over the smooth channel at low Re.

Kilcaslan and Sarac [47] completed a study that compared flow channels with cylindrical or triangular shaped roughness with smooth channel flow for flows with Reynolds numbers from 250 to 7000. The rib geometries were kept at a fixed relative roughness pitch of 6.67. The wall temperature was held constant at 50^{o}C. According to the study, the maximum heat transfer occurred with cylindrical ribs, while triangular rib heat transfer was only slightly lower and smooth channel was much lower still. The study also showed that the pressure drop observed in the channels was slightly higher in the triangular ribbed channel when compared with the cylindrical rib. The Nusselt number was slightly higher for the cylindrical ribbed channel than in the triangular ribbed channel.

1.3 Conclusions and Summary of Literature Review

The literature shows that commercial fuel cells do not presently meet the government cost and performance goals for automotive and distributive energy applications. Tubular SOFC have been highly developed in industry. The technology is able to withstand the material expansion issues that stunt SOFC development; however, the technology involves costly manufacturing processes and has low potential for high power density base on its stacking scheme. Planar fuel cells have simpler manufacturing processes and greater potential for power density. The literature also shows increasing durability of the planar design in industry. From this review it is apparent that while tubular SOFCs have a stronger industrial base, planar SOFCs have the most potential at delivering the lower costs required for commercialization. For this reason, the following study focuses on SOFCs with planar geometry.

To optimize SOFC performance and thermal gradients, past work has focused on fuel cell material development, but fuel cells remain present commercially unviable, leaving in doubt the effectiveness of proceeding solely down this research avenue. The process of developing and testing new materials is expensive and can increase the cost of materials in a field where material cost need to decrease. Using numerical models to study these materials decreases the cost of material R&D, but the literature has shown that the field must look at the wider picture. Conclusions from literature do show the importance of design choices to SOFC performance, such as:

- Increasing power density can decrease the cost, particularly material and operational costs.
- Gas concentration resistance significantly contributes to a cell's overall polarization resistance, and concentration resistance depends on operational parameters such as gas concentration, temperature, and polarization.

- An optimal design is one which can minimize both the area of the electrolyte obstructed by interconnects and the distance the current from the reaction has to travel before it can be collected.
- Decreasing the height of the flow channel can effectively increase the heat/mass transfer within a flow channel.
- Textured electrodes can increase power density by increasing the active area of the electrolyte, as seen in the MOLB design.
- Increasing fresh reactant flow to the electrode/electrolyte assembly can increase power density and efficiency, as seen in the split channel model.

Mixing created by enhanced heat transfer devices can address some of these design choices. However, limited work has focused on improving SOFCs based on increasing the hydrodynamic and thermal performance of the reactant flows. The enhance heat/mass transfer literature has shown that:

- Enhanced heat transfer techniques can be used to increase transport and transfer area within channels.
- Rib design must be optimized:
    - flow behind tall ribs in laminar cases can lead to stagnation rather than enhancement.
    - gradual constriction and expansion can result in no separation at low flow rates.
- Short ribs keep mixing near the wall and decrease the pressure drop.

The use of enhanced heat transfer techniques which increase both the transfer and transfer area within a fuel cell could benefit the cell in two ways: increasing the convection coefficient would lead to lower concentration gradients while increased surface area would lead to additional reaction sites. This concept applied to a planar SOFC could produce a fuel cell that addresses the issues facing electrochemical, hydrodynamic, and thermal performance of SOFCs. Hence, the addition of mixing mechanisms within the flow channel of a fuel cell could increase the mass transport properties of the cell and, subsequently, increase the performance of the cells.

1.4 Objectives and Approach

Based on the findings of the literature survey, the objectives of the current research are summarized below:

1. Determine if mixing can be enhanced in channels with low Re flow.
2. Determine if the use of mixing enhancement techniques can improve the performance of SOFCs.

A fuel cell add-on module will be incorporated into the commercial CFD software, FLUENT and a planar SOFC fuel cell model developed. This model will be validated against numerical and experimental data in literature.

Models of air and fuel flow channels will be constructed and operated under conditions simulating the flow in a planar SOFC. These channels will then be adapted to study various shaped ribs at varied spacing. After the effect of channel ribs on hydrodynamic mixing has been investigated, the optimal rib spacing and designs will be applied to a full channel model of a SOFC.

Structured grids will be used to create meshes for smooth channeled, ribbed channeled, and corrugated channeled SOFCs. Upon the validation of the FLUENT model of a smooth channeled SOFC, various fin shapes will be explored. Key hydrodynamic, heat transfer, and electrochemical parameters will be investigated.

2. Model Description

To numerically model SOFCs, it is necessary to translate the physical processes within a fuel cell into mathematical concepts. To do this, we must first understand the physical operation of the fuel cell. Then we must determine and understand the laws that describe these processes of operations. These equations that govern the flow, thermal, chemical, and electrochemical systems are intrinsically coupled and can then be used to further understand and analyze the operation of a fuel cell.

The basic components of a general SOFC are two porous electrodes and a solid electrolyte. The basic components and workings of a planar SOFC are found in Figure 2.1. Oxygen flows in the cathode and diffuses through the porous electrode until it reaches the electrolyte. The oxygen molecules absorb electrons from the external electrical circuit and ionize at the junction of reactant, electrolyte, and electrode, called the triple phase boundary (TPB). The oxygen ions conduct through the electrolyte towards the anode. Meanwhile, fuel has been fed to the anode and has diffused to the TPB on the anode side of the cell. The fuel molecules are oxidized by the oxygen ions from the electrolyte. Each oxygen ion combines with a hydrogen molecule and releases the two electrons that it carried across the electrolyte. The electrons are collected in the interconnect, or current collector, and are removed to the external circuit. The electrons are able to move through the external circuit from one side of the fuel cell to the other because of the potential difference, or voltage, that exists between anode and cathode which is the result of excess electrons at the anode and limited electrons at the cathode. To achieve equilibrium, electrons pass through the external circuit from anode to cathode generating current. These electrons react with oxygen, as mentioned, thus sustaining the process. The electrochemical processes are described in more detail below.

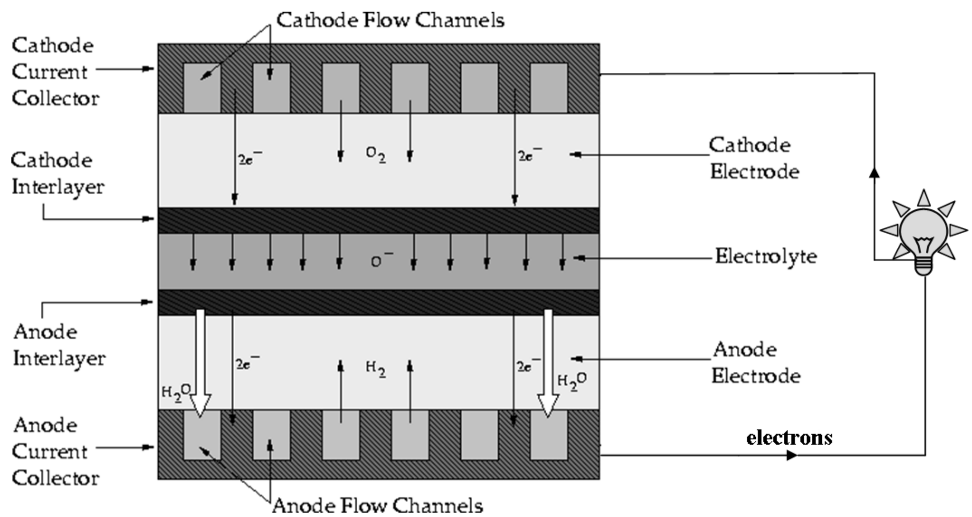

Figure 2.1 Planar SOFC operation

2.1 Electrochemical Modeling

At a basic level, SOFCs are electrochemical reactors that convert chemical energy to electrical energy. In fuel cells operating on hydrogen and air, the general equation for this reaction is:

$$H_2 + \frac{1}{2}O_2 \rightarrow H_2O + \text{heat} \tag{2.1}$$

However, this reaction does not occur directly. The oxygen takes four electrons from the external circuit and is reduced at the cathode in the reaction:

$$O_2 + 4e^- \rightarrow 2O^{2-} \tag{2.2}$$

The two oxygen ions conduct through the electrolyte and combine with hydrogen at the anode to form water in the reaction:

$$H_2 + O^{2-} \rightarrow H_2O + 2e^- \tag{2.3}$$

The water enters the flow stream and is removed from the fuel cell while the electrons are transported through the external circuit back to the cathode side of the cell.

The current produced by the fuel cell is related to the rate of consumption of fuel within the cell. The general expression for this current is:

$$I = \frac{zF}{M}\dot{m} \tag{2.4}$$

where z is the stoichiometric number of moles of electrons per mole of reactant ($z = 2$ when hydrogen is considered and $z = 4$ when oxygen is considered), F is the Faraday constant, M is the molar weight of the fuel, and $\dot{m}$ is the mass consumption rate of the reactant. The electrical power produced by the fuel cell can then be given by:

$$P = VI \tag{2.5}$$

where V is the voltage, or electrical potential difference, produced by the cell.

The ideal voltage this circuit can attain is called the Nernst potential. This is also called the open circuit voltage (OCV). In the ideal voltage, all the available energy in the reacting fuel is transformed into useful electrical power. This potential is expressed by the Nernst equation which is written:

$$V_{ideal} = -\frac{\Delta G^o}{zF} + \frac{RT}{zF}\ln\left(\frac{P_{\mathrm{H_2}} P_{\mathrm{O_2}}^{1/2}}{P_{\mathrm{H_2O}}}\right) \tag{2.6}$$

where ΔG^o is the Gibbs energy, R is the gas constant, and $P_{\mathrm{H_2}}, P_{\mathrm{O_2}}$, and $P_{\mathrm{H_2O}}$ are the partial pressures of the chemical species.

2.1.1 Polarization Losses

The operational voltage of a SOFC is decreased from its OCV because of irreversible losses. These losses are often called polarization, overpotential, or overvoltage and are reported in a fuel cell's polarization curve, shown in Figure 2.2. Multiple phenomena contribute to polarization in a fuel cell. Three main sources of these losses are activation polarization, ohmic polarization, and concentration polarization.

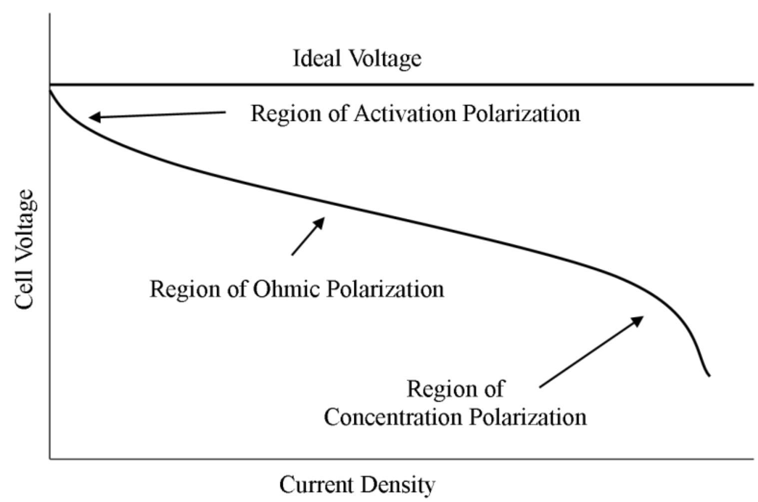

Figure 2.2 Ideal and actual fuel cell voltage/current characteristic polarization curve

Activation polarization

Activation polarization is the loss that results from the energy barrier that must be overcome for the electrochemical reaction to occur. The activation energy barrier is overcome by a sufficiently high temperature of reaction or by the use of extra electrical potential such that the electrode reaction proceeds at the desired rate. This voltage required is the activation polarization. The activation polarization is largest at low current densities but is less significant at higher current densities. Activation polarization occurs at both electrode/electrolyte interfaces in SOFCs. But the cathode side generally has a lower exchange current density, than the anode side; that is, the current density for the forward and reverse reaction to proceed is lower for the cathode at equilibrium. This will result in greater activation losses on the cathode side of the cell.

The Tafel equation often used to approximate the resulting voltage drop, ϕ_{act}:

$$\phi_{\text{act}} = \frac{RT}{\alpha zF}\ln\left(\frac{j}{j_0}\right) \tag{2.7}$$

where α is the electron transfer coefficient of the reaction at the electrode being addressed, j is the current density, and j_0 is the exchange current density of the electrode. This equation is most applicable for fuel cells where activation losses are high as is the case in low- and medium-temperature fuel cells.

In reality, the losses are the result of complex surface electrochemical reaction steps, and the rate parameters and activation energy of one or more rate-limiting reaction steps controls the voltage drop under specific conditions. The high temperatures of a SOFC result in higher reaction rates and lower activation energy of reactions, which results in a less significant activation polarization. Because of the decreased activation requirements, the Tafel equation is not a good approximation for activation. Instead, the losses in SOFCs are determined by solving the Butler-Volmer equation for the activation polarization. The Butler-Volmer equation relates the activation polarization and the rate of reaction as:

$$j = j_0\left[\exp\left(\frac{\alpha zF\phi_{\text{act}}}{RT}\right) - \exp\left(-\frac{(1-\alpha)\,zF\phi_{\text{act}}}{RT}\right)\right] \tag{2.8}$$

where j is the net current density and j_0 is the exchange current density or the current densities for the forward and reverse reaction at equilibrium; α is the electron transfer coefficient which is an additional kinetic parameter and represents how an applied potential favors one direction of reaction over the other or the change in the electrical potential across the reaction interface changes the sizes of the forward versus the reverse activation barrier. Equation (2.8) shows the general form of the Butler-Volmer equation; however, the equation is solved for the activation polarization, ϕ_{act}.

Ohmic polarization

Ohmic polarization is caused by the transport resistance of ions in the electrolyte and the transport resistance of electrons though the electrodes. Both ions in the electrolyte and electrons in the electrodes obey Ohm's law. This allows the ohmic polarization, ϕ_{ohmic}, to be written as the simple relation:

$$\phi_{\mathrm{ohmic}} = IR \tag{2.9}$$

where I is the current flowing though the cell, and R is the total cell resistance. The cell resistance includes electronic, ionic, and contact resistances:

$$R = R_{\mathrm{electronic}} + R_{\mathrm{ionic}} + R_{\mathrm{contact}} \tag{2.10}$$

Any of these components can dominate the ohmic resistance, depending on the cell type. Often, the ionic resistance dominates in planar SOFC. But in thin-electrolyte cells, contact resistance can dominate. Three general methods of reducing this polarization are: use of high conductivity electrodes, use of appropriate interconnect design and materials, and use of thin electrolytes.

Concentration Polarization

Concentration polarization is the voltage loss due to reductions of reactant gas concentration that cause reductions in the partial pressures of the reactant. As a reactant is consumed at the electrode by electrochemical reaction, it is often diluted by the products of the reaction. Finite mass transport rates limit supply of fresh reactant to and the evacuation of products from the electrodes. In SOFCs, gas diffusion controls mass transfer. Fick's first law of diffusion is often used to describe the effect of the rate of mass transport to an electrode surface on current production:

$$I = \frac{zFD\ \ C_{\mathrm{B}} - C_{\mathrm{S}}}{\delta} \tag{2.11}$$

where D is the diffusion coefficient of the reacting species, C_{B} is its bulk concentration, C_{S} is its surface concentration, and δ is the thickness of the diffusion layer.

The maximum rate at which the reactant can be supplied to an electrode determines the limiting current, I_{L} . Beyond this value, the reactants cannot reach the reaction surface to fully supply the reaction, such that the reaction rate will decrease. From Fick's law, the concentration polarization, ϕ_{conc}, can be written:

$$\phi_{\mathrm{conc}} = \frac{RT}{zF}\ln\left(1 - \frac{I}{I_{\mathrm{L}}}\right) \tag{2.12}$$

For Eqn. (2.12) to be valid, activation polarization is assumed to be negligible in comparison with the concentration polarization. This is reasonably appropriate for a high temperature fuel cell.

The cumulative effect of these polarizations affects the voltage across the cell as follows:

$$V_{\mathrm{actual}} = V_{\mathrm{ideal}} - \phi_{\mathrm{act}} - \phi_{\mathrm{ohm}} - \phi_{\mathrm{conc}} \tag{2.13}$$

2.2 Fluid and Thermal Modeling

In an operating fuel cell, the flow, thermal, chemical, and electrochemical systems are intrinsically coupled. As described above, the ability of the fuel cell to transport products and reactions can greatly affect the performance of the cell. Heat generation and absorption affect the temperature distribution and the reaction rate. To calculate flow and temperature, the conservation laws in thermodynamics and fluid mechanics are used.

2.2.1 Conservation Equations

Conservation of Mass

The mass of a species in a reacting mixture of gasses is determined by solving the species continuity equations:

$$\frac{d\rho_i}{dt} + \nabla\bullet\ \rho_i v\ = S_{m,i} \tag{2.14}$$

where ρ_i is the species density, v is the fluid velocity, t is the time, and $S_{m,i}$ is the rate of production of the species i due to the electrochemical reactions. This equation can also be used to determine the conservation of charge. Considering charge as species e:

$$\frac{d\rho_e}{dt} + \nabla \bullet \ \rho_e v_d \ = I_{\text{gen}} \tag{2.15}$$

Here we have the charge density, ρ_e, and drift velocity, v_d, which is the current density relating to the current generation rate, I_{gen}. The current source is regulated by the Butler-Volmer equation, Eqn. (2.8).

Conservation of Species

The conservation of species relates closely to the principle of conservation of mass. This conservation law makes sure that the mass of each chemical species is conserved in the fuel cell. It is written as follows, similarly to Eqn. (2.14):

$$\frac{d\rho_i c_i}{dt} + \nabla \bullet \ \rho_i c_i v \ = -\nabla \bullet \Upsilon_i + S_{s,i} \tag{2.16}$$

where c_i is the mass fraction of each species, Υ_i is the diffusive mass flux of the species, and $S_{s,i}$ represents a species source in the fuel cell.

Conservation of Momentum

The Navier-Stokes equations, the basis for all fluid dynamics models, describe the motion of a fluid:

$$\frac{d}{dt} \ \rho v \ + \nabla \bullet \ \rho v^2 \ = \nabla p + \nabla \bullet \ \mu \nabla v \ + \rho g \tag{2.17}$$

On the left-hand side of the Eqn. (2.17) are the momentum terms, and on the right hand side are the force terms. The surface forces are encapsulated in the pressure term, p, and the stress term, $\mu \nabla v$. The body forces are in the gravitational term, $\rho \mathrm{g}$.

Conservation of Energy

The temperature profiles and local heat fluxes inside the cell can be determined through the energy equation:

$$\frac{d\rho_e}{dt}+\nabla\bullet\left[v\left(\rho_e e+p\right)\right]=\nabla Q+S_h \tag{2.18}$$

where S_h is the volumetric heat source, Q is the heat flux vector, and e is the total energy per unit mass. The sum of the specific internal energy, the specific kinetic energy, and the potential energy in a fluid is the energy per unit mass:

$$e=c_v T+\frac{v^2}{2}+gh \tag{2.19}$$

where c_v is the specific heat at constant volume and g is the acceleration of gravity. Since the working fluid in SOFCs is a mixture of gasses, the potential energy, gh, and kinetic energy, $v^2/2$, terms are often neglected. The heat source in Eqn. (2.18) incorporates viscous dissipation and the heat generated or absorbed by the chemical reactions.

2.2.2 Porous Flow Equations

In understanding transport in the porous electrodes, we must first understand the nature of porous material. Porous material consists of a matrix of solid material with voids or holes in it. The fraction of the total volume that the void spaces make up is described as porosity, ε. The concept of transport in the porous electrodes is that fluid can be flowing around the solid phase material and will interact with it. In a SOFC, these interactions affect the movement of the fluid, the transportation of heat, and the electrochemical reactions. Because of the complexity of the interfaces between solid and fluid material in porous media, properties are often averaged over the entire volume. For example, the velocity of fluid in porous media, the Darcy velocity, v_{d}, is the average fluid velocity over both the solid and the fluid spaces in the media.

In a porous medium, the equation for conservation of mass is altered very little, using the Darcy velocity instead of the fluid velocity. The use of the Darcy velocity accounts for the porous media effects in the electrodes. The general form for the mass conservation equation in porous media is:

$$\varepsilon\frac{d\rho_i}{dt}+\nabla\bullet\left(\rho_i v_{\mathrm{d}}\right)=S_i \tag{2.20}$$

where the velocity in Eqn. (2.14) is replaced with the Darcy velocity.

Since the flow though the SOFC studied is laminar, simplifications can be made to the equations of flow in the porous medium. In laminar flow, pressure drop is proportional to velocity and the internal resistance factor is negligible. The convective acceleration and diffusion terms are also ignored, reducing the model of flow in porous media to Darcy's Law:

$$\Delta p = -\frac{\mu}{\kappa} v \tag{2.21}$$

where κ is the permeability of the porous media and μ is the dynamic viscosity. This relation can be written as:

$$\frac{dp}{dx} = \frac{\mu}{\varepsilon} \nabla^2 v \tag{2.22}$$

This equation directly compares to the Stokes flow equation, Eq. (2.17) when only the pressure term and the stress term are relevant.

The energy equation in porous media can more easily be written as a composite of two phase-specific equations:

$$\begin{gathered} \varepsilon \frac{d\rho_e}{dt} + \nabla \bullet \left(\varepsilon \rho_e v e \right) = \varepsilon \nabla Q + S_h \\ \left(1-\varepsilon\right) \frac{d\rho_e}{dt} + \nabla \bullet \left(\left(1-\varepsilon\right) \rho_e v e \right) = \left(1-\varepsilon\right) \nabla Q + S_h \end{gathered} \tag{2.23}$$

where the terms in the energy equation for the fluid region are multiplied by the porosity and the terms in the energy equation for the solid region are multiplied by $\left(1-\varepsilon\right)$. The properties used in the calculation of the energy equation in each region are also specific to the phase of that region.

2.3 SOFC Performance

There are many ways to quantify the performance of a fuel cell. Some performance characteristics express for how useful the fuel cell is. These characteristics, (i.e., power, voltage, and current described in Section 2.1) determine if the fuel cell can fulfill a specific task. Other performance parameters express how well a fuel cell completes a task. The main characteristic in this category is efficiency since the fuel cell's potential for efficiency is what is driving the industry.

Efficiency can be determined in many different methods to suit the needs of the researcher. In fuel cells, the most flattering method of calculating efficiency is theoretical efficiency: the comparison of the total amount of energy that exists in the fuel, the enthalpy, *H*, with the amount of useful energy that can be released in a reaction, the Gibbs energy. The theoretical efficiency is written:

$$\eta_{\mathrm{FC}} = \frac{\Delta G}{\Delta H} \quad \text{or} \quad \eta_{\mathrm{FC}} = \frac{\frac{\Delta G}{zF}}{\frac{\Delta H}{zF}} = \frac{1.185}{1.254} = 94.5\% \qquad (2.24)$$

The second method for calculating the theoretical efficiency in Eqn. (2.24) is useful when considering the ΔG term as the theoretical cell potential and the ΔH term as the cell potential independent of heat effects, or thermoneutral potential. Because of the high temperatures in the SOFC, the reactions in the cell produce water vapor. In this case, the enthalpy of hydrogen would be the lower heating value (LHV) of the fuel. The theoretical efficiency of fuel cells calculated from the LHV of hydrogen is 94.5 percent. In lower temperature fuel cells, which produce liquid water, the higher heating value (HHV) must be used in calculating the efficiency. This results in a lower theoretical efficiency of 83%.

Of course, in actually fuel cell operation, all of the Gibbs energy is not converted to electric potential. The actual fuel cell efficiency compared the fuel cell operational potential to the thermoneutral potential:

$$\eta_{\mathrm{voltage}} = \frac{\mathrm{V}_{\mathrm{actual}}}{1.254} \qquad (2.25)$$

This representation uses the thermoneutral potential calculated with the LHV of hydrogen.

Not all hydrogen that reacts in the fuel cell is reflected in the generated current. This can be caused by crossover reactions, when hydrogen or oxygen leaks through the electrolyte and react in the flow channels, or it can be caused by internal currents. The current efficiency is written:

$$\eta_{\mathrm{current}} = \frac{I}{I + I_{\mathrm{loss}}} \qquad (2.26)$$

Typically, current loss is very low, and its effects on the fuel cell efficiency are negligible at high current densities.

The hydrogen supply can also affect the efficiency of the fuel cell. Fuel efficiency, or fuel utilization rate, is an important consideration in most energy generation devices. However, this value can be misleading in fuel cells. Since the fuel utilization rate is directly linked to the current in the cell, causing the fuel efficiency to be largely related to fuel input rates:

$$\eta_{\mathrm{fuel}} = \frac{\dot{m}_{\mathrm{used}}}{\dot{m}_{\mathrm{in}}} = \frac{IM}{zF\dot{m}_{\mathrm{in}}} \tag{2.27}$$

Here, the fuel efficiency is written as the ratio of fuel consumed in the cell to the fuel that enters the cell. The operating condition in fuel cells, namely the fuel flow rate, is often selected to achieve fuel efficiencies between 80 and 90 percent. In this fuel cell study the fuel flow rate remained constant between the cases, so the fuel efficiency can add value to the efficiency calculation.

The total fuel cell efficiency is the product of the individual component efficiencies:

$$\eta_{\mathrm{total}} = \eta_{\mathrm{FC}}\eta_{\mathrm{voltage}}\eta_{\mathrm{current}}\eta_{\mathrm{fuel}} \tag{2.28}$$

The total efficiency only reflects the efficiency of the fuel cell. In a fuel cell system, the balance of plant components (e.g., pumps, reformers, etc.) will each contribute terms to the total system efficiency and will further reduce total system efficiency.

3. Model Implementation in FLUENT

As seen above, the models that govern SOFC operation are complex. To limit the time and effort required to develop a full SOFC model, the commercial CFD code FLUENT has been used. FLUENT offers a SOFC add-on module to assist in developing SOFC models. This sub-model was designed to marry the electrochemical processes to the thermal-fluid models.

To generate a model in FLUENT, we must first create mesh geometries suitable for supporting the numerical equation. To create a proper model to run in FLUENT, the first step is to create the geometry of the model and create a mesh on which to build the numerical calculations. Gambit is the meshing package used to generate the geometry, generate the mesh, and specify the types of boundary conditions. Gambit produces case files that FLUENT can read. Once the base case file is read into FLUENT, the appropriate equations and boundary values are set. These boundary conditions and equations define the physical operation of the SOFC. However, there are many peculiarities that need to be understood about the methods the FLUENT-SOFC module uses to model a SOFC. These alterations to the physical processes in the previous section may not be intuitive but are essential to the operation of the model.

3.1 Description of Base Model

The base model for this study is a benchmark case defined in Pakalapati [48]. The flow configuration in the model is co-flow, where both reactant flows enter the channels from the same side of the cell, Figure 3.1.a. The model makes use of symmetry within the fuel cell to simplify the model to a half flow channel model depicted in Figure 3.1.b. Details of the unit cell geometry of the SOFC investigated are given in Table 3.1.

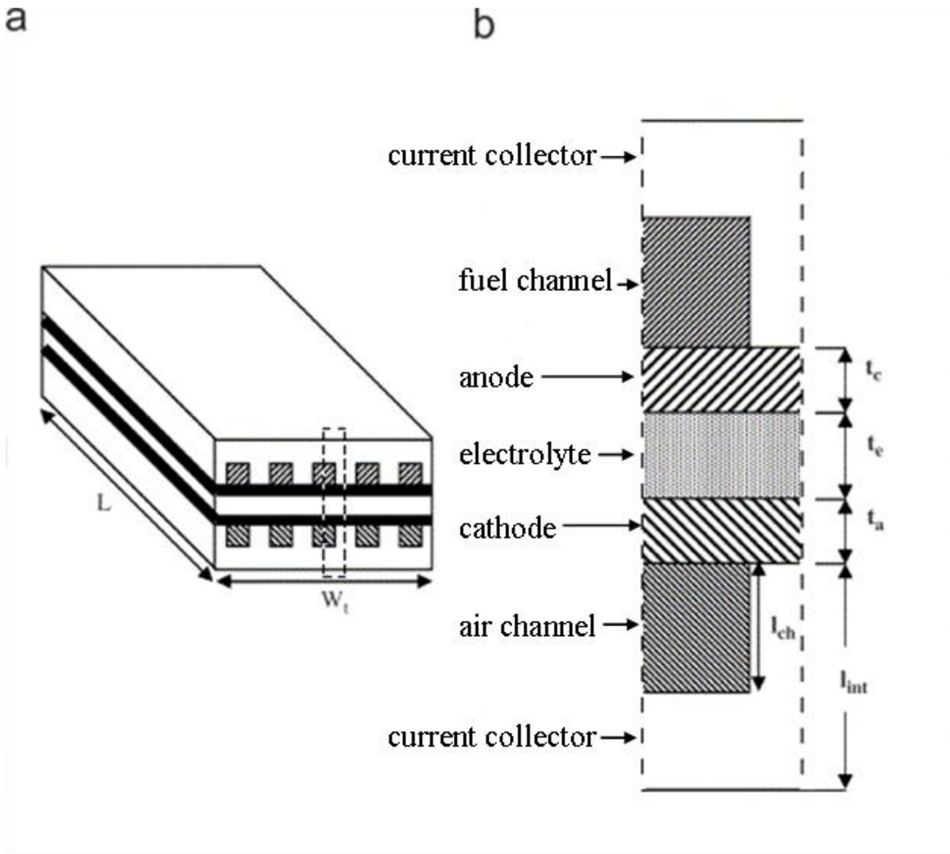

Figure 3.1 Geometry of base model SOFC (a) Three-dimensional drawing of the planar SOFC and (b) Configuration of unit cell SOFC

Table 3.1 Unit cell SOFC dimensions

Parameter	**Value**
Anode thickness (mm)	**0.05**
Electrolyte thickness (mm)	**0.15**
Cathode thickness (mm)	**0.05**
Interconnect thickness (mm)	**0.5**
Channel length (mm)	**20**
Height of fuel and air channels (mm)	**1.0**
Width of fuel and air channels (mm)	**1.5**
Active area (mm^2)	**40**

The geometry described above was meshed in Gambit, as shown in Figure 3.2. The numerical model contains the interconnects, flow channels, and electrodes from Figure 3.1.a above. In comparison to Figure 3.1.a, the electrolyte is excluded in Figure 3.2 because FLUENT models it as a plane surface separating the electrodes. Information on how FLUENT account for electrolyte thickness is found in Section 3.2. The grid generated consists of 224,000 nodes. The grids generated in the interconnect and flow channel zones utilize 200 nodes along the length of the cell, 20 along the width, and 25 along the height. The grids generated in the electrode zones utilize 3 nodes along the thickness of the electrolyte. The low node count in the electrodes is required to maintain a low node skewness ratio. The mesh sizes in the test geometries vary; however, the 3 node count along the thickness of the electrolyte is maintained throughout the tests. Further information on the test geometry grids can be found in the respective sections of the results chapter.

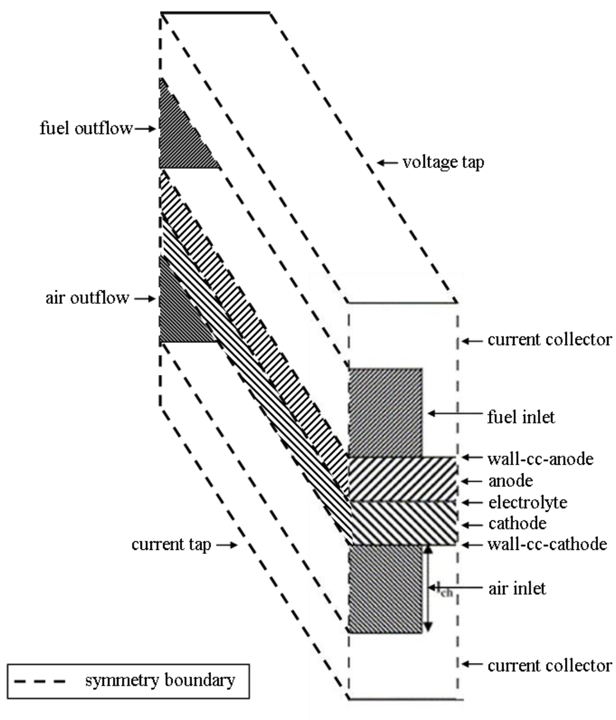

Figure 3.2 Configuration of unit cell in Gambit and FLUENT

Gambit offers the option to set and name boundary conditions and zones in the mesh. By specifying the different boundaries and zones, each entity receives a different identifier when the model is imported into FLUENT. This eases the process of preparing the fuel cell model within FLUENT. The user assigns the properties in each volume, or continuum, separately in FLUENT, so it is helpful to add descriptive names to the volumes and to specify whether the volume is a solid or a fluid zone before the model is imported. The zone names and types created in Gambit are listed in Table 3.2. Note that the porous electrodes are specified as a fluid zone. FLUENT requires this to calculate the characteristics of the fluid filling the voids in the porous material. There are also several key surfaces within the model with boundary conditions that require adjustment in FLUENT. It is necessary to properly prepare these surfaces within Gambit. These surface zones and their associated boundary types are listed in Table 3.3.

Table 3.2 Volume zone settings in Gambit and FLUENT

Continuum Zone	Type
Anode	**fluid**
Cathode	**fluid**
Air [flow channel]	**fluid**
Fuel [flow channel]	**fluid**
CC-anode-solid [current collector]	**solid**
CC-cathode-solid [current collector]	**solid**

Table 3.3 Surface zone boundary conditions in Gambit and FLUENT

Surface Zone	Type	Description
inlet-air	**mass flow inlet**	**Inlet into air channel**
inlet-fuel	**mass flow inlet**	**Inlet into fuel channel**
outflow-air	**pressure outlet**	**Outlet from air channel**
outflow-fuel	**pressure outlet**	**Outlet from fuel channel**
electrolyte	**wall**	**Surface between electrodes for electrochemical calculations in FLUENT**

voltage-tap	**wall**	**Surface of anode current collector for circuit**
current-tap	**wall**	**Surface of cathode current collector for circuit**
wall-cc-anode	**wall**	**Contact surface between anode and collector**
wall-cc-cathode	**wall**	**Contact surface between cathode and collector**
symmetry-cc	**symmetry**	**4 surfaces of symmetry boundary on current collector side of fuel cell**
symmetry-ch	**symmetry**	**6 surfaces of symmetry boundary on channel side of fuel cell**

When the grid is read into FLUENT, the particulars of the case are set. The first specification needed is the length scale of the grid. Gambit meshes do not contain units, so the length scale of millimeters must be selected to properly size the model. The electrolyte boundary condition also requires further classification. Plane walls created in Gambit have two surfaces when loaded into FLUENT. Each side of the physical wall can have differing properties depending on the volume it is facing. FLUENT requires separate settings on each side of the electrolyte wall for the electrochemical calculations, so it is convenient to rename these walls. The two walls are renamed electrolyte-anode and electrolyte-cathode—named for the volume that each surface contacts.

3.1.1 Basic Transport Formulation in FLUENT

After the geometry of the fuel cell is properly defined, the numerical equations can be formulated within the model. Many of the basic fluid flow equations are built in as defaults in FLUENT and will operate once flow conditions are set in a latter process. However, the SOFC module in FLUENT requires the energy equation to be enabled. The equation is used to calculate the conductive and convective heat transfer within the model. The model also makes use of a laminar flow assumption.

Since a fuel cell is an electrochemical reactor, the *species transport and reaction* function must be enabled. In this function, s*pecies transport* enables the modeling of multi-species transport and mixing by solving conservation equations describing convection, diffusion, and reaction sources for each species component in the model. The *volumetric reaction* option, used in this investigation, enables the calculation of reacting flow using finite-rate formulation. Disabling the *inlet diffusion* function allows us to specify the mass fractions entering the fuel cell at the inlets. The *diffusion energy source* is enabled to include the effect of enthalpy carried by diffusing species in the energy equation. *Full multicomponent diffusion* is enabled to calculate the diffusive mass flux of the chemical species. The *thermal diffusion* function is enabled; this causes heavy molecules to diffuse less rapidly than lighter molecules towards heated surfaces. These inputs create the backbone of the model that is available in the standard FLUENT package.

3.1.2 FLUENT SOFC Module Formulation

The SOFC module includes additional inputs specific to electrochemical modeling. The *control panel* interface contains the options to enable various submodels contained in the SOFC module. The *enable electrolyte conductivity* submodel allows the ionic conductivity of the electrolyte to change as a function of temperature. The *enable surface energy source* submodel includes the heat addition due to the electrochemistry and all reversible processes. The *enable volumetric energy source* submodel includes the ohmic heating in the electrically conducting zones of the model. The *disable CO electrochemistry* submodel is selected for cases when carbon monoxide is not present in the fuel. All submodels are enabled in the present investigation. Also included in the SOFC control panel are the parameters that describe the electrolyte and electrical characteristics of the system. These parameters and the assigned values can be found in Table 3.4.

Table 3.4 SOFC control panel parameters

Parameter	Value
Current underrelaxation factor	**0.4**
Total system current (Amp)	**0.0 to 0.84**
Leakage Current Density(Amp/m^2)	**0.0**
Electrolyte thickness (m)	**0.00015**
Electrolyte resistivity (ohm-m)	**0.1948**

The *electric field input panel* defines the volumes and surfaces that form the electrical circuit in the model. The SOFC module allows five regions to be defined with individual conductivities. In the present model there are three conductive regions: the anode, the cathode, and the two current-collectors, which can be defined together. The surfaces between the conductive materials must be specified to allow current to flow in the model. These surfaces are assigned contact resistances to account for the electric losses due to non-ideal connection between the materials. To complete the circuit, one of the external surfaces needs to be grounded (the voltage tap) and a second surface needs to be designated as the surface from which the current is being drawn (the current tap). The electric field parameters with associated values can be found in Table 3.5.

Table 3.5 Electric field input parameters

Entity	Parameter	Value
Anode	**conductivity (1/ohm-m)**	**30384**
Cathode	**conductivity (1/ohm-m)**	**12872**
cc-anode-solid cc-cathode-solid	**conductivity (1/ohm-m)**	**3078**
wall-cc-anode	**contact resistance (ohm-m)**	**1e-7**
wall-cc-cathode	**contact resistance (ohm-m)**	**1e-8**

The *activation panel* defines parameters associated with the electrochemical reactions. Here the anode and cathode exchange current density is set. This quantifies the forward and reverse electrode reaction rates at the equilibrium potential. Traditionally this value is on a per area basis (Amp/m^2); however, in the present version of the FLUENT module, the exchange current density needs to be placed in terms of amps. The option of setting a temperature dependent exchange current density is included here but was not utilized in this investigation. The anode and cathode mole fractions set in this panel act as reference values for the inlet flow conditions. In this investigation, the default stoichiometric exponents and the Butler-Volmer transfer coefficients were maintained. The activation parameters with assigned values can be found in Table 3.6.

Table 3.6 Activation panel input parameters

Parameter	Value
Anode exchange current density (Amp)	**5500**
Cathode exchange current density (Amp)	**5500**
H_2 reference value (moles/moles)	**1**
O_2 reference value (moles/moles)	**1**
H_2O reference value (moles/moles)	**1**

The *anode interface setup* panel is used to specify the surface that represents the anode electrode interface with the electrolyte. Similarly, the *cathode interface setup* panel is used to specify a surface as the interface between the cathode electrode and the electrolyte. The *tortuosity setup* panel is used to specify the effective diffusive path length factor in the porous regions of the model. Here the anode and cathode regions were designated to have a tortuosity value of 3. This is a typical value—used because tortuosity needs to be measured experimentally. This completes the definition SOFC module specific properties.

3.1.3 Material Property Formulation

The material properties and boundary conditions are defined in the standard FLUENT processes. The properties used in this investigation were taken from Pakalapati [48]. This was done so that it would be possible to verify the code. It is often not possible to exactly match all of the conditions which exist between models due to limitations on what parameters are reported. However, it is important to match as many independent parameters as possible for a meaningful comparison. The first aspects of the model that must be addressed are the material properties. In FLUENT, materials are entries to a database. In this investigation, four materials needed to be created: anode-material, cathode-material, interconnect-material, and electrolyte-material. Each material created can be referenced while setting the boundary conditions of the fuel cell zones to specify the zone material. The material properties are given in Table 3.7.

Table 3.7 Material properties values

Parameter	Value
Density (kg/m^3)	
Anode	**6600**
Cathode	**6600**
Electrolyte	**6600**
Interconnect	**6600**
Heat Capacity (J/kg-K)	
Anode	**400**
Cathode	**400**
Electrolyte	**400**
Interconnect	**400**
Thermal conductivity (W/m-K)	
Anode	**3**
Cathode	**3**
Electrolyte	**2**
Interconnect	**3.5**

Defining the fluid is a peculiarity in FLUENT, since the code wants the material in each zone to be defined even if it is not a solid. Thus, the fluid mixture considered in the model is also created in the *material properties* panel. At this point in the model set-up, all FLUENT needs to know are the species which could exist within the fluids of the model. The SOFC module only requires this one mixture to be created in the *material properties* panel which contains H_2O, O_2, H_2, and N_2. It is important to have the species listed in that order, since FLUENT calculates the last species from the previously listed ones to save computational space. These species are separated into the two separate flow channels when the mass flow inlet properties are specified later in the set up procedure. This fluid mixture utilizes incompressible ideal gas assumptions for the majority of properties. However, the mass diffusivity is associated with the user-defined function that contains the information defined in the SOFC module panels described above.

3.1.4 Boundary Condition Formulation

Several additional boundary conditions were required by FLUENT. Each of the continuum zones have parameters that need to be described before the model will function properly. In the anode and cathode, the porous structure and source terms must be properly enabled and defined. In the *porous zone* tab, the viscous resistance caused by the fluid moving at low velocities through porous material is specified. The material porosity is also defined, and the material is designated to be either the anode or cathode material defined above. In the *source terms* tab, we associate the source terms to the calculated quantities that require their use. The SOFC module contains a user defined function which includes the source terms for mass, chemical species, and energy. The source terms associated in the anode zone are for mass, energy, H_2O, and H_2. These parameters are parallel to those set in the cathode zone; however, the species with the associated source term is O_2. The input parameters for the electrodes can be found in Table 3.8.

Table 3.8 Electrode boundary condition properties

Parameter	Value
Viscous Resistance ($1/m^2$)	
Anode	**1e-8**
Cathode	**1e-8**
Porosity	
Anode	**0.2**
Cathode	**0.2**
Source Terms	
Anode	**mass, H_2O, H_2, energy**
Cathode	**mass, O_2, energy**

Similarly, the interconnects require the material to be specified. Each interconnect also acts as an energy source for the cell, so the user-defined source must be associated with the energy quantity in the interconnect.

The final boundary conditions that require input parameter are the mass flow inlets. The mass flow is assumed to be normal to the boundary in this investigation. The temperature and species fractions were determined from Pakalapati [48]. The flow rate was calculated from Eqn. (2.29):

$$\dot{m}_{fuel}^{inlet} = \frac{2I}{2F}\frac{1\times10^{-3}}{\eta_{H_2} X_{H_2}^{inlet}} \tag{2.29}$$

where I is the cell current, η_{H_2} the hydrogen utilization efficiency, and $X_{H_2}^{inlet}$ is the mass fraction of hydrogen entering the cell. The air entering the cell is likewise calculated from Eqn. (2.30):

$$\dot{m}_{air}^{inlet} = \frac{32I}{4F}\frac{1\times10^{-3}}{\eta_{O_2} X_{O_2}^{inlet}} \tag{2.30}$$

where η_{O_2} is the oxygen utilization efficiency and $X_{O_2}^{inlet}$ is the mass fraction oxygen entering the cell. These parameters and associated values are found in Table 3.9.

Table 3.9 Mass flow boundary parameters

Parameter	**Value**
Fuel Inlet	
Mass flow rate (kg/s)	**2.03×10^{-8}**
Fuel utilization	**0.85**
Total temperature (K)	**1173**
H_2 mass fraction	**0.5**
H_2O mass fraction	**0.5**
Air Inlet	
Mass flow rate (kg/s)	**2.38×10^{-6}**
Air utilization	**0.125**
Total temperature (K)	**1173**
H_2 mass fraction	**0.233**

3.2 FLUENT Fuel Cell Adaptation

This section describes the adaptations that FLUENT makes to the governing equations used for modeling flow and reactions in a SOFC. Included in this section are the adaptations FLUENT makes to the basic models for SOFC geometry, fluid flow, heat transfer, and mass transport. Traditionally in FLUENT, a user would need to create additional code to couple electrochemical reactions to the heat and fluid flow functionality in the software. Recently, FLUENT created the SOFC module which combines electrochemical capability with its CFD functionality. The module has the ability to calculate Nernst voltage, keep track of current distributions, and the electric potential field across the fuel cell.

3.2.1 Geometry

As described in brief above, the geometry of a fuel cell becomes simplified in the FLUENT–SOFC module. Since the important reactions occur on the surfaces of the electrolyte, the electrolyte is modeled as a plane surface with no thickness in the fuel cell mesh geometry. The thickness of the electrolyte is a user input that is included, mathematically, in the modeling. In FLUENT modeling, a plane wall has two distinct surfaces that contain properties associated to the volume that it contacts. In the electrolyte, the surfaces act as separate triple phase boundaries (TPBs) for the cathode and anode. To couple these surfaces, a condition known as the jump condition, is placed between the surfaces and is used to calculate the effect of the electrolyte thickness on the fuel cell processes.

3.2.2 Electrochemistry

Conservation of charge governs the FLUENT electrochemical model. The present FLUENT model calculates steady-state solutions of fuel cell operation. FLUENT simplifies the charge conservation law in Eqn. (2.15) by removing the transient term, thus leaving:

$$\nabla \bullet J = 0 \text{ or } \nabla \bullet \sigma \nabla \vec{V} = 0 \tag{3.1}$$

where FLUENT represents the current density, J, as a function of conductivity, σ, and electric potential field, $\vec{V}$. FLUENT solves this Laplace equation by enforcing flux conservation on each control volume. For control volumes away from the electrolyte, the flux from a control volume to its neighbor is given by Ohm's law in Eqn. (2.9) where the gradient is approximated using the numerical difference of electric potential between the volumes. This gradient is the voltage, V, in each control volume. At the electrolyte interface, Ohm's law must be used with a relation for voltage difference. For normal flux, there are three separate voltage coupling relations: anode voltage to anode-electrolyte interface voltage, cathode voltage to cathode-electrolyte interface voltage, and the jump condition across the electrolyte which relates anode-electrolyte interface voltage to cathode-electrolyte interface voltage. These relations are:

$$V_{\text{cathode}_{\text{centroid}}} = V_{\text{cathode}_{\text{wall}}} - I\rho_{\text{cathode}} D_{\text{cathode}} \tag{3.2}$$

$$V_{\text{anode}_{\text{centroid}}} = V_{\text{anode}_{\text{wall}}} - I\rho_{\text{anode}} D_{\text{anode}} \tag{3.3}$$

$$V_{\text{anode}_{\text{wall}}} = V_{\text{cathode}_{\text{wall}}} - I \left(\rho_{\text{ele}} \delta_{\text{ele}}\right)_{\text{eff}} \tag{3.4}$$

Here, D is the distance from electrode cell center to the electrolyte and δ_{ele} is the thickness of the electrolyte. FLUENT simultaneously solves these three equations to compute the current flow between each node, I, based on the values of the electric field in the anode and cathode.

In the electrochemical model, the two sides of the electrolyte are separated by a local potential difference that reflects the losses occurring under electrical loads. This equation is written as:

$$V_{\text{cell}} = V_{\text{ideal}} - I\rho_{\text{ele}}\delta_{\text{ele}} - \phi_{\text{act}} \tag{3.5}$$

where the voltage drop across the cell is equal to the Nernst voltage reduced by ohmic losses across the electrolyte and activation losses across the electrode-electrolyte interfaces. Care must be taken in calculating the potential difference across the electrolyte, because FLUENT treats the electrolyte as an impermeable wall. To properly couple the electrochemical behavior at the TPBs to the electrical field calculation, the electrochemical effects are included in the jump condition. These effects include: voltage due to Nernst, voltage reduction due to activation, and ohmic losses due to resistivity within the electrolyte. The interface condition that relates the potentials on either side of the electrolyte has the following form:

$$V_{\text{cell}} = V_{\text{jump}} - \phi_{\text{s}} \tag{3.6}$$

Here, ϕ_s represents the ohmic losses in the solid conducting regions of the cell and the jump potential, V_{jump}, is calculated from:

$$V_{\text{jump}} = V_{\text{ideal}} - \phi_{\text{ele}} - \phi_{\text{act,a}} - \phi_{\text{act,c}} \tag{3.7}$$

In Eqn. (3.7), ϕ_{ele} represents the ohmic polarization of the electrolyte, $\phi_{\text{act,a}}$ and $\phi_{\text{act,c}}$ represent the activation polarization of the anode and cathode and V_{ideal} represents the Nernst potential.

A term for concentration polarization, ϕ_{conc}, does not appear in Eqn. 3.7. The concentration polarization is not directly calculated within the FLUENT-SOFC module. The FLUENT model relies on the effect of concentration being reflected in the partial pressures from the Nernst equation, Eqn. (2.6). This is a weakness in the present version of the model and limits the abilities of the model at high current densities.

The activation polarization is the additional potential that the electrochemical reaction requires to overcome the energy barrier in the chemical bonds of the reactants. The potential is closely related to the rate at which the reaction proceeds. FLUENT adapts the full expression of the activation polarization given in the Butler-Volmer equation from Eqn. (2.8). FLUENT found it useful to linearize the Butler-Volmer relation to aid in the computational process. Using the previous computational step value for current, I_{old}, the Taylor series expansion is:

$$\phi(I) \approx \phi_0 - \phi_1 (I - I_{old}) \tag{3.8}$$

$$\phi_0 = \phi_{act}(I_{old}) \tag{3.9}$$

$$\phi_1 = -\left.\frac{\partial \phi_{act}}{\partial I}\right|_{I=I_{old}} \tag{3.10}$$

With this approximation substituted into Eqn. (3.5), the formula for the voltage jump across the electrolyte becomes:

$$V_{jump} \approx (N - \phi_0 + \phi_1 I_{old}) - I(\rho_{ele}\delta_{ele} + \phi_1) \tag{3.11}$$

The first bracketed term is now a constant and the second term is linear with the local density. During calculation, this form allows the activation overpotential to respond to changes in local current density. Even though the Butler-Volmer relation is nonlinear, the linearized form in FLUENT becomes more accurate as the solution reaches convergence and is exact at convergence.

The ohmic polarization involves the ionic losses through the electrolyte, the electrical resistance in the conducting porous electrodes and solid conductors, and the contact resistance. FLUENT uses Ohm's law, in Eqn. (2.9) where *R* is the total effective resistance calculated from ionic losses through the electrolyte, electrical resistance in the conducting porous electrodes and solid conductors, and the contact resistance.
where, I is the current and R is the effective resistance of the material or interface.

3.2.3 Fluid and Thermal Modeling

Conservation Equations

FLUENT models obey the basic conservation laws for mass, species, momentum, and energy. The only "adaptation" that the FLUENT-SOFC model makes to Eqns. (2.14), (2.16), (2.18) is to quantify the source terms. The momentum conservation law, Eqn. (2.17), contains no source term and is not adjusted in the fuel cell module.

The electrochemical modeling within the FLUENT-SOFC package calculates the species sources and sinks based on the current at the reaction surface. The general form of this equation is:

$$S_x = -\frac{aI}{zF} \tag{3.12}$$

where S_x is the source or sink of a species and a is the stoichiometric coefficient for the species. The species source represents the rate at which the number of moles of the species that are created or destroyed per unit area.

The species sources calculation can be used to determine the mass sources and sinks. Moles are related to mass by molecular weights of atoms. Multiplying Eqn. (3.12) by the species molecular weight and summing the equations at an electrode results in the rate of mass production at the electrode:

$$S_m = \sum_x -M_x \frac{a_x I}{zF} \tag{3.13}$$

where, M_x is the molar weight of the species and *x* represents each species.

In the energy conservation law, the FLUENT-SOFC module clarifies two terms from Eqn. (2.18): the heat flux vector and the volumetric heat source. The heat flux vector consists of the net heat flux into the element and the net work done on the element due to the transportation of the fluid:

$$Q = k_{\mathrm{eff}} \nabla T - \sum_{x} h_x \vec{D}_x \quad \bar{\bar{\tau}}_{\mathrm{eff}} \bullet \vec{\mathrm{v}} \tag{3.14}$$

where k_{eff} is the effective conductivity of combined solid and fluid, h_x is the sensible enthalpy, and $\vec{D}_x$ is the diffusion flux of each species in the fluid. In the conducting zones of the fuel cell, FLUENT adds a source term to account for ohmic heating:

$$S_h = I^2 * R_{\mathrm{ohmic}} \tag{3.15}$$

where I is the current and R_{ohmic} is the ohmic resistance of the conducting material. This resistance occurs in the interconnects, the electrodes, and the electrolyte. Because of how the electrolyte is modeled as a plane surface in FLUENT, the ohmic heat produced in the electrolyte must be added to the cells neighboring the electrode-electrolyte interface.

Heat is also produced at the electrode-electrolyte interface by the electrochemical reactions taking place. The total energy balance on the electrolyte interface includes the enthalpy flux of all species and is reduced by the work leaving the system. For the hydrogen reaction, the balance is:

$$\dot{Q}'' = h''_{\mathrm{H_2}} + h''_{\mathrm{O_2}} - h''_{\mathrm{H_2O}} - i\Delta V \tag{3.16}$$

where $\dot{Q}''$ is the waste heat generation due to irreversibilities and h is the total enthalpy of the species. The final term in the energy balance is the energy converted to electric work. The source term that is added to the energy equation is:

$$S_h = \frac{Q}{\mathrm{Volume}} \tag{3.17}$$

Since a portion of the hydrogen reaction and electric work occurs on both sides of the electrolyte, a portion of S_h is applied to either side of the electrolyte interface. FLUENT divides the heat evenly but notes that the equal distribution of the heat energy is arbitrary.

3.3 Solution Controls and Convergence

Due to the small scale of the fuel cell model and processes, the convergence criteria for the conserved quantities are lower than the default FLUENT values. These values represent the absolute value of the difference in value of the general variable in a cell from the influence of neighboring cells and source term

$$R^{\varphi} = \sum_{\text{cells P}} \left| \sum_{\text{nb}} a_{\text{nb}} \varphi_{\text{nb}} + b + a_P \varphi_P \right|. \tag{3.18}$$

Here, R^{φ} is the residual, a_{nb} are the influence coefficients from the neighboring cells, b is the contribution of the source term, and φ_P is the value of the considered variable in cell P. These values examined are scaled and are unitless:

$$R^{\varphi} = \frac{\sum_{\text{cells P}} \left| \sum_{\text{nb}} a_{\text{nb}} \varphi_{\text{nb}} + b + a_P \varphi_P \right|}{\sum_{\text{cells P}} \left| a_P \varphi_P \right|}. \tag{3.19}$$

The scaling is essential for judging the changes of the solution in cases with very small variable values. The residuals in the fuel cell module are small due to the small scale of the processes, thus, the convergence criteria must be small. These values are found in Table 3.10.

Table 3.10 Convergence criteria

Residual	Convergence Criterion
Continuity	**1×10^{-6}**
X-velocity	**1×10^{-6}**
Y-velocity	**1×10^{-6}**
Z-velocity	**1×10^{-6}**
Energy	**1×10^{-8}**
H2O	**1×10^{-6}**
O2	**1×10^{-6}**
H2	**1×10^{-6}**
UDS-0 (cell voltage)	**1×10^{-7}**

4. Results

4.1 Preliminary observations

The effects of rib design on the function and performance of a SOFC were examined using the basic model discussed in the previous section. A comparison was made between the results from this three-dimensional model with a plane channel model and the model presented in Pakalapati [48]. However, before discussing the results of these models, a short discussion about data presentation and the preliminary rib spacing study, as well as an overview of the fuel cell model results, are presented.

4.1.1 Data Presentation

The parameters to be compared are velocities (presented as vectors), power density, pumping power, fuel cell voltage, fuel utilization, and temperature (presented as contours). The voltages reported in this study will be reported as a plot of surface averaged values and in a contour plot visualization. While FLUENT calculates the voltage at every node in the electrolyte mesh, the surface average of the voltage across the electrolyte represents the voltage produced by the cell that enters the external circuit. Thus, the surface averaged voltage in the fuel cell model is reported to generate the operation curve, or polarization curve. This value is universally used to determine the power density and performance of a fuel cell. Alternatively, knowing the voltage at specific locations along the fuel cell can be useful when designing a fuel cell. To determine the effects of cell design on voltage, distributed data are presented in contour plots. Each voltage contour plot shows the voltage on the cathode-side surface of the electrolyte. The data reviewed in the contour plots are from the case which achieved peak power density.

The power density has been determined by two methods for this study. Though the scientific jargon describes the power performance as a density as if it were calculated on a per volume basis, the power density is generally calculated as a surface flux using the area of the electrolyte as its basis. These distinctions are not often considered in analysis as most fuel cell electrolytes are flat such that the area of the electrolyte would reflect (i.e. be proportional to) the volume of the cell in model comparisons. When texture is added to the electrolyte in an attempt to enhance mixing, the increase in the area of the electrolyte does not necessarily increase the volume of the fuel cell. This benefit is not reflected in the power density performance parameter. Since the volume of the device is an essential parameter for mechanical engineering applications, the power density is reported as the <u>actual power density</u> based on the actual area of the electrolyte and as the <u>plan power density</u> which is based on the projected area of the electrolyte.

The velocity vectors are compared in this study to qualitatively compare the amount of flow mixing in the flow channel designs modeled. The velocity vectors can be visualized in two ways, either by the use of streamline plots or by the use of vector plots. In two-fluid models, the velocity vectors are used to present data because the mass fluxes contain information about the velocities and local void fractions of both liquid and vapor. In homogeneous (i.e., single-phase) flows, less information is required to characterize the mass flux. In these cases, velocity vectors are sufficient for presenting mass flux data. Pathlines can also be used to visualize the mass flux within the model. The lines represent the paths traveled by particles in equilibrium with the fluid motion. In this study, velocity vectors are used for flow visualization. Since we focused on mixing in the air channel side of the fuel cell, the mass flux data are calculated and displayed on the symmetry boundary in the center of the air flow channel. The data reviewed are from the case which achieved peak power density.

The pumping power considered in this study is calculated from the pressure drop between the flow inlet and outlet. The addition of mixing mechanisms inherently increase the pumping power required for the flow. Since we are attempting to increase the ability of a fuel cell to generate electric power, the parasitic pumping power is an important consideration.

The temperature distribution across the fuel cell electrolyte has little effect on the electrical performance of the fuel cell, but it is an important factor in the mechanical performance of a SOFC fuel cell. A major challenge in the design of SOFCs is ensuring sufficient mechanical stability in the ceramic fuel cell components to withstand thermal expansion rates. Thermal expansion rates vary between materials and are a function of temperature. A large temperature gradient across the fuel cell electrolyte could cause the ceramic to crack. Fuel and air would then be free to crossover to the opposing flow channel. Fuel crossover greatly decreases the performance and function of a fuel cell.

The temperature distributions in this study are calculated at the peak power density and are presented on the electrode-electrolyte interface.

4.1.2 SOFC Reference Case

The first step after developing the model was to validate the code. Validation of a model is usually done by comparing the results to either experimental results or to the results of another independent model, which has the same operating conditions. Sometimes it may not be possible to exactly match all conditions between the model and the test cases due to limitations imposed by modeling assumptions. However, it is important to match the independent parameters as much as possible for a meaningful comparison.

Full experimental or numerical results for solid oxide fuel cell with sufficient details to validate models are very difficult to obtain in literature. However, the SOFC model parameters presented in Pakalapati [48] were used as a reference case with the characteristics listed in Table 4.1. This model presented the most complete set of model input parameters for use in comparisons. The mass flow rates in this case are used throughout the study to determine if the addition of mixing techniques would increase the fuel utilization within a SOFC.

Table 4.1 Properties of SOFC model

Attribute	Value
Geometry	**Plane channel**
Electrolyte area	**40 cm^2**
Air flow rate	**$2.38e^{-6}$ kg/s**
Fuel flow rate	**$2.03e^{-8}$ kg/s**
Air and Fuel Inlet Temperature	**1173 K**
Length[1]	**20 mm**

[1] Length was scaled down from 100 mm in the Pakalapati model to reduce computational time.

The Pakalapati model [48], however, did not present data for validation across a wide range of operating conditions. Pakalapati modeled a fuel cell operating at 300 mAmp/cm^2 and predicted a cell voltage of 0.728 V. In this study, a SOFC operating at similar conditions had a predicted cell voltage of 0.802 V. This difference in output voltage is likely caused by the sum of the effects caused by the differences between the models including, cell length, electrode exchange current density, and fuel composition. To validate the model over a wider range of operating currents, the model was compared to other results in the literature.

Figure 4.1 shows a comparison of the plane channel model's polarization curve with several polarization curves from literature. The Bessler *et al.* model [49] simulates a fuel cell operating at 1073 K. The fuel cell modeled was 50 mm in length. The electrolyte thickness was 200 μm and electrode thickness was 30 μm. In the Ni *et al.* model [50], a two-dimensional SOFC was modeled over a range of parameters. The model chosen for comparison was a planar anode-supported SOFC operated at 1073 K and. The electrolyte in this model was 8 μm thick, the anode 1000 μm, and the cathode 20 μm thick. The Ramakrishna *et al.* model [34] used in this comparison operated at 1273 K. The fuel cell was 40 mm in length and contained a 0.1 mm thick electrolyte and 0.45 mm thick electrodes. The final model in this comparison is from Chan *et al.* [19]. This two-dimensional model operated at 1073 K and contained a 40 μm thick electrolyte, a 50 μm thick cathode, and a 750 μm thick anode.

It is apparent in Figure 4.1 that the operational curve of a fuel cell depends greatly on the operating parameters. A broad comparison like this one is useful to determine if the results of a model reflect reality. For instance, there is a general range of voltages that will be produced by a fuel cell that is operating properly. The voltage of a fuel cell cannot exceed the theoretical maximum voltage, so the Nernst voltage makes a good limiting case solution. Also, the voltage produced by a fuel cell follows a general pattern. The curve shape generated by the FLUENT model is typical of all SOFCs. In many studies, the authors are not concerned with the effects at the extremes of the operating range because practical operation occurs in the central region of the curve where the peak power density exists. As seen in this comparison, Ramakrishna *et al.* were not interested in the low current operating and did not model the activation region of the polarization curve. Likewise the other models were not concerned with the high current extreme and did not model the concentration loss portion of operation.

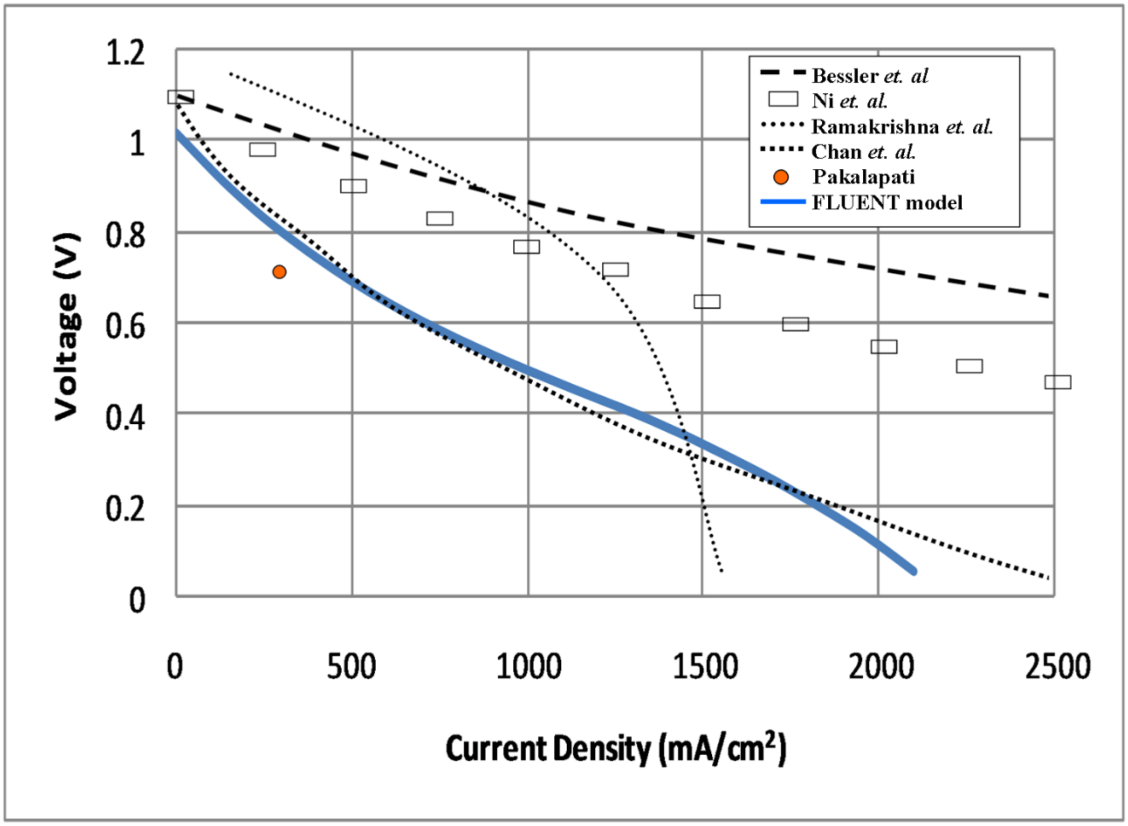

Figure 4.1 Comparison of SOFC polarization curves [19, 34, 48, 49, 50]

Figure 4.1 shows that each model's operation follows the form of the polarization curve as far as the individual interests of the researchers and the fuel cell designs and parameters would allow. Each curve starts at the Nernst voltage particular to the case. As the fuel cell operates at low currents, the activation energy required to initiate the electrochemical reaction is the predominant loss in the cell and decreases the voltage produced by the cell. As current increases, conduction and transport losses become more pronounced. At the highest current levels, the fuel and oxygen reactants are depleted, thus starving the reaction sites and producing a sharp drop in voltage. In this study, only the beginning of the concentration effects was captured. Likewise, the step size between simulated operation points was large in comparison to the range of currents over which the greatest concentration losses occur; hence, the coarse step sizes, combined with the indirect method FLUENT uses to calculate the concentration losses within the fuel cell mentioned in Section 3.2.2, made it difficult to resolve the sharp voltage drop.

Figure 4.2 is a contour plot of the voltage generated at the electrolyte while being operated at peak power density. As mentioned above, the contour plot shows the voltage on the cathode-side surface of the electrolyte. The voltage in the base cell ranged from 0.337 V to 0.395 V. In this diagram, the symmetry boundary that represents the center of the flow channels is the upper edge. The lower boundary is the symmetry boundary that represents the center of the interconnect between flow channels. The boundary that is marked within the contour plot is the boundary between the portion of the electrolyte exposed to the flow channel and the portion connected to the solid interconnect. The fluid flows from the left side of the diagram to the right. The voltage decreases along this direction due to the decrease in reactant concentration in the fluids along the flow path.

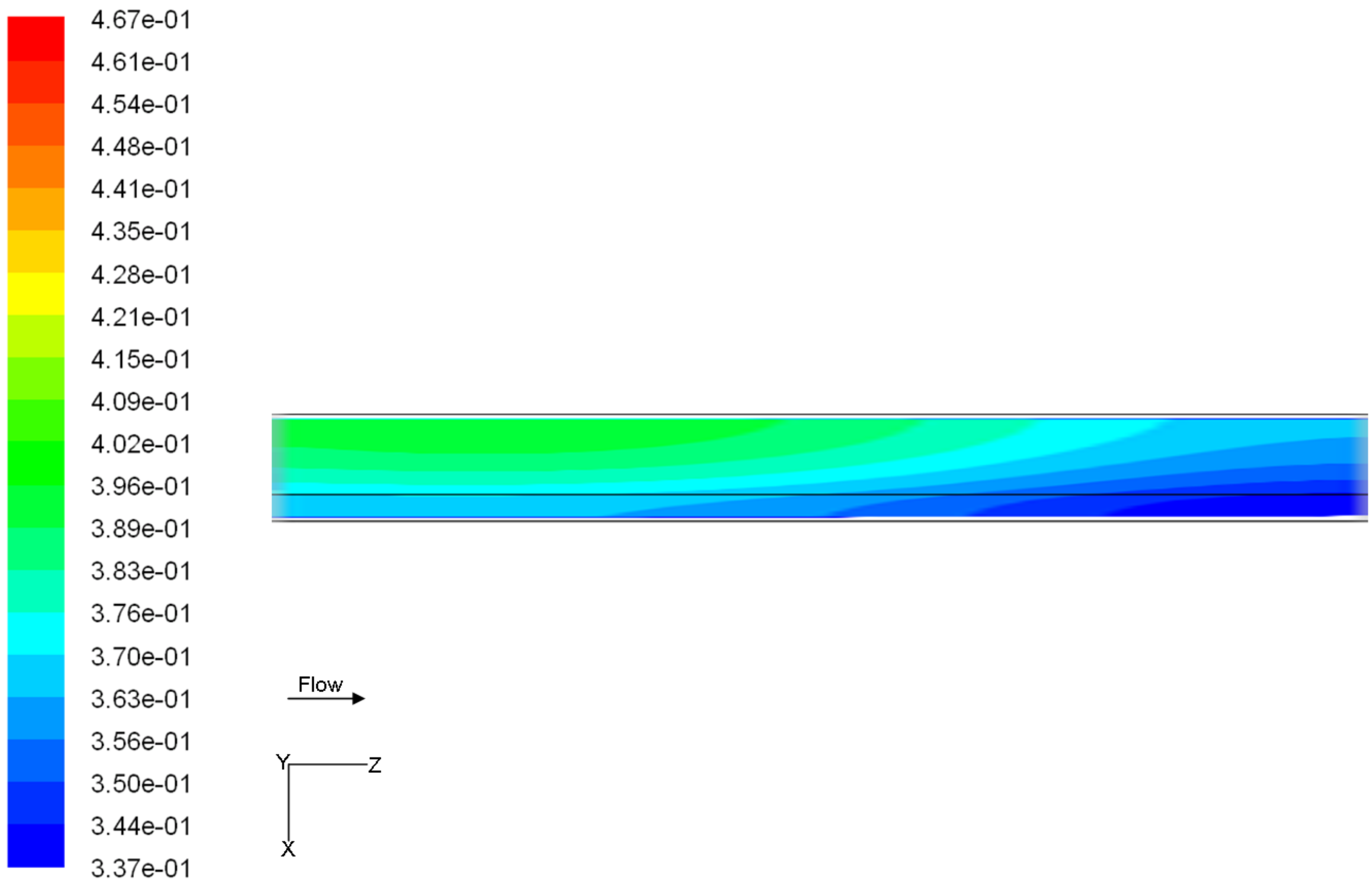

Figure 4.2 Cell voltage distribution on electrolyte in SOFC with plane channel geometry

Power density is derived directly from the polarization curve of a fuel cell. Thus, it is only as accurate as the voltage curve calculated by the model. Figure 4.3 is the power density produced by the plane channel SOFC over a range of operating current densities. Since the power of a fuel cell is a function of current and voltage, $P = IV$, and that voltage has an inverse relation to current, the power density has a parabolic relation to current density. In physical terms, at low current densities, the increase of current is more dominant than the voltage losses. At higher current densities, the voltage losses overshadow the increasing current density so that the net power of the system decreases. Thus, the peak power density calculated in this study was 5254 W/m^2 and occurred at 1300 mA/cm^2.

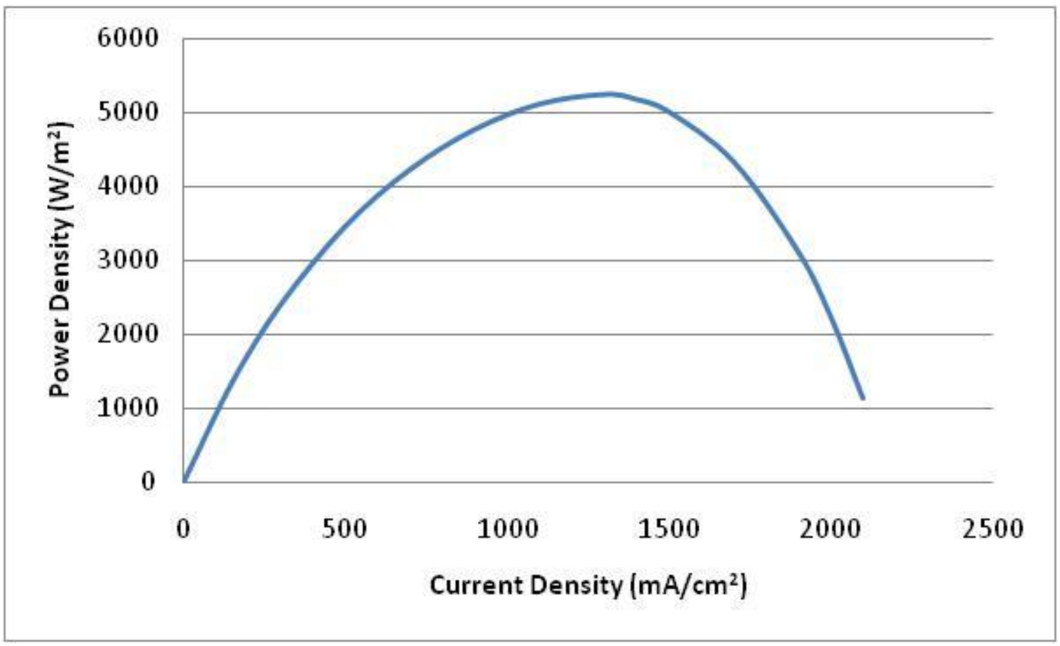

Figure 4.3 Power density curve of a SOFC with plane channel geometry

Figure 4.4 shows the vectors of velocity in the air channel of a SOFC with plane channel geometry. The figure shows typical developing channel flow in the upper channel, which is the air channel. The velocity vectors of the fuel are not displayed in the lower channel in Figure 4.4 because the fuel flow rates are very low in comparison to the air flow rates. As a result, no mixing occurs in the fuel channel rendering the fuel-flow velocity vectors insignificant in this study.

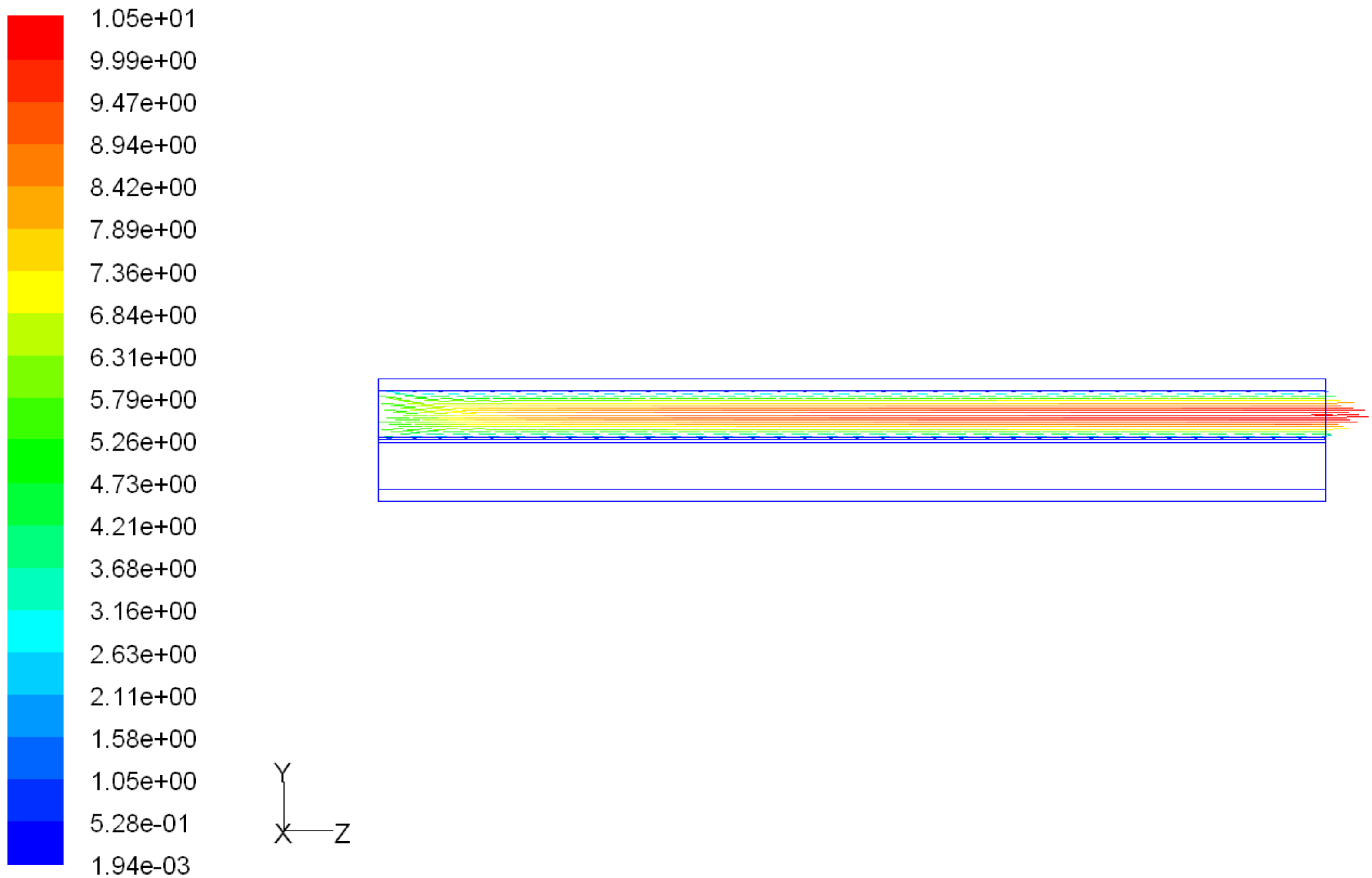

Figure 4.4 Velocity vector plot for a SOFC with plane channel geometry.

Figure 4.5 is a contour plot which shows the distribution of temperature across the plane electrolyte. The temperature of the electrolyte in the plane channel model ranged from 1205 K to 1419 K. In the Pakalapati model [48], the temperature of the electrolyte ranged from 1196 K to 1342 K. The fuel cells in this study do not contain any external heat exchangers, so no external mechanisms affect the temperature of the electrolyte. The air and fuel in this study are assumed to be preheated to a temperature of 1173 K. The elevation of the electrolyte temperature along the length of the cell is due to the exothermic chemical processes and the inability of the fluid flow to remove the heat as the fluid temperature rises. The temperature in the portion of the electrolyte in contact with the interconnect is initially higher than the channel portion because there is no convection to transfer the heat. Along the length of flow, the temperature in the electrolyte contact area is lower than the channel portion due to the limited reactions that can occur in the covered portion.

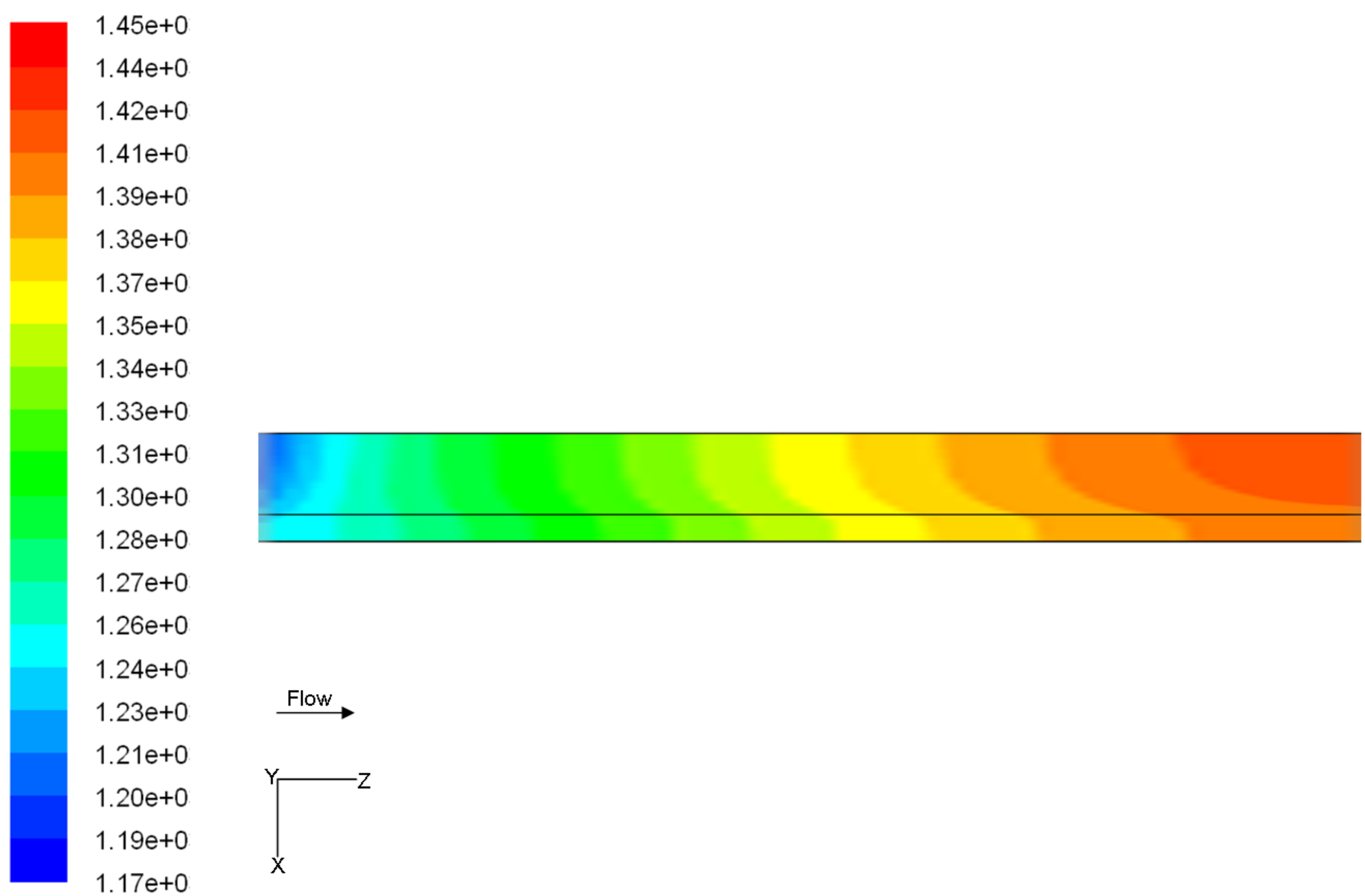

Figure 4.5 Temperature distribution in a SOFC with plane channel geometry

4.2 Hydrodynamic Spacing Study

Before new geometries that might enhance mixing and fuel cell performance were tested in a full fuel cell model, it was useful to simulate simplified, hydrodynamics-only models to determine operable rib spacing. This model contained only the flow channel with typical air and hydrogen flow conditions. The rib spacings tested were based on artificial roughness technology developed for solar air heaters [51].

Solar air heaters and fuel cells are related in that both use low mass flow rates. In solar air heaters, thermal efficiency is generally poor because of an inherently low heat transfer capability between the absorber plate and air flowing in the duct. This can be further attributed to the thick thermal boundary layer which develops in flow with low velocities. Similarly, fuel cells can suffer from low mass transfer capacity between the electrolyte reacting surface and the reactant flow channels. This can be attributed to the equivalent of a thick species concentration boundary layer which develops as reactant species are consumed in the cell and reaction products are introduced to dilute the flow.

The solar air heater field has determined two basic methods for improving performance. The first method involves increasing the area for heat transfer by using corrugated surfaces or fins without affecting the heat transfer coefficient (that is, without affecting the fluid flow). The second method involves increasing the convective heat transfer coefficient by creating turbulence or improved mixing at the heat-transferring surface through the use of artificial roughness [52].

An example of the first method has previously appeared in SOFC literature. The monolithic, or mono-block-layer, fuel cell makes use of a corrugated electrolyte to create compact flow channels, (see Figure 1.7 above). This structure increased the surface area of the reaction plane for electrochemical processes but did not affect the convective heat transfer coefficient. The second method of increasing transfer properties has not been widely studied and is the scope of this study.

4.2.1 Artificial Roughness Geometry

The concept behind artificial roughness in energy devices is simple: produce mixing and/or localized turbulence at the transferring surface while limiting the energy required by pumps to create the flow modifications. The desired condition is to create mixing/turbulence only in the region of flow very close to the heat/mass transfer surface while not disturbing the gross flow in an effort to avoid excessive friction losses. This is achieved by keeping the height of the roughness element small with respect to channel dimension.

The key parameters that guide the design of artificial roughness are the roughness element height (e) and pitch (p). Since these characteristics are considered in reference to the channel dimension, they are usually specified in terms of dimensionless parameters as the relative roughness height (e/D) with respect to channel diameter and relative roughness pitch (p/e) with respect to roughness height [52].

The most important effect produced by the presence of a protrusion, or rib, on the flow pattern, is the generation of two separation regions, one on each side of the rib. The vortices generated are responsible for the mixing/turbulence, as well as in the generation of frictional losses [52]. Prasad and Saini completed a study to understand and optimize the combination of pitch and height for maximum heat transfer enhancement [53]. Figure 4.6 shows the flow patterns downstream of a rectangular rib as the rib height and pitch are changed. Due to flow separation downstream of a rib, reattachment of the shear layer does not occur for a pitch ratio of less than about 8. Maximum heat transfer has been found to occur in the vicinity of a reattachment point. For relative roughness pitch considerably less than 8, reattachment will not occur, thus resulting in a decrease in heat transfer enhancement. An increase in the pitch ratio beyond about 10 will also result in a decrease enhancement. Therefore, there exists an optimum combination of pitch and height for maximum enhancement which needs to be determined for flow in the SOFC flow channels.

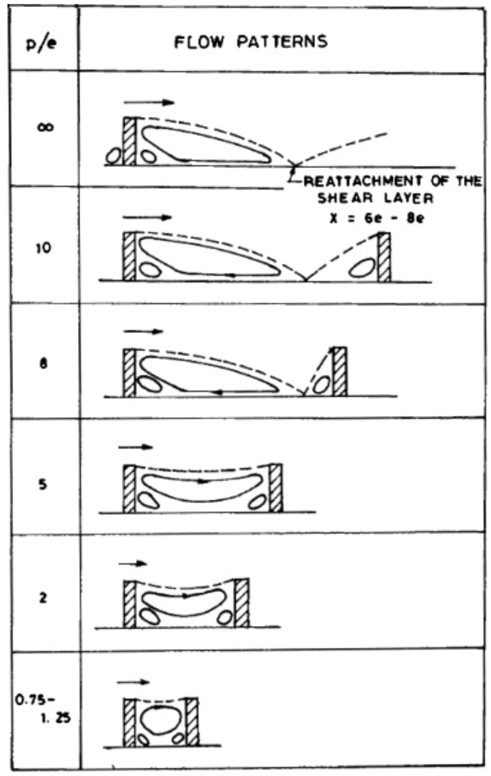

Figure 4.6 The effect of relative roughness pitch on downstream flow pattern [53]

To determine the optimal roughness geometry for the fuel cell modeled in this study, the relative roughness height and relative pitch ratio must be determined. In this study, the flow ducts are 1.0 mm high by 1.5 mm wide. The hydraulic diameter of a duct is the ratio of a duct's flow area to its wetted perimeter. The hydraulic diameter for a rectangular duct is

$$D_h = \frac{2LW}{L+W} \tag{3.20}$$

where W is the width and L is the height of the channel. For the fuel cell geometry in this study, the hydraulic diameter is 1.2 mm. The rib size for the roughness geometry was chosen to be 0.5 mm high by 1.0 mm in length to create a rib that would potentially be easy to manufacture. From this dimension, the relative roughness height is 0.4 mm. The approximate optimal relative pitch ratio from Prasad and Saini was 8, so the approximate pitch for the ribs in the hydrodynamic spacing study was 3.2 mm [53]. Hence, the pitch values studied were 3 mm, 3.5 mm, 4 mm, and 5 mm. Additionally, triangular shaped ribs were tested at a 5 mm pitch.

The flow channel geometry for the hydrodynamic spacing study is representative of the fuel cell geometry. The channel is 1.0 mm by 1.5 mm by 20 mm. To simplify the model for the spacing study, only two ribs were created in the geometry. These ribs were placed 7.0 mm down the length of the channel so that they were beyond the entrance effects of the flow. A generic geometry is shown in Figure 4.7. The meshing scheme for this geometry was 40 by 15 by 200 nodes to pick up the flow details around the rib down the length of the flow. To maintain continuity between the hydrodynamic study and the fuel cell study, the flow conditions in Table 4.1 fuel cell model are also used in the hydrodynamic study.

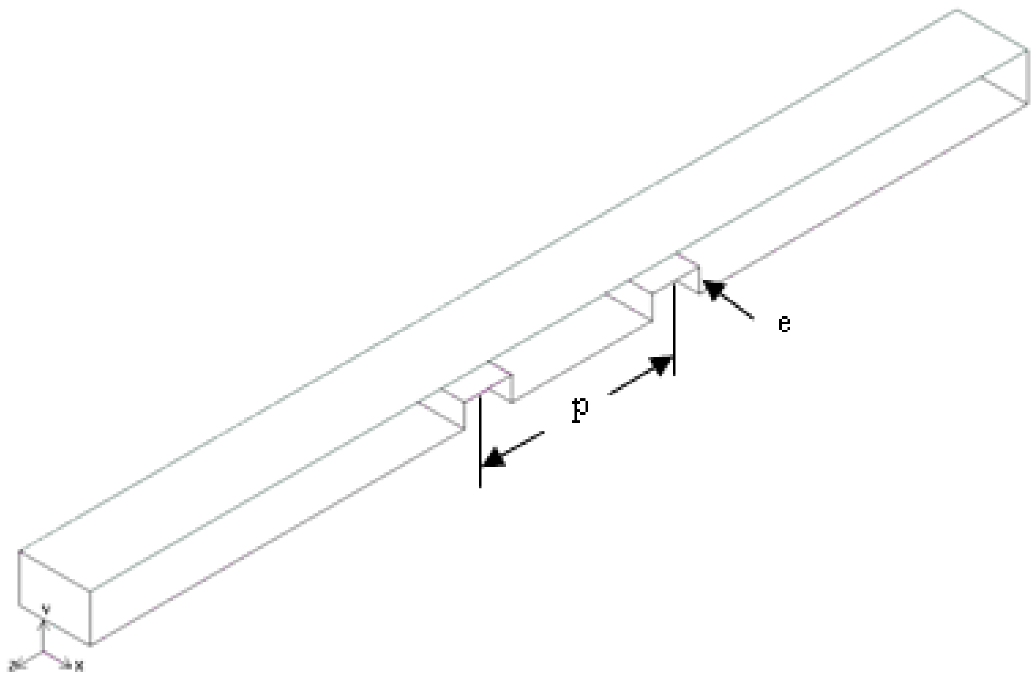

Figure 4.7 Artificial roughness geometry where e is the height of the roughness and p is the pitch

4.2.2 Hydrodynamic Spacing Study Results

The results from the hydrodynamic study were analyzed qualitatively based on the mass flow characteristics. As mentioned above, velocity vector plots are used to depict the mass flow and any mixing that occurred in the cases studied. The velocity vectors are presented on the symmetry boundary to avoid interference from side-wall effects. Figure 4.8 shows the velocity vector plot for each hydrodynamic model.

Figure 4.8.A shows the 3 mm relative pitch geometry modeled with air flow. This case is an example of a flow where separation occurs without reattachment occurring ahead of the following rib. The flow increases velocity as it travels across the rib and begins to flow into the space between the ribs. However, the flow near the wall between the ribs in a single recirculating region rather than the two regions which would indicate flow reattachment geometry.

Figure 4.8.B shows the 3.5 mm relative pitch modeled with air flow. This case achieves reattachment of the flow to the wall. Notice how the flow only has a small attached flow area before the flow is forced to separate again. This reattachment-separation point creates optimal enhancement. The 3.5 mm pitch design was further developed for the SOFC model.

Figure 4.8.C shows that 4 mm relative pitch geometry modeled with air flow. This case shows continued reattachment of flow with the wall between the ribs. Figure 4.8.D shows the length of reattached flow extending in the 5 mm pitch air channel. These two cases demonstrate the separation and circulating flow pattern desired; however, the length of reattached flow between the ribs must remain minimal in an optimal rib design. The reattachments points are the essential component of the enhancement. The extended attached flow area represents unenhanced flow area.

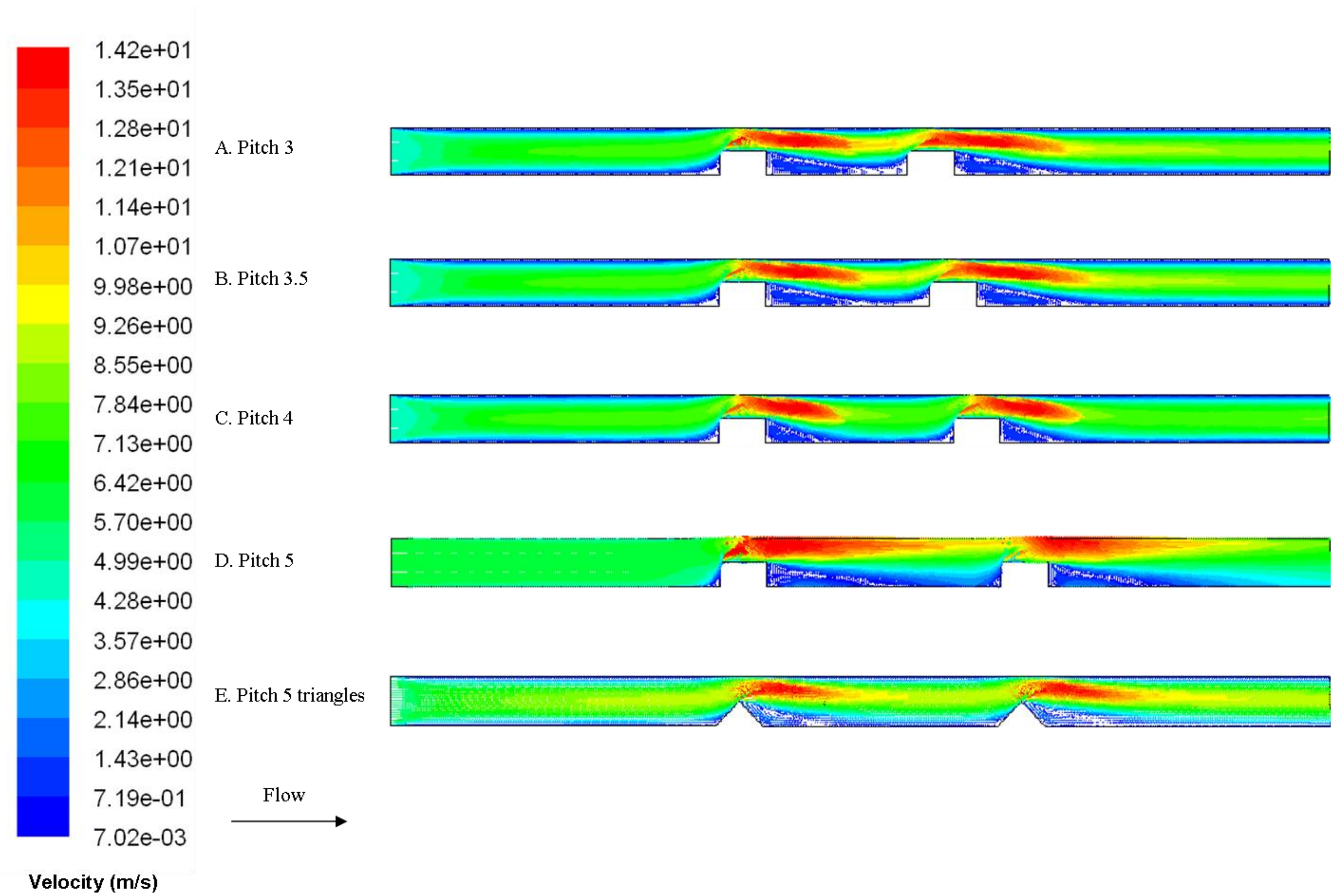

Figure 4.8 Velocity Vectors of air flow channels with rib protrusions

Triangular ribbed geometries produce similar results, as shown in Figure 4.8.E, the 5 mm pitch triangular ribbed geometry. The air flows over the rib with a less significant recirculation region prior to the rib and produces a recirculating region in the shadow of the rib. Like the rectangular ribbed model, the flow has reattached for two thirds of the length between the ribs.

The fuel flow hydrodynamic studies were less successful than the air flow studies. Figure 4.9 shows the 3 mm, 4 mm, 5 mm pitch rib geometry and 5 mm triangular rib geometry fuel channels flows. In these cases the flow increases velocity as the flow moves over the ribs; however, the flow quickly returns to the average fluid velocity downstream of the rib. This figure shows that the flow remains attached to the rib as it passes over. The flow continues downstream and there is no recirculation region. The flow attachment is due to the highly laminar nature of the flow inherent in the low mass flow rate of fuel in the SOFC model.

4.2.3 Hydrodynamic Study Conclusions

Base on this preliminary study, a rib pitch of 3.5 mm was selected for development in a full electrochemical model of a SOFC channel. This represents a relative roughness pitch of 7 which agrees with the information given in the solar air heater literature [53].

Due to the low flow rate of the hydrogen fuel, the hydrodynamic spacing study indicated that mixing was not achievable in the hydrogen flow channels. Therefore, fuel channel ribs were not developed for the fuel cells in the following study.

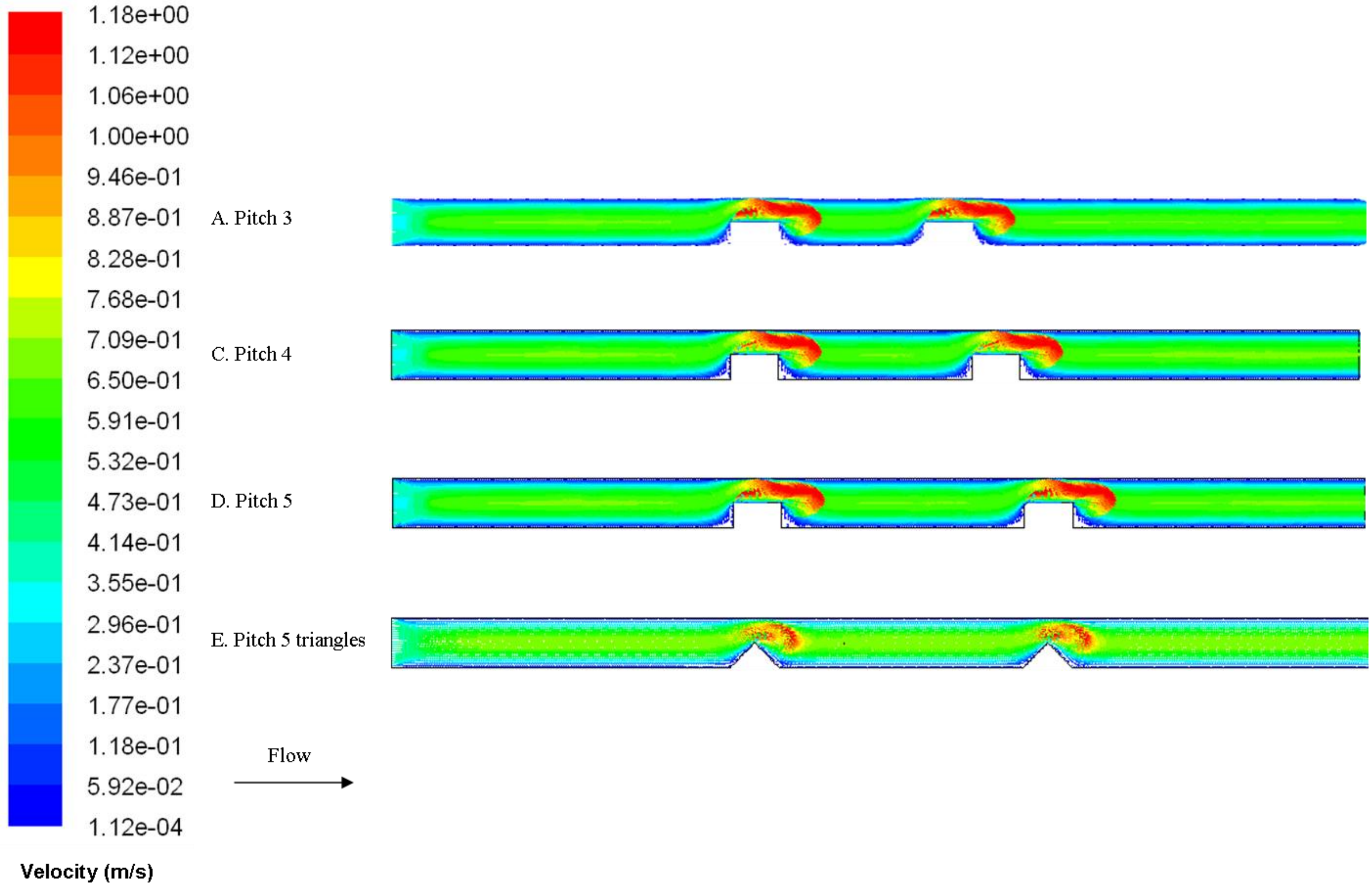

Figure 4.9 Velocity Vectors of fuel flow channels with rib protrusions

4.3 Comparison of SOFC Performance with Enhanced Geometry

The SOFC channel model allows us to study the effects of design changes of a fuel cell's performance without requiring a full model which would be computationally expensive. To reduce the computational demands of the study, the results from the above hydrodynamic spacing study were used to guide the rib spacing in the SOFC geometries studied.

As in the base case outlined in Section 4.1, the parameters compared in this study are velocities (presented as vectors), power density, pumping power, fuel cell voltage, fuel utilization, and temperature (presented as contours). Recall that the voltage reported in this study will be reported as a plot of surface averaged values and in a contour plot visualization. The power density is reported as the actual power density, based on the actual area of the electrolyte and as the plan power density, based on the projected area of the electrolyte. The velocity vectors are used to depict mixing in the flow channels. The pumping power is reported in a plot determined from the pressure drop between the flow inlet and outlet. The temperature distribution in this study is reported in contour plots to qualitatively describe the temperature gradients in the cells.

The contour and vector plot data presented here are from data corresponding to an input current of 0.56 Amp. This value is in the region of the polarization curve in which regular fuel cell operation occurs and was chosen to maintain continuity between the results presented.

4.3.1 Description of Channel Geometries

Six SOFC electrolyte designs were compared in this investigation. These designs included a plane channel control case, a porous cathode ribbed case, three sawtoothed electrolyte cases, and a parallel ribbed case for further comparisons. Descriptions of these geometries can be found in Table 4.2. S of these fuel cell channels can be found in Figure 4.10.

Table 4.2 SOFC Geometry Electrolyte Area

Geometry	Area in mm^2	% Increase relative to plane channel
Plane Channel	**40**	**-**
3.5 mm Pitch Ribs	**40**	**0**
Sawtooth 1	**46.4**	**16**
Sawtooth 2	**41.6**	**4**
Sawtooth 3	**46**	**15**
Sawtooth 4	**46**	**15**

Figure 4.10.B shows the first flow field design with two ribs with a pitch of 3.5 mm built into the porous cathode material. The ribs were made part of the electrode for two reasons. First, in fuel cell manufacturing, it would be simpler to print extra material at the rib locations while applying the cathode layer or to mill the material around the ribs out of the channel, than to introduce a new non-porous rib material. Second, the porous nature of the rib allows for the reactant species to more easily diffuse to the triple phase reaction boundary (TPB) at the electrolyte than a non-porous rib would.

Figure 4.10.C shows the sharp edged sawtooth design. It utilizes a trailing edge at a pitch of 3.5 mm similar to a continuous rib pattern design. The design uses repeat units to create multiple separation and reattachment locations. The design also increases the area of the TPB which will increase the reaction occurring in the fuel cell.

Figure 4.10.D shows the gradual edged sawtooth design, which utilized a symmetrical chamfered rib with a 3.5 pitch to create mixing. The design allows us to determine the effect of the shape of a rib obstruction on the flow pattern.

Figure 4.10.E shows the compact sawtooth geometry. The compact sawtooth was created to have a similar TPB area as the sharp edged sawtooth design to limit the effect of area on the performance comparison of the two designs.

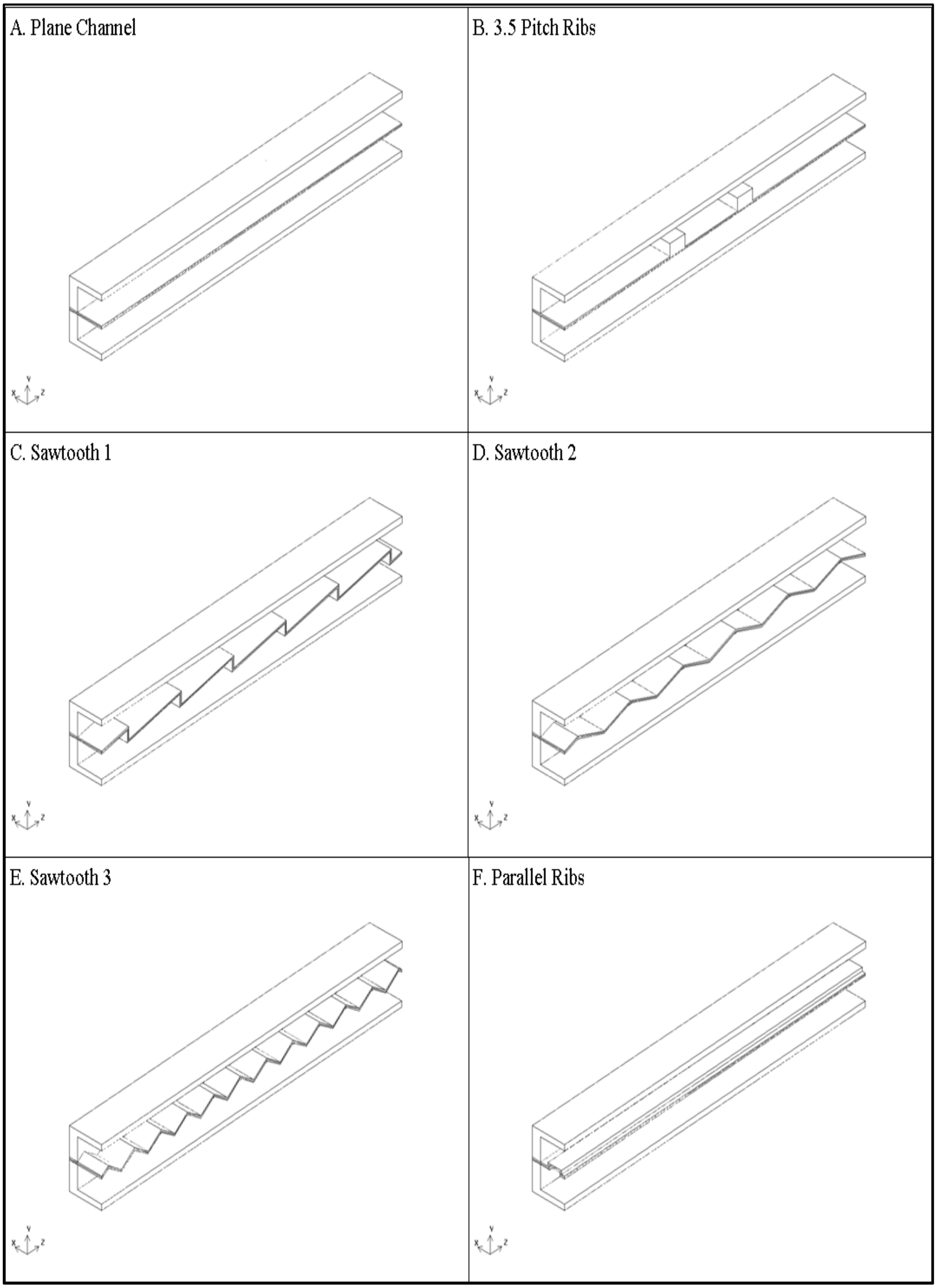

Figure 4.10 SOFC half channel geometries

Figure 4.10.F shows the final rib design with a rib that runs in parallel with the flow along the length of the channel. This design was created to compare the performance increase of the sharp edged sawtooth channel design and the compact sawtooth channel design. The parallel rib channel design shares the 46 mm^2 area of the two channel designs; however, it does not contain any artificial roughness so that no mixing would be induced in the flow stream. This fuel cell design can be considered a baseline comparison case for the mixing designs of similar area.

Of these designs, only the 3.5 mm pitch rib case is a true roughness rib. The sawtooth electrolyte designs were favored because the designs inherently increased the reaction area of the cell, which boosts fuel cell production. The parallel rib case was created to compare the enhancement of the fuel cell from the increased area but without the added effect of artificial roughness. The gradual edged sawtooth also allows us to study the effect of area on fuel cell performance, since it has a smaller electrolyte area than the other sawtooth flow designs. The area of the reaction surfaces of each of the cells is found in Table 4.2.

4.3.2 Comparison of Mixing in SOFC with Enhanced Geometry

4.3.2.1 Cell Voltage

The cell voltage of a fuel cell is a good indicator of how well the fuel cell is producing electrical energy and how easily the reactants are being transported to the TPB reaction sites. The former consideration is easily determined from the polarization curve over a range of operating conditions. The useful electrical energy being produced by the cell will be reflected in the voltage measured across the external circuit of the cell. The latter performance consideration is more easily understood by viewing the contours of voltage at the TPB. In these images we can visualize where the reactions are occurring readily and where the reactions occur more slowly.

Figure 4.11 is a comparison of the cell voltage of a single channel SOFC operating with the different flow channel designs. Each curve starts at the same theoretical potential showing that each fuel cell has the ability to operate at the same level. However, the losses in each fuel cell model show how design parameters can affect performance in different manners. As the fuel cell operates at low currents, the activation losses in each design produce similar voltages. As current increases, there are fewer losses in the three cases with increased actual electrolyte area: Sawtooth1, Sawtooth3, and the parallel rib case. After 1400 mA/cm^2, where the peak power density is measured, the voltage in the Sawtooth3 case decreases more rapidly than the Sawtooth1or parallel rib case. Sawtooth2, the gradual sawtooth design, showed a small increase in voltage over the plane channel case. This reflects the small increase in area of the design over the plane channel. The Sawtooth1, Sawtooth3, and the parallel rib designs showed similar voltage increases roughly proportional to the increase of area of the electrolyte. Table 4.3 compares the area and voltage increase of the designs from the plane geometry at 0.56 Amp. The cathode rib case showed decreased concentration losses at high currents, which was the desired goal with the used of mixing techniques. However, the voltage of the cathode rib case is slightly lower than the plane case at low and moderate currents. This strange behavior of the cathode rib case can be better understood by studying the contours of current.

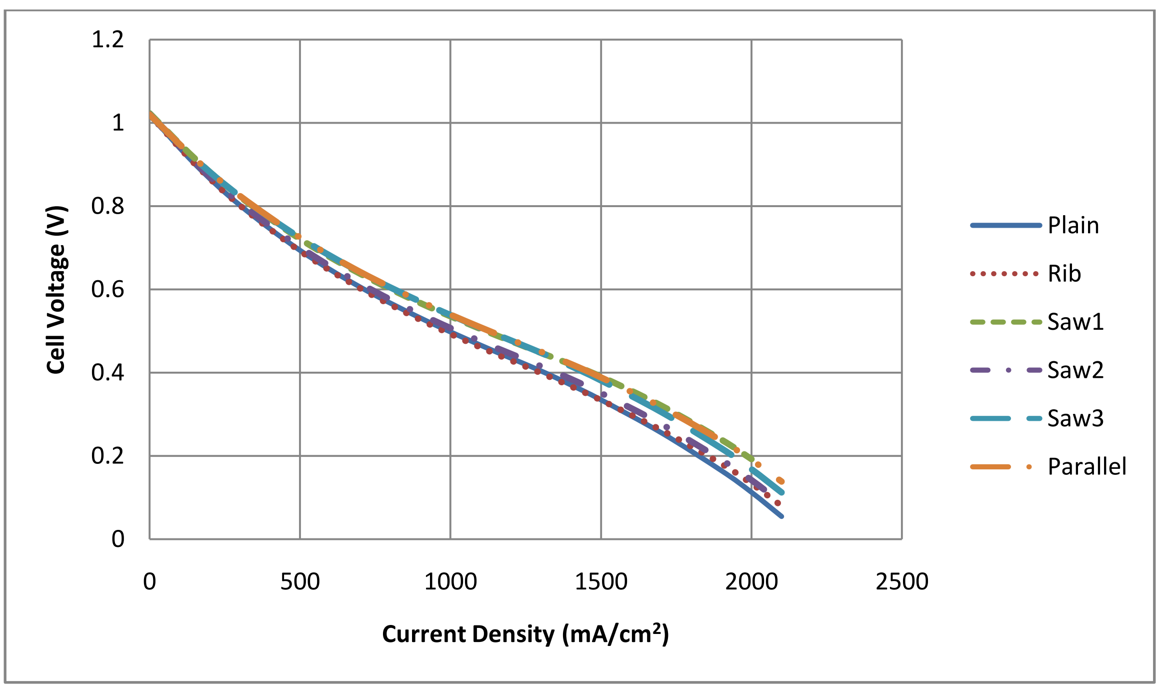

Figure 4.11 Polarization curve comparing the cell voltage of the SOFC flow designs at various current operating conditions

Table 4.3 Comparison of cell voltage increase with electrolyte area increase at peak power density

Geometry	% Increase in Electrolyte Area relative to plane channel	% Increase in Voltage relative to plane channel
Plane Channel	**-**	**-**
3.5 mm Pitch Rib	**0**	**-0.9**
Sawtooth1	**16**	**13.3**
Sawtooth2	**4**	**3.8**
Sawtooth3	**15**	**12.1**
Parallel Rib	**15**	**13.5**

The voltage contour plot in Figure 4.12 shows how well the voltage is being produced at specific locations on the electrolyte. Figure 4.12.A shows the voltage being produced in the plan channel fuel cell. The limitations to reactions under the current collector are apparent by the low voltage at the edge of the cell. The wall effect from the velocity boundary layer on the current collector wall can also be seen. The flow along the wall has a low velocity causing the reactant concentration near that wall to dilute with products. This is apparent from the greater voltage near the symmetry boundary and the thickening of the low voltage region along the length of the flow.

The transport limitations caused by the two porous ribs in case B are apparent from Figure 4.12.B. The voltage produced is highest as the air flow enters the channels since there is the greatest concentration of reactants. The voltage level decreases towards the outlet of the cell, which is expected as fuel and oxygen are depleted from the cell; however, Figure 4.12.B also shows two regions of decreased voltage near the center of the cell. These represent the locations of the porous ribs. The ribs are sufficiently thick to inhibit the diffusion of oxygen to the electrolyte under the ribs. The path the molecules must take is tortuous so the reactants take a longer time and more difficult path while diffusing to the TPB to react. Beyond the ribs, the voltage of the ribbed case is greater than the plane channel case. This is because fewer reactions can occur under the porous ribs, thus, there are more reactants available near the outlet of the cell as compared to the planar case. This helps explain why the ribbed case generated higher voltage than the planar case at high current densities. In effect, the ribbed fuel cell does not run out of reactant fuel as quickly as the plane channel case.

The sawtooth 2, or gradual sawtooth, geometry shows a slight voltage increase over the planar and ribbed cases in Figure 4.12.D. The area of the electrolyte in this design increased 4% and is responsible for much of the increase. In this design we can begin to see the effect of sawteeth on the performance of a cell. Along the inclining portion of the electrolyte, the voltage decreases and along the declining portion the voltage increases. This effect mainly occurs under the current collector, and it is likely that the reactants are consumed before they can fully diffuse under the solid structure.

Figure 4.12 parts C, E, and F show the voltage contour plot of the cell designs with the greatest increase in electrolyte area over the plane channel case. The voltage generated in these cells is greater than the plane channel and cathode ribbed cases. This is likely due to the increased cell area and decreased actual current density. Like the gradual sawtooth contour plot, these plots show an increased voltage in the troughs and a decreased voltage at the peaks of the ribs. Since, the contour plot of the parallel rib case in Figure 4.12.F shows an increased voltage as compared to the control case. This seems to indicate that the increased voltage is a function of the increased area.

The effect of increased reaction area can be further understood from the locations of the current density on the electrolytes in the cell designs. In Figure 4.13, it is apparent that that plane channel and the ribbed case have a greater current density than the cell designs with increased area. This is inherent in the operation of this model. Current is set by the user and must be distributed across the entire area: the greater the area, the more diffuse the current is. In Figure 4.13, the current density is greatest near the edge of the current collectors. This is caused by the gathering effect as the current travels towards the external circuit. The current density is low at the entrance because there is no reactant flow into the electrodes at the entrance and a limited amount of reactants have managed to diffuse to the TPB surface. The current density is greatest at the portion of the electrolyte where the most reactions occur. On the other hand, the polarization losses on the voltage increase with current, so the elevated current densities in the fuel cells with smaller areas explain low voltages seen in Figure 4.12.

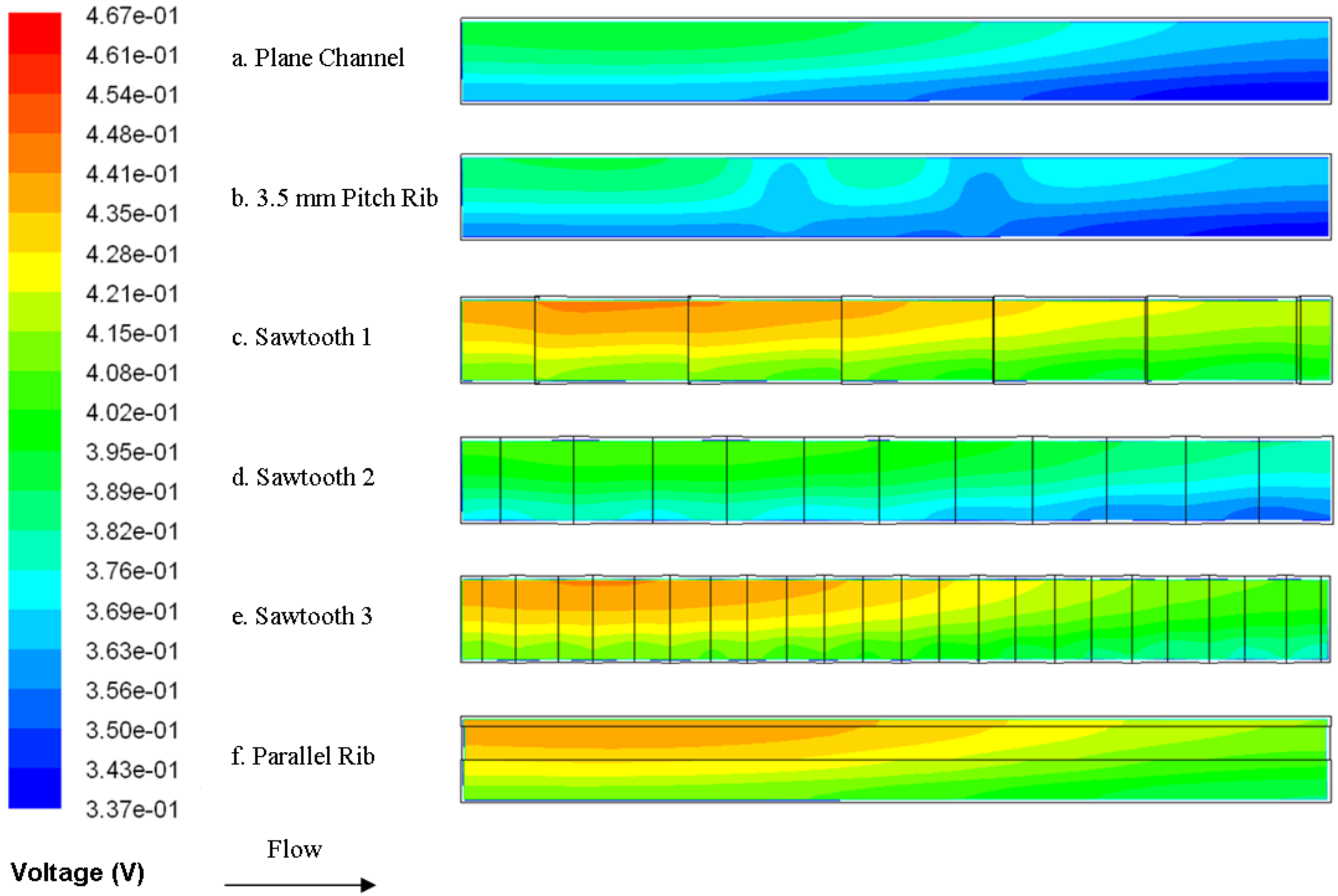

Figure 4.12 Cell voltage contour plot comparison of a single SOFC flow channel with varying geometries

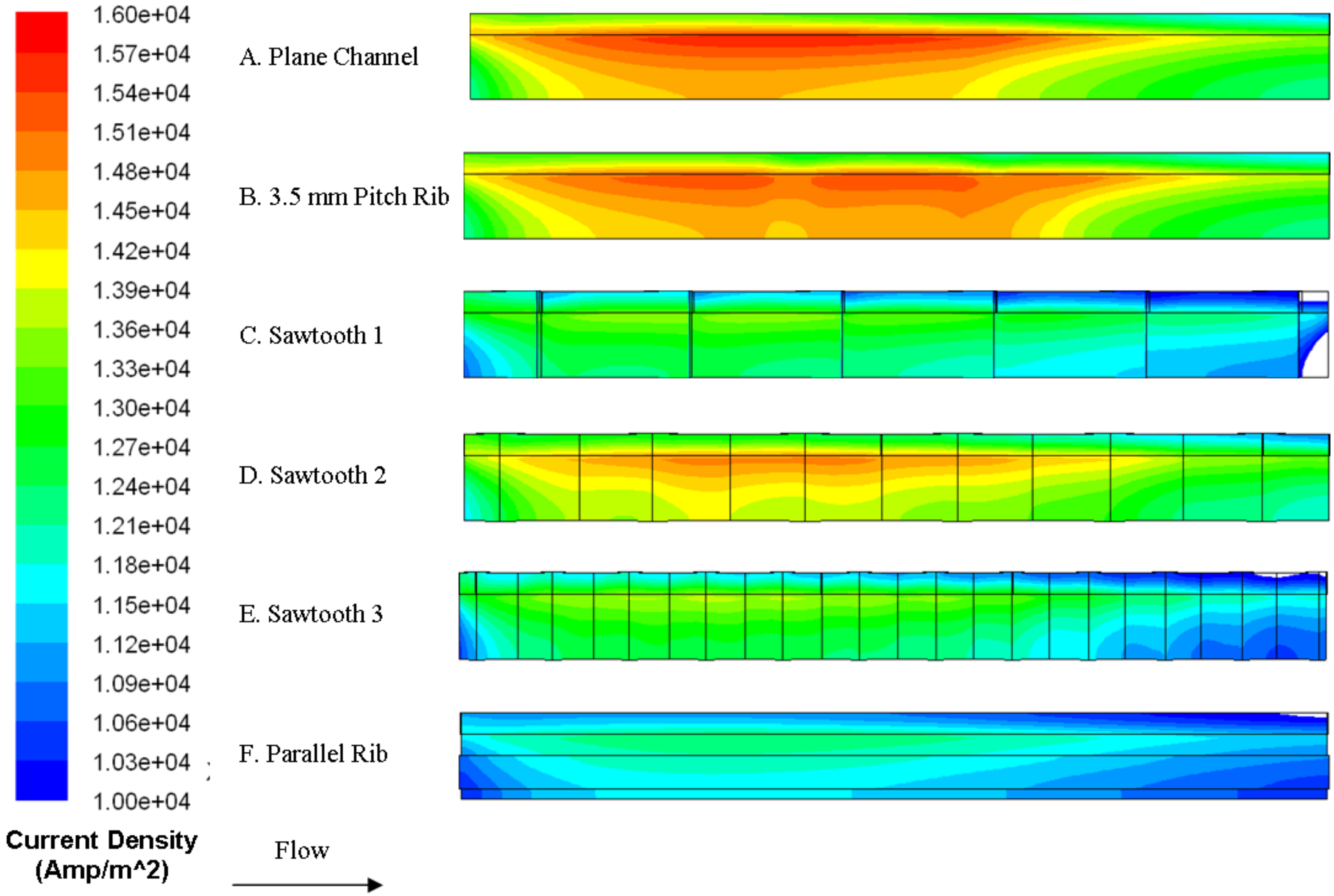

Figure 4.13 Current density contour plot comparison of a single SOFC flow channel with varying geometries

4.3.2.2 Power Density

The power density of a fuel cell is another valuable indicator of how well the fuel cell performs. After all, the purpose of a fuel cell is to generate power. It is standard practice in the fuel cell field to present the power production capability of a fuel cell as value averaged over the area of the electrolyte. This allows cell designs from different laboratories or manufacturers to be compared easily. From an engineering standpoint it would be more interesting to know the *volumetric* power generating capacity, which is more useful when building the fuel cell into a building, automobile, or cell phone. To do this, the power would have to be averaged over the volume of the fuel cell. In the traditional planar fuel cells, the commonly used area power density is proportional to the volumetric power density; however, as we increase the electrolyte areas in this study while maintaining the cell volume, the traditional power density does not make as useful a comparison. For this reason, the power densities presented here are calculated from both the plan area and the actual area.

Figure 4.14 shows the power density based on the plan area of the SOFC electrolyte. Since the power is calculated solely from the information in the polarization curve (Figure 4.11), it is expected that the plane channel and rib geometries would have the lowest power densities. In fact, the percent increase in power density in the data compared at 0.56 Amp is the same as the percent increase in voltage at 0.56 Amp (Table 4.4). The SOFC designs with the greatest electrolyte area generated the highest voltage curves above and have the highest peak power density in Figure 4.14. It is also important to note the shift in the peak power density to higher currents for the fuel cell designs with mixing devices. This indicates that the mixing devices allow the fuel cell to utilize more of the reactants at high currents when the reactants are more dilute.

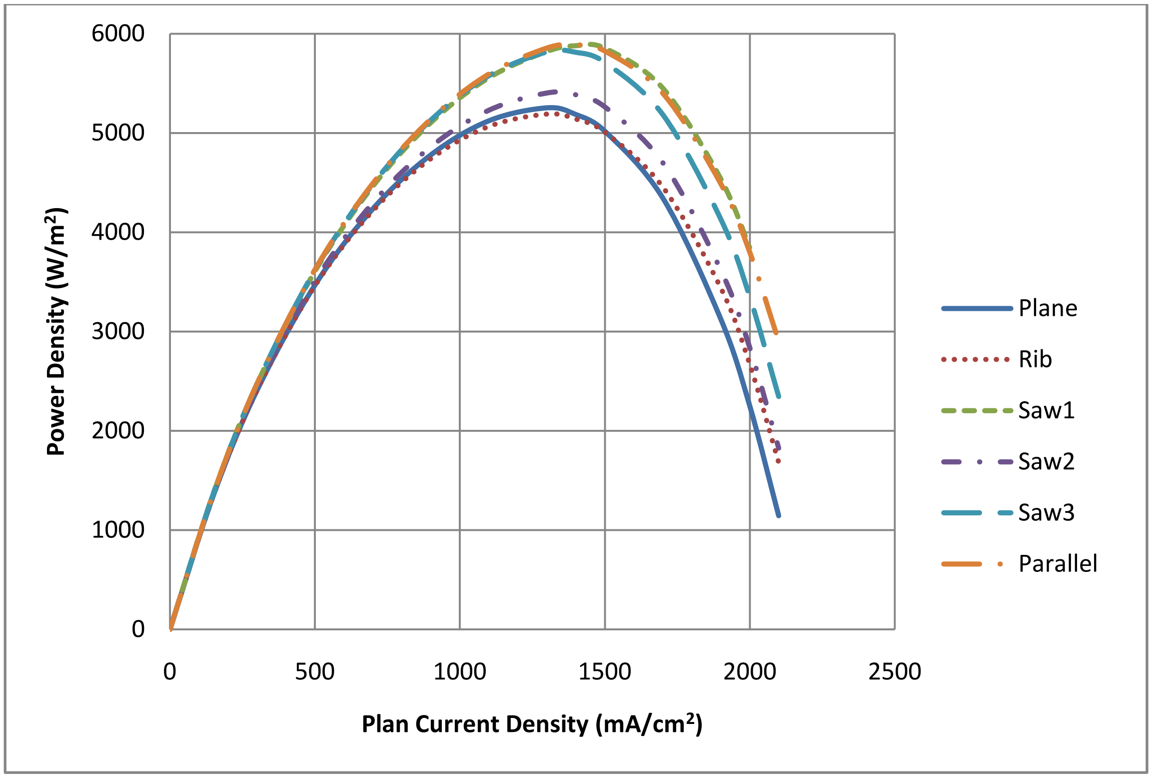

Figure 4.14 System power density based on electrolyte plan area

Table 4.4 Comparison of power density (plan area) increase with electrolyte area increase at peak power density

Geometry	% Increase in Electrolyte Area relative to plane channel	% Increase in Power Density relative to plane channel
Plane Channel	-	-
3.5 mm Pitch Rib	**0**	**-0.9**
Sawtooth1	**16**	**13.3**
Sawtooth2	**4**	**3.8**
Sawtooth3	**15**	**12.1**
Parallel Rib	**15**	**13.5**

However, the increase in power density is not seen when comparing the fuel cell designs by their actual electrolyte area, Figure 4.15. To give this plot additional meaning, this curve represents the power density proportional to the materials needed to form the more complex electrodes and electrolyte. In Figure 4.15, the cell designs with mixing devices achieve a lower power density than the plane channel case. The change in power density with respect to the plane channel geometry is given in Table 4.5. In the rib case, this decrease in power density is likely caused by the increased concentration polarization losses under the ribs (Figure 4.12). The parallel rib case also underwent a decrease in power. This could indicate that the decrease in power among the cells with increased area may be due to the decrease in fuel relative to the reacting surface. The results interpreted based on the actual area of the cell also indicate that the mixing devices did not enhance the performance in the manner desired. To understand the limitations of the mixing techniques, the velocity vectors are presented below.

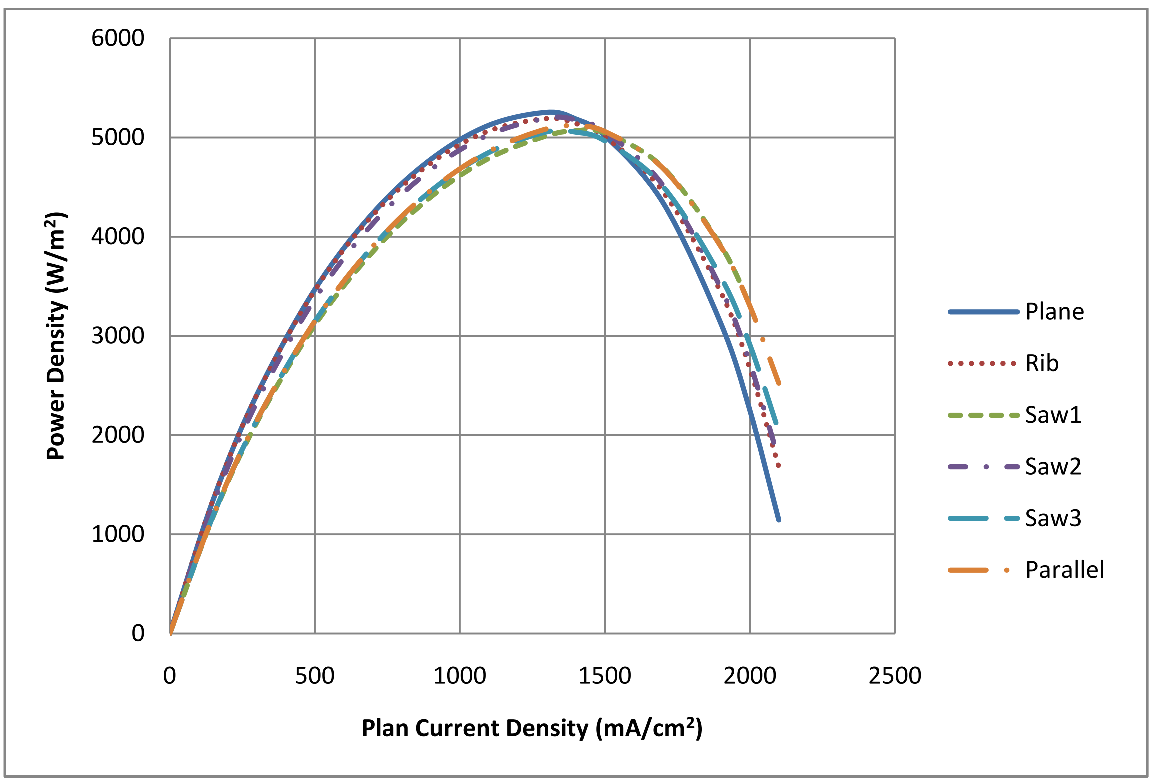

Figure 4.15 System power density based on electrolyte actual area

Table 4.5 Comparison of power density (actual area) increase with electrolyte area increase at peak power density

Geometry	% Increase in Electrolyte Area relative to plane channel	% Increase in Power Density relative to plane channel
Plane Channel	-	-
3.5 mm Pitch Rib	**0**	**-0.9**
Sawtooth1	**16**	**-2.3**
Sawtooth2	**4**	**-2.1**
Sawtooth3	**15**	**-2.5**
Parallel Rib	**15**	**-1.4**

4.3.2.3 Velocity Vectors

The velocity vector plots let us visualize the flow patterns in each test case to understand the reactant flow that occurs in the SOFC channel designs. The results give us a qualitative look at the amount of mixing that was achieved by each design. Figure 4.16.B shows the velocity vector representation of mixing in a SOFC air flow channel with two porous cathode material ribs. Here we can see the flow is affected by the ribs. The velocity of the flow increases above the rib as a portion of the bulk flow avoids the obstacle; however, the porous rib was not as productive in generating mixing as a non porous rib. The momentum of the flow allows air to diffuse through the porous ribs at a nearly unaffected velocity. The flow that is diffusing through the trailing edge of the rib fills the separation region which might have resulted in a solid rib cases limiting the effect of enhanced mixing.

Figure 4.16.C shows the velocity vector plot of the mixing generated in the sharp edged sawtooth design. The bulk of the flow is swept over the sawtoothed rib sections and recirculation regions are evident in the shadow of each sharp edge. The flow reattaches to the electrode wall midway along the following incline and separates again after the next channel diameter change. This is the desired flow separation and

reattachment for enhanced mixing and heat transfer; however, it is possible that mass transfer concentration losses within the separation region counteracted the improvements that occurred elsewhere along the flow.

Figure 4.16.D shows the velocity vector plot of the mixing generated in the gradual 3.5 mm pitch sawtooth design. The mixing in this design occurs to a lesser extent than the sharp-edged sawtooth design. As the flow passes over the ribs, it settles more smoothly back to the electrolyte surface and there is limited recirculation at the base connecting each rib pair.

Figure 4.16.E shows similar results as the gradual sawtooth design. As the bulk of the flow passes above the sawtooth ribs, the fluid between the ribs separates from the electrode surface and recirculates. The flow does not reattach to the TPB surface until the peak of the following rib. This design further demonstrates that mixing can be generated in fuel cell flow channels; however, the fact that the flow does not reattach until the crown of the next rib results in a non-ideal mixing profile for enhancement.

Figure 4.16.F shows the velocity vector plot of the flow in the parallel rib channel design. Because there is no artificial roughness in the channel, the flow acts the same as a plane channel flow with a slightly elevated velocity due to the decreased channel area.

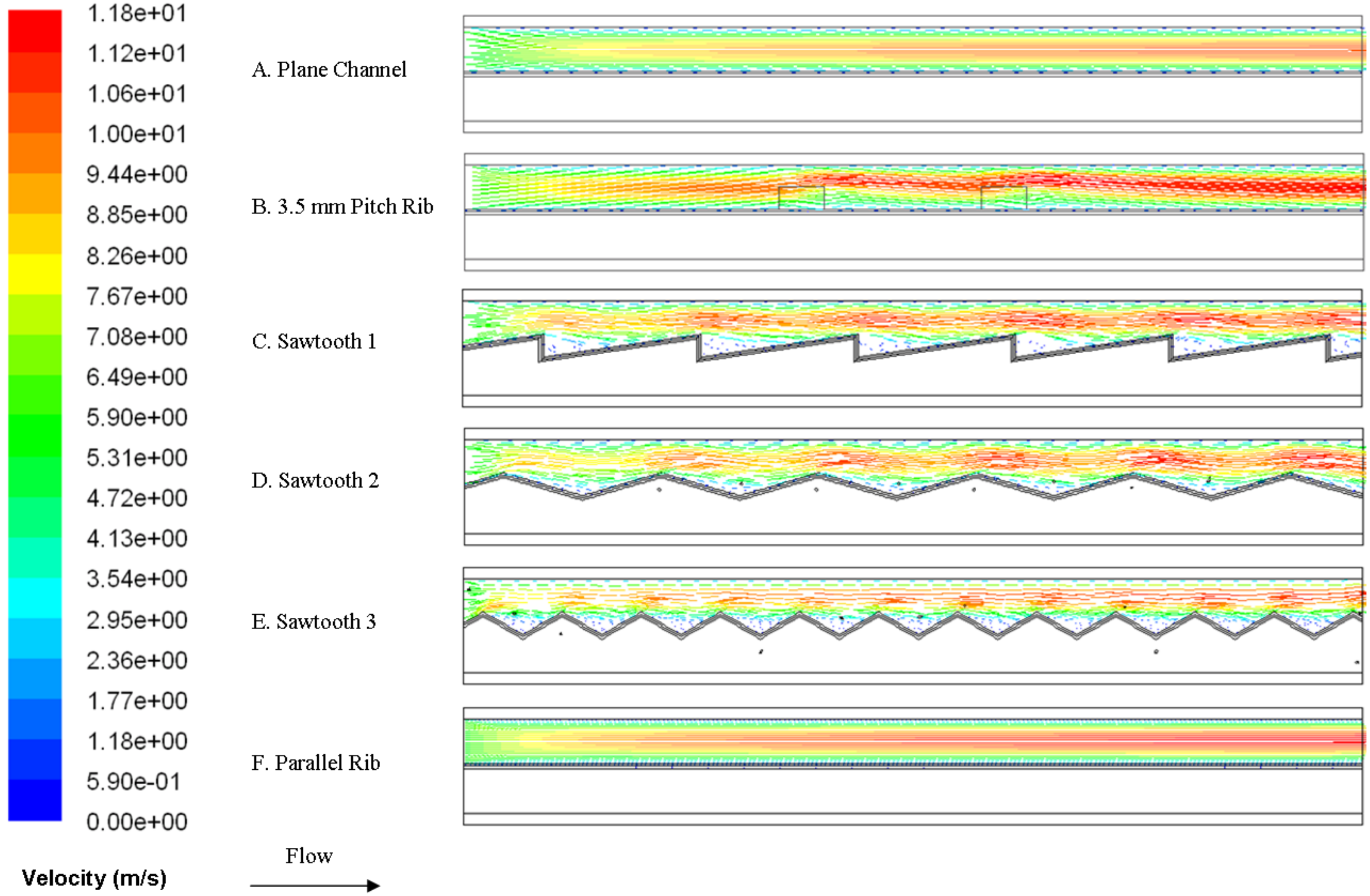

Figure 4.16 Velocity vectors of SOFC with varied geometry

4.3.2.4 Pumping Power

The buildup of pressure in the flow channels is one of the detriments of the use of mixing techniques to increase the performance of energy systems. In each fuel cell design, the pressure increases on the incline of the ribs due to the narrowing of the flow channel. As the pressure increases, more energy is required to pump the fluid through the flow channels. It is illogical to include these enhancement techniques if the net power gained is not sufficient to generate the power needed for pumping. Because the flows in SOFC have such low velocities, the pumping power required for the flows is very low (Table 4.6). Even a 94% increase in pumping power only results in 0.5 mW of increased power required. Since, the cells produce over 5000 W/m^2, or 0.2 W, the power required for pumping is insignificant, requiring less than 1% of the power produced in the fuel cell.

Table 4.6 Comparison of air pumping power increase with the addition of mixing techniques

Geometry	Pumping Power (W)	% Increase in Pumping Power relative to plane channel	% of Power produced by fuel cell required for pumping
Plane Channel	**2.59E-04**	**-**	**0.12**
3.5 mm Pitch Rib	**3.44E-04**	**33.2**	**0.17**
Sawtooth1	**3.93E-04**	**52.0**	**0.17**
Sawtooth2	**3.59E-04**	**39.0**	**0.17**
Sawtooth3	**5.02E-04**	**94.0**	**0.22**
Parallel Rib	**3.45E-04**	**33.5**	**0.15**

4.3.2.5 Temperature Distribution

The temperature gradients across a SOFC are an often overlooked performance parameter. As the temperature of the ceramic components of a fuel cell increases, the materials expand at different rates depending on their coefficient of thermal expansion.

If there are large temperature gradients in the cell, part of the material could expand less than another part causing the material to crack. To prevent these failures, the heating of the fuel cell must be controlled. The main source of heat in the fuel cell is ohmic heating. This heat must be carried away via conduction within the solid materials and convection in the fluid. Figure 4.17 shows the temperature profiles on the electrolytes of each cell design. The profile in Figure 4.17.A is a typical temperature profile for planar SOFCs. The area under the current collector is at a lower temperature because there are fewer reactions to generate heat. The temperature in the cell steadily increases along the channel as the reactant fluid gains heat from the electrolyte. As the fluid heats, the temperature gradient between it and the heated surface decreases and the fluid looses some of its ability to transfer heat.

The effect of the ribs on heat transfer within the channel is apparent in Figure 4.17.B. The leading rib is apparent in the 1128K contour partway down the channel. The fluid here is still relatively cool and able to transfer heat, but the rib is limiting reactions so there is less heat generated at the electrolyte. The second rib appears after the 1345K contour protruding halfway down the channel. This rib also limits the heat generation and causes the electrolyte under it to be cooler than the area to either side. The temperature of the rib channel is greater than the plane channel at the outlet because the ribbed channel geometry is capable of more reactions near the outlet and thus more heat generation.

In the sawtooth designs, Figure 4.17.C-E, the temperature gradient is gradual along the incline of the rib and greater at the top and in the shadow of the ribs. The increase in temperature rise in the shadow of the rib is likely caused by decreased convection in the stagnant separated flow in the shadow of the rib.

The parallel-rib design, Figure 4.17.F, results in a similar temperature profile as the plane channel case. The parallel-rib design experienced more heat generation from reactions than the plane case, but had an increase heat transfer surface to remove the heat.

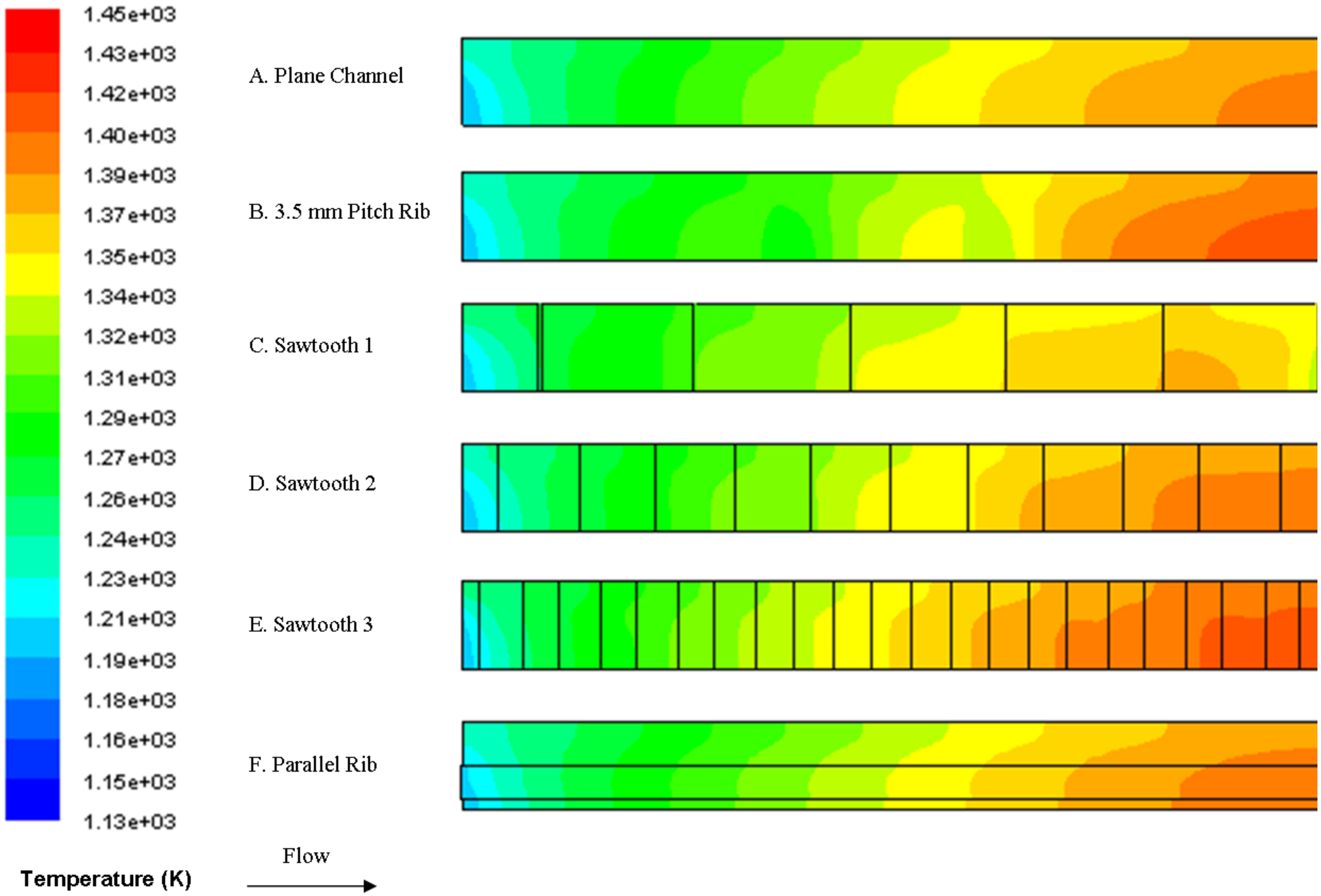

Figure 4.17 Electrolyte temperature contour plot comparison of a single SOFC flow channel with varying geometries

5. Conclusions

An examination of literature concerning SOFCs indicated that limited information exists on increasing the performance of SOFC by enhancing the structure or geometry of a planar SOFC. However, literature also suggests that careful engineering of the flow field design might have a beneficial impact on SOFC performance. The literature survey provides four guidelines for creating SOFC geometries with well engineered flow fields:

- An optimal design is one which can minimize both the area of the electrolyte obstructed by interconnects and the distance the current from the reaction has to travel before it can be collected.
- Decreasing the height of the flow channel can effectively increase the heat/mass transfer within a flow channel.
- Textured electrodes can increase power density by increasing the active area of the electrolyte, as seen in the MOLB design.
- Increasing fresh reactant flow to the electrode/electrolyte assembly can increase power density and efficiency, as seen in the split channel model.

The literature also suggested that mixing created by enhanced heat transfer devices can address some of these design optimizations. However, limited work has focused on improving SOFCs based on increasing the hydrodynamic and thermal performance of the reactant flows.

Based on the conclusions drawn from literature, it was determined that FLUENT provided the most accessible CFD simulation software for fuel cell applications. Six selected fuel cell flow geometries were studied to determine if the used of enhanced heat transfer techniques could increase fuel cell performance in two ways: increasing the fluid mixing to reduce concentration gradients and increasing surface area leading to additional reaction sites.

The baseline SOFC was validated against data from the literature. It was discovered that it is difficult to find sufficiently detailed models in literature to exactly validate a numerical model, as many details regarding input parameters often are not reported. Nevertheless, several references were found that gave sufficient information for comparison, and agreement was reasonable.

The conclusions from the modeling of hydrodynamic flow mixing in fuel cell channels and from the modeling of SOFC operation are listed below:

1. Mixing techniques can create mixing in channels depending on the value of Re. While the flow rates in the fuel flow channel are too low to create mixing, mixing in the air flow channels is optimally created by solid rectangular ribs at a 3.5 mm pitch spacing.
2. Mixing devices have insignificant impact on pumping power. At such low flow rates, the parasitic power required for pumping is less than 1% of the power produced.
3. Mixing, albeit modest, can be induced in the air flow of SOFC fuel cells. The use of porous cathode ribs was ineffective at creating mixing; however, mixing was enhanced only slightly by the three sawtooth electrolyte geometries.
4. Enhanced mixing in the SOFC did not increase the performance of the SOFC; however, the increase in electrolyte area from the mixing devices was responsible for increased voltage in the cell. The increased cell voltage with respect to the planar case was roughly proportional to the increase in area of the electrolyte. After comparing the increase in power density of the fuel cell on an actual area basis, mixing techniques showed no improvement over the plane channel case.
5. Mixing mechanisms that increase surface area are useful in the SOFC to increase the reacting area of the electrolyte. On a volumetric power density basis, the geometries with mixing techniques that increased surface area of the electrolyte, increased power density in proportion to the increase in area with respect to the plane channel case.
6. The use of ribs slightly increased the temperature rise across the length of fuel cell flow; however, there was no significant increase in temperature gradients were created by the ribs.

From this study it is apparent that increasing the area of a SOFC with cross-flow roughness can improve the volumetric power density of the cell without detriment to the pumping requirements or thermal gradients in the cell

6. Works Cited

[1] EPA, Greenhouse Gas Emissions from the US Transportation Sector, March 2006.

[2] EIA, Annual Energy Outlook 2005 with Projections to 2025, 2005.

[3] EPA, Inventory of U.S. Greenhouse Gas Emissions and Sinks: 1990-2006, April 2008.

[4] DOE, Future Fuel Cells R&D Program, <http://www.fossil.energy.gov/programs/powersystems/fuelcells>.

[5] DOE, Hydrogen Fuel Cell Program, <http://www.hydrogen.energy.gov/about.html>.

[6] N. Garland, The President's Hydrogen Fuel Initiative: Durability Requirements, in: Fuel Cells Durability—Stationary, Automotive, Portable, 1st ed., Knowledge Foundation, 2005.

[7] J. Milewski, A. Miller, Influences of type and thickness of electrolyte on solid oxide fuel cell hybrid system performance, J. Fuel Cell Sci. and Technology 3 (2006) 396.

[8] Yamamoto, O., Solid oxide fuel cellls: fundamental aspects and prospect, Electrochim. Acta 45 (2000) 2423-2435.

[9] Minh, N., Ceramic Fuel Cells, J. Am. Ceram. Soc. 76 (1993) 563-588.

[10] Sammes, N., Smimova, A., & Vasylyev, O., Fuel Cell Technologies: State and Perspectives. Springer, 2005.

[11] S.P.S. Badwal and K. Foger, Solid oxide electrolyte fuel cell review, Ceramics International, 22 (1996) 257-265.

[12] L. Blum et al., Worldwide SOFC technology overview and benchmark, Int. J. App. Ceram. Tech., reprinted in: Progress in Solid Oxide Fuel Cells, ed. The American Ceramic Society, Wiley & Sons Inc., 2006.

[13] Fuel Cell Today, "Acumentrics and partners to test SOFC mCHP in European homes," 02 Oct 2008. <http://www.fuelcelltoday.com/online/news/articles/2008-10/Acumentrics-to-Test-SOFC-mCHP-in>

[14] Schmidt, Doug, Progress in Acumentrics Fuel Cell Program presented at 8th Annual Solid State Energy Conversion Alliance (SECA) Workshop, 05 Aug. 2007.

[15] Fuel Cell Today, “Acumentrics SOFC fuel cell tops 10,000 operating hours,” 08 Sept 2008. <http://www.fuelcelltoday.com/online/news/articles/2008-09/Acumentrics-SOFC-Fuel-Cell-Tops->.

[16] “Fraunhofer unveils weather-resistant mini fuel cells, SOFC station,” Fuel Cell Bulletin, 2005 (2005) 2.

[17] <http://www.cfcl.com.au/System_Evolution/>

[18] < http://www.hexis.com/downloads/hexis_prospekt_englisch_web0703.pdf>

[19] Chan, S., Khor, K., & Xia, Z., A complete polarization model of a solid oxide fuel cell and its sensitivity to the change of cell component thickness, J. of Power Sources, 93 (2001) 130-140.

[20] Chan, S., & Xia, Z., Polarization effects in electrolyte/electrode-supported solid oxide fuel cells, J. Appl. Electrochim., 32 (2002) 339-347.

[21] Bessler, W., & Gewies, S., Gas concentration impedance of solid oxide fuel cell anodes, J. Electrochem. Society, 154 (2007) 548-559.

[22] Lin, Z., Stevenson, J., & Khaleel, M., The effect of interconnect rib size on the fuel cell concentration polarization in planar SOFCs, J. Power Sources, 117 (2003) 92-97.

[23] Li, P.W., Chen, S., & Chyu, M., To Achieve the best performance through optimization of gas delivery and current collection in solid oxide fuel cells, J. fuel cell science and technology, 3 (2006) 188-194.

[24] Ji, Y., *et al.*, Effects of transport scale on heat/mass transfer and performance optimization for solid oxide fuel cells, J. Power Sources, 161 (2006) 380-391.

[25] Hasan, A., Ekkad, S., & Mensah, P., Simulations of dimensional effects in solid oxide fuel cells, ASME Summer Heat Transfer Conference paper number HT2005-72394, July 17-22, 2005.

[26] Ackerman, J.P., J.E. Young, U.S. Patent No. 4476198, October 9, 1984.

[27] Nagela, FP et al., Performance comparison of planar, tubular and Delta8 solid oxide fuel cells using a generalized finite volume model, J. Power Sources, 184 (2008) 143-164.

[28] Vora, Shailesh, SECA Program at Siemens, presented at 9th Annual Solid State Energy Conversion Alliance (SECA) Workshop, 05 Aug. 2008.

[29] Hwang, J., Chen, C., & Lai, D., Computational analysis of species transport and electrochemical characteristics of a MOLB-type SOFC, J. of Power Sources, 140 (2005) 235-24.

[30] Hwang, J., Chen, C., & Lai, D., Detailed characteristic comparison between planar and MOLB-type SOFCs, J.of Power Sources, 143 (2005) 75-83.

[31] Hwang, J. Mass/charge transfer in mono-block-layer-built-type solid-oxide fuel cells, J. of Fuel Cell Science and Technology, 2 (2005) 164-170.

[32] Yang, Y., Wang, G., Zhang, H., & Xia, W., Computationa analysis of thermo-fluid and electrochemical characteristics of MOLB-type SOFC stacks, J. of Power Sources, 173 (2007) 233-239.

[33] Yang, Y., Wang, G., Zhang, H., & Xia, W., Comparison of heat and mass transfer between planar and MOLB-type SOFCs, J. of Power Sources, 177 (2008) 426-433.

[34] Ramakrishna, P., Yank, S., & Shon, C., Innovative design to improve the power density of a solid oxide fuel cell, J. of Power Sources, 158 (2006) 378-384.

[35] Yamaguchi, T, *et al*., Evaluation of extruded cathode honeycomb monolith-supported SOFC under rapid start-up operation, Electrochim. Acta, 54 (2009) 1478-1482.

[36] Web, R., Principles of Enhanced Heat Transfer, Wiley & Sons: New York, 1994.

[37] Han, J., Glicksman, L., & Rohsenow, W., An investigation of heat transfer and friction factor for rib-roughened surfaces, International Journal of Heat and Mass Transfer, 21 (1978) 1143-1156.

[38] Murata, A., & Mochizuki, S., Comparison between laminar and turbulent heat transfer in a stationary square duct with transverse or angled rib turbulators, Int. J. Heat and Mass Transfer 44 (2001) 1127-1141.

[39] Tatsumi, K., Iwai, H., & Inaoka, K., Numerical simulation for heat and fluid characteristics of square duct with discrete rib turbulators, Int. J. Heat and Mass Transfer 45 (2002) 4353-4359.

[40] Gao, X., & Sunden, B., Heat transfer and pressure drop measurements in rib-roughened rectangular ducts, Exp. Thermal and Fluid Sci. 24 (2001) 25-34.

[41] Gao, X., & Sunden, B. PIV measurement of the flow field in rectangular ducts with 60 degree parallel, corssed and V-shaped ribs, Exp. Thermal and Fluid Sci. 28 (2004) 639-653.

[42] Tanda, G., Heat transfer in rectangular channels with transverse and V-shaped broken ribs, Int. J. Heat and Mass Transfer 47 (2004) 229-243.

[43] Nagano, Y., Hattori, H., & Houra, T., DNS of velocity and thermal fields in turbulent channel flow with transverse-rib roughness, Int. J. Heat and Fluid Flow 25 (2004) 393-403.

[44] Layek, A., Saini, J., & Solanki, S., Heat transfer and friction characteristics for artificially roughened ducts with compound turbulators, Int. J. Heat and Mass Transfer 50 (2007) 4845-4854.

[45] Focke, W., On the mechanism of transfer enhancement by eddy promoters, Electrochim. Acta 28 (1983) 1137-1146.

[46] Olsson, C., & Sunden, B., Experimental study of flow and heat transfer in rib-roughened rectangular channels, Exp. Thermal and Fluid Sci. 16 (1998) 349-365.

[47] Kilicaslan, I., and Sarac, H., Enhancement of heat transfer in compace heat exchanger by different type of rib with holographic interferometry, Exp. Thermal and Fluid Sci. 17 (1998) 339-346.

[48] Pakalapati, SR. A new reduced order model for solid oxide fuel cells, Electronic Thesis, Mechanical Engineering, West Virginia University, 2006.

[49] Bessler, W.G., S. Gewies, and M. Volger, A new framework for physically based modeling of solid oxide fuel cells, Electrochim. Acta, 53 (2007) 1782-1800.

[50] Ni, M., M.K.H. Leung, and D.Y.C. Leung, Parametric study of solid oxide fuel cell performance, Energy Conversion and Management 48 (2007) 1525-1535.

[51] Sparrow, E.M. and Tao, W.Q., Enhanced heat transfer in a flat rectangular duct with streamwise periodic disturbances at one principal wall, J Heat Transfer 105 (1983) 851-861.

[52] Varun, R.P. Saini and S.K. Singal, A review on roughness geometry used in solar air heaters, Solar Energy 81 (2007) 1340-1350.

[53] Prasad, B.N., J.S. Saini, Effect of artificial roughness on heat transfer and friction factor in a solar air heater, Solar Energy 41 (1988) 555-560.